https://doi.org/10.15388/vu.thesis.30

VILNIUS UNIVERSITY

Linas
PETKEVIČIUS

Numerical and Symbolic Modeling of Reaction-Diffusion Processes in Bioreactors

DOCTORAL DISSERTATION

Natural Sciences,
Informatics N 009

VILNIUS 2020

This dissertation was written between 2015 and 2019 at Vilnius University. Doctoral dissertation preparation was partially funded by the Research Council of Lithuania (Researcher groups projects Grant), project 'Computational modelling of open biological systems: bacteria grow and microreactors' (Grant No. S-MIP-17-98), and scholarship given by Research Council of Lithuania (No. P-DAP-19-337).

Academic supervisor – Prof. Dr. Romas Baronas (Vilnius University, Natural Sciences, Informatics – N 009).

https://doi.org/10.15388/vu.thesis.30

VILNIAUS UNIVERSITETAS

Linas
PETKEVIČIUS

Skaitinis ir simbolinis reakcijos-difuzijos procesų bioreaktoriuose modeliavimas

DAKTARO DISERTACIJA

Gamtos mokslai,
informatika N 009

VILNIUS 2020

Disertacija rengta 2015 – 2019 metais Vilniaus universitete. Disertacijos rengimą iš dalies parėmė projektas ‘Kompiuterinis atvirų biologinių sistemų modeliavimas: augančios bakterijos ir mikroreaktoriai’, finansuojamas Lietuvos Mokslo Tarybos (Mokslininkų grupių projektai) lėšų (projekto nr. S-MIP-17-98) ir LMT stipendija P-DAP-19-337.

Mokslinis vadovas – prof. dr. Romas Baronas (Vilniaus universitetas, gamtos mokslai, informatika – N 009).

Table of Contents

List of Figures

List of Tables

Notation

D – diffusion coefficient
E – the concentration of enzyme
K_{M} – the Michaelis constant
P – the concentration of product
r – the distance (radius)
S_{m} – the concentration of substrate (the lower index indicate the domain m - microbioreactor, d - diffusion layer, b - bulk.)
t – the time
$\mathrm{V}_{\mathrm{max}}$ – the maximal enzymatic rate

Abbreviations

BSTR – batch stirred tank reactors
CA WoS – Clarivate Analytics Web of Science
CSTR – continuous stirred tank reactors
FDM – finite difference method
HPM – homotopy perturbation method
GDH – glucose dehydrogenase
LAC – laccase
MR – microbioreactor
PDE – partial differential equation

Introduction

Research context and motivation

Chemical reactions surround all of us in various situations in our lives. On the other hand, materials do not interact with each other by chemical reactions if not all necessary conditions are met. In various fields, such as chemical, environmental, food and pharmaceutical industries [44, 101, 112], chemical reactions are triggered by enzymes[1]. This trigger effect is known as (bio)catalysis process in which enzymes increase the rate (or enables) of a chemical reaction. A lot of breakthroughs in recent years have been made in applications of enzymes, e.g., the most fascinating one - ability to dissolve plastic [87, 117]. The special environment/device, where the chemical reactions take place is often called (bio)reactor. We use a simplified mathematical model of process kinetics in bioreactors where (bio)catalyst is enzyme E, the material is substrate S, and product P is produced as a result of reaction (see Figure 1). In general, biocatalyst is such a material which allows to produce new or faster reactions between the substances [75].

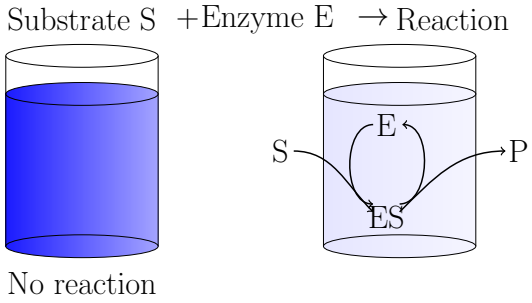

Figure 1: The usage of biocatalyst (enzyme) to enable chemical reactions ((bio)catalysis process).

A variety of definitions of bioreactors can be found in literature. In some of them, it is defined as a tank or a container in which various products could be produced; such as, manufacturing of beer [26] (see Figure 2). However, tank or a container is limited in terms of number of controllable reactions that can take place. According to other definitions, a bioreactor is a chemical device or designed material that enables chemical reactions [94]. An example could be bioreactor based on microbioreactors, which are immobilized with

[1]Enzymes are biological catalysts (biocatalysts).

enzyme[2] (see Figure 2). In this thesis we concentrate on bioreactors based on microbioreactors.

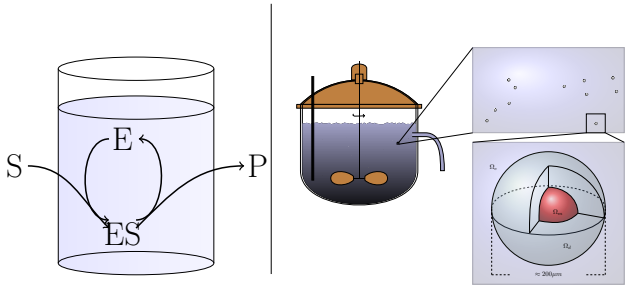

Figure 2: The bioreactor (left) and bioreactor based on microbioreactors (right).

The usage as well as demand of bioreactors are growing. According to the report by Global Market Insights, the global demand for bioreactors in the USA reached US$270 million by the year 2018 and expected to be expand up to US$700 million till 2025 [3]. A similar growth is expected in other markets for bioreactors globally.

Similar trends can be found in scientific community. The Clarivate Analytics Web of Science [4] database indicates that the number of scientific papers on immobilized enzymes gradually increases, while applications of bioreactors are in high demand since 2004 (see Figure 3).

This research concentrates on the investigation of enzyme immobilized bioreactors, which have proved to be reliable and low-cost in various commercial systems within chemical, environmental, food and pharmaceutical industries [44, 101, 112]. The particle-based bioreactor systems are typically compared based on their effectiveness [19–21]. However, usually the system is simplified and the reaction part is assumed to be linear, which covers only small range of practical cases. Mathematically microbioreactors are modeled as a core and outer (Nernst) layer. Model which have two layers is called bi-layer model.

The recent experiments have demonstrated the construction of microcatalysts using non-specific glucose dehydrogenase (GDH) and oxygen reducing laccase (LAC) that have been wired via carbon nanotubes and gold nanoparticles [93, 94]. In this thesis the hypothesis: is it possible to model the chemical kinetics of a microbioreactor with nanotubes, with a model model formulated in one-dimensional space (unitary microbioreactor with a shell layer) is investigated.

[2] Immobilized enzymes – are enzymes which are inert or insoluble into material. In our case this material is a microbioreactor.

[3] https://www.gminsights.com/industry-analysis/bioreactor-market

[4] wcs.webofknowledge.com

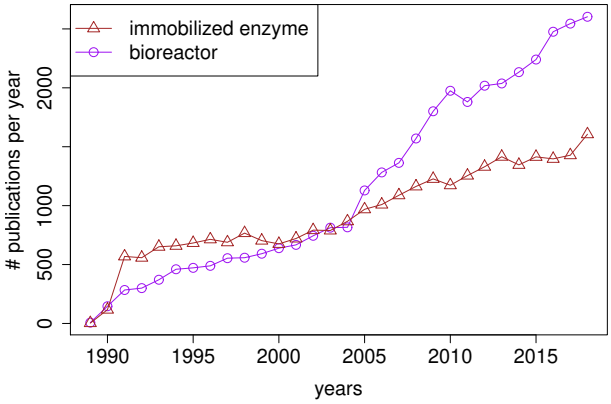

Figure 3: The number of scientific papers per year for separate keywords: *bioreactor* and *immobilized enzyme* in CA WoS database

Aim, object and objectives of the thesis

The object of investigation are mathematical and computational models describing chemical kinetics of bioreactors based on microbioreactor particles. The aim of this work is to properly simulate and optimize bioreactor systems, based on microbioreactors, by suggesting original mathematical and computational models. The objectives are as follows:

1. To generalize existing mathematical models of bioreactors,
2. To develop a mathematical and computational models for a microbioreactor with carbon nanotubes,
3. Propose an algorithm based on the homotopy perturbation method, for mathematical model not considered in literature before, for approximate analytical solution of the nonlinear boundary value problem describing a bi-layer biocatalytic the system,
4. To develop a computational model to be used for the multi-objective optimization of a batch stirred tank reactor based on spherical catalyst microbioreactors,
5. Investigate properties of the open and closed bioreactor systems by using the developed mathematical and computations models.

Research approach and methods

In the dissertation we use numerical schemes (the finite difference method (FDM)) from mathematical modelling theory, the methods of perturbation analysis from the theory of aproximations, scalability analysis from the theory of parallel computing, the three-objective optimization to find the Pareto front from the optimization theory.

Scientific novelty and results

A novel mathematical model of a bioreactor based on carbon nanotubes was proposed. Various bioreactor properties were investigated under different conditions as well as at variuos extensions like additional layers, and non-linear boundary conditions. In more detailed, the results are as follows:

1. A mathematical model of bioreactors was generalized in terms of additional layers, and initial boundary conditions,
2. A new mathematical model for a microbioreactor based on carbon nanotubes substrates conversion was developed,
3. Limitations of the homotopy perturbation method were demonstrated, and recommendations on the method usage were provided,
4. A computational model for the multi-objective optimization of microbioreactor configuration was developed,
5. The model parameter values for all considered microbioreactor models, at which the bioreactor transient effectiveness significantly increases, have been determined.

Practical significance of the results

The mathematical models presented in this thesis describe the bioreactors based on spherical microbioreactor partials. The developed and implemented computational models can be used to numerically investigate the behaviour of such bioreactors, as well as to create more efficient bioreactors in the design phase. The analytical approximations were produced for the limiting cases which allow the biochemists to have analytical solutions of the investigated systems.

By using the developed programs to model microbioreactor action, the dependency of systems efficiency on various parameters, like particle size, and physical conditions, like diffusion and number of outer layers, was investigated. The obtained results show the dependencies of analysed microbioreactor on various physical conditions.

The investigation of various properties described in this thesis can be applied for creation and development of microbioreactors utilizing multiple reactions behaving according the Michaelis-Menten kinetics [6, 12, 44].

The results were used to accomplish the goals of the following project: 'Computational modeling of open biological systems: bacteria grow and microbioreactors' funded by the grant project No. S-MIP-17-98 from the Research Council of Lithuania (Researcher groups projects Grant).

Statements promoted to defend

The main contributions formulated to defend are as follows:

1. The proposed novel mathematical model can be successfully applied to modeling the kinetics for a microbioreactor with carbon nanotubes,
2. The transient effectiveness of a closed system (batch type model) reduces to the effectiveness of an open steady-state system (continuous type models) under large time,
3. Approximations of limiting system cases obtained by the homotopy perturbation method are valid only when the small parameter value falls into the convergence region. For different bioreactor configurations, different values of the of small parameter are needed.
4. The chemical kinetics of a bioreactor, based on a large number of uninteracting microbioreactors, can be successfully modeled by a unit cell (a microbioreactor) and the surrounding shell in one dimensional space.

Results approbation

Three articles were published in the journals with citation index in Clarivate Analytics Web of Knowledge database (WoS) [A1–A2, A4], the forth publication [A2] is in review process stage, one publication was published in periodical and peer-reviewed [A5] journal. The main contribution for the thesis, which was published in articles, covers the development of numerical models and the software for numerical and symbolic solving and validation of these models, digital investigation of the kinetic process behavior under various scenarios.

Additionally, the results were presented in four international conference proceedings [A6–A9].

The results were presented at the following scientific conferences:

1. ESM 2019 (Palma, Spain): *The 33rd annual European Simulation and Modelling Conference*. 28–31th October 2019.
2. ECMS 2019 (Caserta, Italy): *32th European Conference on Modelling and Simulation*. 10–14th June 2019.

3. DAMSS 2018 (Druskininkai, Lithuania): *Data analysis methods for software systems*. 29th November–1st December 2018.

4. AIEEE 2018 (Vilnius, Lithuania): *6th IEEE Workshop on Advances in Information, Electronic and Electrical Engineering*. 8–12th November 2018.

5. NESUS 2018 (Zagreb, Croatia) *3rd NESUS Winter School and PhD Symposium*. 22–25th January 2018. (COST Action IC1305)

6. SIMUL 2017 (Athens, Greece): *The Ninth International Conference on Advances in System Simulation*. 8–12th October 2017.

7. LMD 2017 (Vilnius, Lithuania): *Lithuanian Mathematical Society 58th Conference*, 21–22th June 2017.

8. OR 2017 (Vilnius, Lithuania): *Open Readings*. 14–17th March 2017.

9. DAMSS 2016 (Druskininkai, Lithuania): *Data Analysis Methods for Software Systems*. 1–3rd December 2016.

Structure of the thesis

The thesis consists of four chapters. In Chapter 1 the overview of the researched domain as well as the state-of-the-art models are presented: an introduction to bioreactors, their properties and classification, an overview of the existing mathematical models, as well as the methods and tools used to carry out the simulation processes. Chapter 2 presents the mathematical models including the proposed novel mathematical model of a microbioreactor with carbon nanotubes. Chapter 3 presents the solving of mathematical models of the bioreactors utilizing intermediate substances: the homotopy perturbation method, numerical methods, as well as parallelization of simulation. The investigation of bioreactors based on spherical microbioreactors is presented in Chapter 4, were the modelling results of a microbioreactor with carbon nanotubes are compared with the experimental data.

1. Mathematical Modeling of Process Kinetics in Microbioreactors

In this Chapter scientific literature review is presented. All the necessary definitions, types of bioreactors, general mathematical models as well as computational methods are introduced.

1.1. Bioreactors

The history of bioreactors dates back to the year 1944 when De Beeze and Liebmann have used the first large scale fermentor for the production of yeast [78]. It was a large tank of enzymes. In 1950 Monod, and Novick and Szilard have developed the concept using continuous stirred tank bioreactors [36].

For a long time, in order to receive a reaction product, the initial materials were mixed in stirred bioreactors. In 1974 a particle-based bioreactor was introduced [114]. Particle-based bioreactor containe (commonly, catalyst) particles which enable chemical processses. Such a process mixes particles constantly, therefore it is also called as stirred bioreactors. The use of stirred bioreactors brings some benefits; such as the ability to produce product constantly in large quantities [114]. One of the common assumptions in the analysis of chemical kinetics is that the provided catalyst deactivation is negligible [12]. Such a formulation assume, that under enzyme conservation law the process eventually (under large time) settle the down, so it is called steady state. Steady state processes allow simplification of the whole chain of reactions as it is reduced to a simpler reaction network [4, 107].

The microbioreactors containing immobilized enzyme permit substrate conversion, a use of small volumes of samples and reagents, reduced costs, short processing time and system compactness [60, 101]. Although some enzyme activity is often lost upon the immobilization, improved stability is often gained by confining the enzymes in support materials [77, 88]. Porous[1] silica-based materials are promising supports as their properties can be varied to achieve efficient enzyme loadings to a particle (microbioreactor) [60, 66, 118].

For the development and improvement of highly efficient and productive biotechnological processes a number of physical and biochemical characteristics should be measured and analysed [44, 60, 112]. In many bioreactors, liquid and solid phases are present and the mass transfer is an important consideration [41,

[1] Porous means microbioreactor have voids and enzyme take only fraction of the volume.

44]. In particular, pore and particle sizes determine the total surface area and, therefore, critically affect the ability for binding enzymes [2].

1.1.1. Continuous stirred tank reactors

Continuous stirred tank reactors (CSTR) were developed by Monod, and Novick and Szilard [80, 81, 85]. CSTR kinetics sometimes refers to a black box model, since all of the reactions are lumped into one overall reaction. Typical equations describing the enzymatic kinetics (where there is often one substrate and one product in one reaction), such as the Michaelis-Menten kinetics have been used to formulate steady state processes. Since the tank is continuously, replenishing and mixing, the modeled system is known as an open system.

1.1.2. Batch stirred tank reactors

Batch stirred tank reactor (BSTR) and continuous stirred tank reactor (CSTR) are usually the most commonly used configurations of chemical bioreactors [62, 90]. The most prominent advantages of BSTR are its simplicity and versatility [41, 44]. Typically, the biocatalyst particles are dispersed in the solution, the reactants are injected and the agitation is provided by mechanical stirrers [19, 23]. BSTR, differently from CSTR, is not refilled by the substrate. When the tank is continuously mixed and no new substrate is injected into the system, the modeled system is known as a closed system.

1.1.3. Microbioreactors based on carbon nanotubes

In real world, the chemical processes are much more complicated and involve more substances. In this Section a description of real experiments [93, 94] is presented. The purpose of these experiments were to create synthesis of artificial multi-enzyme systems and demonstrate better understanding of natural electron transfer networks and chains. Based on these experiments the novel model of microbioreactors with carbon nanotubes is presented in Section 2.3.

Recently, the non-specific glucose dehydrogenase (GDH) and oxygen reducing laccase (LAC) have been wired via carbon nanotubes or gold nanoparticles. As a result, the system have demonstrated effective carbohydates conversion by oxygen in the absence of a mediator [93, 94].

Ratautas et al. proposed a microbioreactor based on entraping modified by GDH and LAC nanotubes into controlled pore glass (CPG) carrier (microbioreactor) [93, 94]. The computational model for a batch stirred tank reactor (BSTR) is based on an array of spherical porous microbioreactors loaded with

these enzymes [30]. An investigation of the influence of the physical and kinetic parameters on the transient effectiveness of the bioreactor is presented in Chapter 4.3. The microbioreactor was mathematically modeled by a two-compartment model, based on transient reaction-diffusion equations containing nonlinear terms related to the Michaelis-Menten kinetics of two enzymatic reactions with addition of the mass transfer of the substrate outside the catalyst region [6, 110].

For the modeling the following biochemical reactions taking place in the microbioreactor:

$$\mathrm{L} + \mathrm{E}_{1\mathrm{ox}} \xrightarrow{k_1} \mathrm{P} + \mathrm{E}_{1\mathrm{red}}, \tag{1.1a}$$

$$\mathrm{E}_{1\mathrm{red}} \xrightarrow{k_2} \mathrm{E}_{1\mathrm{ox}} + 2\mathrm{e}^-, \tag{1.1b}$$

$$\mathrm{E}_{2\mathrm{ox}} + 4\mathrm{e}^- \xrightarrow{k_3} \mathrm{E}_{2\mathrm{red}}, \tag{1.1c}$$

$$\mathrm{E}_{2\mathrm{red}} + \mathrm{O}_2 \xrightarrow{k_4} \mathrm{E}_{2\mathrm{ox}} + 2\mathrm{H}_2\mathrm{O}, \tag{1.1d}$$

where L – lactose, O_2 – oxygen, $\mathrm{H}_2\mathrm{O}$ – water, $\mathrm{E}_{i,\mathrm{ox}}$ and $\mathrm{E}_{i,\mathrm{red}}$ are the oxidized and reduced forms of the enzyme E_i, $i = 1, 2$, E_1 stands for GDH, E_2 – for LAC, P is the reaction product, k_1 and k_4 are the rate constants of the enzyme reactions, and k_2, k_3 are the rate constants of the electron transfer (ET) reactions. It is assumed that both enzyme catalyzed processes (1.1a)–(1.1b) and (1.1c)–(1.1d) obey the Michaelis–Menten kinetics.

In this thesis the novel mathematical and computational models for microreactor utilizing reactions (1.1a)–(1.1d) are proposed. Since such a system was not yet investigated, the transient effectiveness of a microbioreactor with carbon nanotubes in the BSTR is analysed. The process duration is numerically analysed for different initial concentrations of the substrate as well as for internal and external diffusion resistances. The performed analysis of CSTR and BSTR allowed us to formulate the resulting model. The comparison of proposed model with the experimental data presented in Section 4.3.

1.2. Mathematical model

The physical experiments are common practice to investigate and create new bioreactors. Another way is to model and simulate the bioreactor action using state-of-the-art techniques of computational modeling [6].

Mathematical modeling of biochemical processes is regarded as an important tool to provide useful information for the analysis, design and operation conditions for the production of various materials including enzymes, proteins

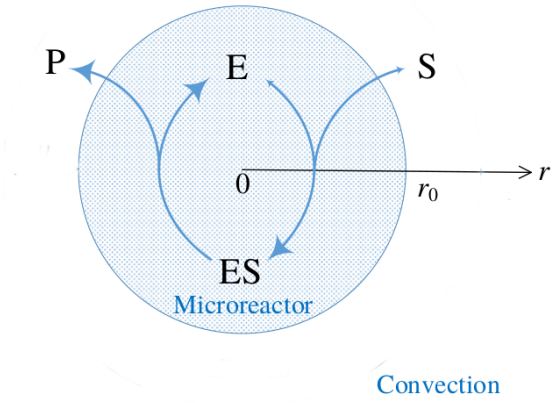

Figure 1.1: Schematic view of a modeled unit cell: a microbioreactor and the surrounding shell

and biofuel [50, 77, 96]. These models are useful for planning efficient process control strategies and predicting the production performance [74, 82, 88]. The computer simulation approach allow us to optimize the microbioreactor configuration with substantially reduced time and cost [77, 89, 111].

For an enzyme-loaded microbioreactor, the enzyme-catalyzed reaction considered:

$$\mathrm{S} \xrightarrow{\mathrm{E}} \mathrm{P}, \tag{1.2}$$

where the substrate (S) binds to the enzyme (E) and is converted to the product (P) [41, 44]. The principal structure of the modeled unit cell is presented in Figure 1.1. The lower letter notations, like $s = s(r,t)$, are representing the model in one dimensional space, where r – the radius of a microbioreactor, t – the time. The capital letters indicate dimensionless models. For example, r_0 represents the radius of a microbioreactor in meters.

At the quasi-steady-state conditions, the kinetics of most enzyme reactions are reasonably well represented by the Michaelis-Menten equation

$$v(s) = \frac{V_{\max} s}{K_{\mathrm{M}} + s}, \tag{1.3}$$

where $s = s(r,t)$ is the substrate concentration, v is the volumetric reaction rate expressed as a function of the substrate concentration s, $V_{\max}$ is the maximal enzymatic rate, and K_{M} is the Michaelis constant [54, 102].

1.2.1. Categorization of chemical kinetic processes

Stochasting modeling [120], Monte-Carlo methods [17] and PDE [19, 23] have been successfully applied to modeling of chemical kinetics. The performance of microbioreactors based on particles has been successfully modeled by second order partial differential equations [19, 23]. Usually, a equations system belongs to the parabolic-type reaction-diffusion equations [4, 41, 44],

$$\tau \frac{\partial s(r,\, t)}{\partial t} = \mathrm{D} \cdot \triangle s(r,\, t) + f(s(r,\, t), \nabla s(r,\, t), r, t), \tag{R-D}$$

where $\triangle$ – the Laplace operator to define the diffusion process, f – reaction term[2], D – the diffusion coefficient. The most common forms of the reaction-diffusion processes (reaction term f) are as following:

$$\tau \frac{\partial s(r,\, t)}{\partial t} = \mathrm{D} \cdot \triangle s(r,\, t) + \frac{V_{\max} s(r,\, t)}{K_{\mathrm{M}} + s(r,\, t)}, \tag{RMM-D}$$

$$\tau \frac{\partial s(r,\, t)}{\partial t} = \mathrm{D} \cdot \triangle s(r,\, t) + A + B \cdot s(r,\, t). \tag{Rt-D}$$

The reaction-diffusion processes with the non-linear Michael-Menten kinetics part (RMM-D) are considered. The limiting cases are: $\tau = 0$ or $\lim_{t \to \infty} f(r,t) = g(r)$ called steady-state (*SS*) or stationary; $\mathrm{D} = 0$ no diffusion; $V_{\max} = 0$ no chemical reactions;

Limiting cases for (Rt-D): when $K_{\mathrm{M}} \gg s_0$, then $A = 0$ – the reaction term approches a linear process, while case $s(r,\, t) \gg K_{\mathrm{M}}$ or $s \sim 0$ – barely depends on the concentration.

1.2.2. Governing equations

The equations of the simplest bioreactor model (see Figure 1.1) have the following form:

$$\frac{\partial s_{\mathrm{m}}(r,t)}{\partial t} = \underbrace{\mathrm{D} \cdot \triangle s_{\mathrm{m}}(r,t)}_{\text{diffusion term}} + \underbrace{\frac{V_{\max} s_{\mathrm{m}}(r,t)}{K_{\mathrm{M}} + s_{\mathrm{m}}(r,t)}}_{\text{reaction term}}, \tag{1.4}$$

where $s = s_{\mathrm{m}}(r,t)$ is the concentration of substance in a microbioreactor, t is time, r is the distance from the particle center, D is the diffusion coefficient, K_{M} is a constant describing the chemical kinetics also known as the Michaelis

[2]Reaction–diffusion systems contains two term: difusion and reaction, respectively.

constant, and $\triangle$ is the Laplace operator, defined in spherical coordinates. A microbioreactor is defined in region $0 < r < r_0$ [4]. In such a case the radius of a microbioreactor is r_0 (see Figure 1.1).

The first part (diffusion term) of the differential equation defines the diffusion of matter by the Second Law of the Fick [48]. The second part (reaction term) of the equation defines the chemical reaction. This part is required if the substance undergoes chemical reactions as a reagent or as a reaction product. Depending on the type of bioreactors and the chemical reactions that take place therein, the chemical kinetics can be defined by the Michael-Menten kinetic equation [12, 102].

Having an equation system that defines the concentration of substances in bioreactors, the process dynamics is formulated as a partial differential equation (PDE) [14, 75].

In order to uniquely define the formulated task, the concentrations of substances are usually defined by the initial conditions inside and outside the domain Ω and boundaries Γ at the initial time $(t = 0)$, i.e.,

$$s_{\mathrm{m}}(r,0) = f(r), \quad r \in \Omega; \tag{1.5}$$

$$s_{\mathrm{m}}(r,0) = g(r), \quad r \in \Gamma, \tag{1.6}$$

where Ω is open domain, while Γ is the boundary of the domain, f and g are known functions under consideration [12, 102]. In open systems the initial conditions are defined as follows:

$$s_{\mathrm{m}}(r,0) = 0, \quad 0 < r < r_0; \tag{1.7}$$

$$s_{\mathrm{m}}(r,0) = s_0, \quad r = r_0, \tag{1.8}$$

i.e, no substrate appears in a particle (for example when particle is thrown into the solution), and the uniform concentration within a solution [4, 18]. The boundary conditions define the concentrations of substances at the border of the domain boundaries.

The simplest boundary condition states that the concentration of the substance on the border is constant and does not change over time $(t = 0)$, i.e.,

$$s_{\mathrm{m}}\Big|_{\Gamma} = \text{const.} \tag{1.9}$$

The iliustrative example of equation (1.9) is:

$$s_{\mathrm{m}}(r_0,t) = s_0, \quad t > 0. \tag{1.10}$$

1.2.3. Dimensionless model

The system described above have multiple dimensional parameters. To simplify the model, dimensionless models are considered [12]. In order to

define the main governing parameters of the one layer model (1.4)–(1.9), the dimensional variable r and the unknown concentration $s_{\mathrm{m}}(r,t)$ are replaced with the following dimensionless parameters:

$$R = \frac{r}{r_0}, \;\; S_{\mathrm{m}} = \frac{s_{\mathrm{m}}}{K_{\mathrm{M}}}, \;\; S_0 = \frac{s_0}{K_{\mathrm{M}}}, \;\; T = \frac{\mathrm{D_m} t}{r_0^2}, \tag{1.11}$$

where R is the dimensionless distance from the microbioreactor center and $S_{\mathrm{m}}(R)$ is the dimensionless concentration, while S_0 is the dimensionless substrate concentration in the bulk solution. Finally, T is dimensionless time. The dimensionless thickness of the microbioreactor equals one $R_0 = \frac{r_0}{r_0} = 1$.

The governing equations (1.4) in the dimensionless coordinates are expressed as follows ($0 < R < 1$):

$$\frac{\partial S_{\mathrm{m}}}{\partial T} = \triangle S_{\mathrm{m}} - \sigma^2 \frac{S_{\mathrm{m}}}{1 + S_{\mathrm{m}}}, \tag{1.12}$$

where σ is the Thiele modulus or the Damköhler number [49, 103, 112] defined as:

$$\sigma^2 = \frac{V_{\max} r_0^2}{K_{\mathrm{M}} \mathrm{D}_{S,\mathrm{m}}}. \tag{1.13}$$

The dimensionless factor σ^2 essentially compares the rate of enzyme reaction ($V_{\max}/K_{\mathrm{M}}$) with the diffusion through the enzyme-loaded microbioreactor ($\mathrm{D_m}/r_0^2$). If $\sigma^2 \ll 1$, the enzyme kinetics controls the bioreactor action. On the other hand action is under diffusion control, when $\sigma^2 \gg 1$ [12].

In case when $K_{\mathrm{M}} \gg s_0$, the reaction term (1.12) approaches a linear function (see categorization (Rt-D)) of concentration under steady-state $\partial S_{\mathrm{m}}/\partial T = 0$, then the analytical solution of concentration S is known:

$$S(r) = \frac{S_0 \sinh(\sigma R)}{R \sinh(\sigma)}. \tag{1.14}$$

1.2.4. Characteristics of microbioreactors

In many industrial processes, especially in the production of low-value added products like bio-pesticides, bio-fertilizers, bio-surfactants [116], it is important to continuously improve efficiency [42, 44]. The productivity is especially important, since this ensures an efficient utilization of the production capacity, i.e., bioreactors [19–21].

The effectiveness factors characterize the interaction between diffusion and reactions in microbioreactors, the outer layer and the bulk [15, 42]. Reactants have to diffuse through the external diffusion layer and pores of the

support for the reaction to take place, and, therefore, the actual rate can be limited by the rate at which the diffusing reactants reach the catalyst. Typically, the designers seek for reaction-limited regime in a microbioreactor, since in this case reaction and diffusion occur on different time scales and one is in the best possible position to measure reaction [45].

Since the effectiveness of a bioreactor can be defined with respect to the substrate concentration at the catalyst surface or with respect to the bulk concentration, the internal and external effectiveness factors are often used in biochemical engineering [42, 44]. Additionally, the effectiveness factor is also used when taking into consideration the partitioning effect [113].

The effectiveness factors are usually defined for the stationary mode of biocatalytic systems [15, 44, 55]. Although the transient effectiveness factors in porous catalyst particles can be considered [19], after a very short time the substrate concentration inside the particles becomes constant. Then the effectiveness of a bioreactor system in the beginning of the process is not important for overall effectiveness of the system acting in the flow mode [44].

The internal effectiveness factor η_{i} for the microbioreactor can be defined as the ratio of the actual volume-averaged rate of the reaction over the whole microbioreactor to the rate of the reaction at the inner surface of the microbioreactor [14, 41, 44],

$$\eta_{\mathrm{i}} = \frac{\left(4\pi \int_0^{r_0} v(s_{\mathrm{m,s}}(r)) r^2 \mathrm{d}r\right) / (4\pi r_0^3/3)}{v(s_{\mathrm{m,s}}(r_0))} = \frac{3\int_0^{r_0} v(s_{\mathrm{m,s}}(r)) r^2 \mathrm{d}r}{r_0^3\, v(s_{\mathrm{m,s}}(r_0))}. \tag{1.15}$$

The factor η_{i} can be also expressed in terms of the dimensionless model, as follows:

$$\eta_{\mathrm{i}} = \left(3\int_0^1 \frac{S_{\mathrm{m,s}}(R)}{1+S_{\mathrm{m,s}}(R)} R^2 \mathrm{d}R\right)\left(\frac{1+S_{\mathrm{m,s}}(1)}{S_{\mathrm{m,s}}(1)}\right). \tag{1.16}$$

For η_{i} values near one, the entire microbioreactor is reacting at the same rate as at the inner surface because the substrate concentration decrease in the microbioreactor is insignificant. For η_{i} values near zero, almost all the substrate reacts at the surface of the microbioreactor, while the reaction rate decreases in comparison to the rate at the inner surface at the same substrate concentration [44].

The external effectiveness factor η_{e} is defined as the ratio of the reaction rate that would occur if the substrate concentration over the whole microbioreactor equal to the concentration at the outer surface of the microbioreactor. It would be obtained if the concentration everywhere in the microbioreactor is equal to the concentration S_0 in the bulk [44, 113],

$$\eta_{\mathrm{e}} = \frac{v(s_{\mathrm{d,s}}(r_0))}{v(s_0)} = \frac{(1+S_0)\, S_{\mathrm{d,s}}(1)}{(1+S_{\mathrm{d,s}}(1))\, S_0}. \tag{1.17}$$

The external effectiveness factor is a measure of the influence of the external mass transfer resistance on the rate of the observed reaction. If it is significantly

less than unity, the mass transfer resistance restricts the supply of the substrate to the microbioreactor surface. Thus limits the catalytic activity of the enzyme, whereas the reaction is not limited by the external mass transfer if the factor equals unity [44].

The influence of partitioning can be expressed as follows:

$$\eta_{\mathrm{p}} = \frac{v(s_{\mathrm{m,s}}(r_0))}{v(s_{\mathrm{d,s}}(r_0))} = \frac{(1+S_{\mathrm{d,s}}(1))\,S_{\mathrm{m,s}}(1)}{(1+S_{\mathrm{m,s}}(1))\,S_{\mathrm{d,s}}(1)}. \tag{1.18}$$

The overall effectiveness factor η_{o} can be calculated from the internal and external effectiveness factors as well as from the effectiveness factor due to partitioning [113],

$$\begin{aligned} \eta_{\mathrm{o}} &= \eta_{\mathrm{i}} \times \eta_{\mathrm{e}} \times \eta_{\mathrm{p}} = \frac{3\int_0^{r_0} v(s_{\mathrm{m,s}}(r))r^2\mathrm{d}r}{r_0^3\, v(s_0)} \\ &= \left(3\int_0^1 \frac{S_{\mathrm{m,s}}(R)}{1+S_{\mathrm{m,s}}(R)}R^2\mathrm{d}R\right)\left(\frac{1+S_0}{S_0}\right). \end{aligned} \tag{1.19}$$

Summarising definitions (1.15)–(1.19), the overall (total) effectiveness factor η_{o} can be defined also as the ratio of the average reaction rate actually observed in the microbioreactor to the rate evaluated at the bulk concentrations of the substrate [102, 113].

The process duration is another important characteristic of biotechnological processes [55]. A minimization of time-cost is often sought by the designers of biotechnological processes [108]. The holding time t_{h} and the corresponding dimensionless time T_{h} required for complete enzymatic conversion of the whole amount of the substrate initially added to bioreactor system (spherical diffusion shell) were accepted as the measures of time-cost of the bioreactor operation,

$$t_{\mathrm{h}} = \left\{ t : \int_0^t \int_0^{r_0} v(s_{\mathrm{m}}(r,t))\, r^2\,\mathrm{d}r\,\mathrm{d}t = \frac{(r_1^3 - r_0^3)s_0}{3} \right\}, \quad T_{\mathrm{h}} = \frac{\mathrm{D_m}t_{\mathrm{h}}}{r_0^2}. \tag{1.20}$$

Since radius r_0 fixed and the commulatively used concentration is monotonicaly increasing, the time t_{h} is set to.

1.3. Perturbation methods for approximate solutions

Over the last two decades, some nonlinear reaction-diffusion equations have been analytically solved by applying the homotopy perturbation method (HPM) [56]. This method, which is a combination of homotopy in topology and classic perturbation techniques, provides a convenient way to obtain approximate solutions for a wide variety of problems arising in different fields, including

reaction-diffusion equation involving the Michaelis-Menten kinetics [67, 100]. However, often accurate analytical solutions obtained by HPM are not expressed in the closed form and the accuracy of the constructed closed-forms of analytical expressions of the substrate concentration is not satisfactory: approximation is not sufficient enought or not valid [92]. Nevertheless, a variety of applications show the usefulness of HPM in solving reaction-diffusion equations [7].

Let us consider a non-linear differential equation in a domain Ω with a solution function $S = S(r)$:

$$A(S) = f(\mathbf{b}), \;\; \mathbf{b} \in \Omega, \tag{1.21}$$

with the boundary conditions:

$$B(S, S_{\mathbf{b}}) = 0, \;\; \mathbf{b} \in \partial\Omega, \tag{1.22}$$

where A is a differential operator, $f(\mathbf{b})$ is a known analytical function, B is a boundary operator, $\partial\Omega$ is a boundary of an area Ω.
By splitting the expression $A(S)$ to the linear $L(S)$ and non-linear $N(S)$ parts, we get:

$$A(S) = L(S) + N(S). \tag{1.23}$$

Then the equation (1.21) can be rewritten as:

$$L(S) + N(S) - f(\mathbf{b}) = 0. \tag{1.24}$$

Using the homotopy technique [57], we construct a homotopy with, parameter ε that satisfies the following equation:

$$\begin{aligned} H(u,\varepsilon) &= (1-\varepsilon)\cdot \underbrace{[L(u) - L(u_{\text{in}})]}_{\text{linear part}} + \\ &+ \varepsilon \cdot \underbrace{[A(u) - f(\mathbf{b})]}_{\text{solution}} = 0. \end{aligned} \tag{1.25}$$

By inserting (1.23) into (1.25), we can rewrite the homotopy:

$$\begin{aligned} H(u,\varepsilon) &= \underbrace{[L(u) - L(u_{\text{in}})]}_{\text{linear part}} + \varepsilon \cdot L(s_{\text{in}}) + \\ &+ \varepsilon \cdot \underbrace{[N(u) - f(\mathbf{b})]}_{\text{non-linear}} = 0, \end{aligned}$$

where ε is a also known as the deformation parameter, $\varepsilon \in [0,1]$, and u_{in} is a a known function which satisfies the boundary conditions (1.22). From Eq. (1.26) we have the limiting cases of the homotopy H when the parameter ε equals zero or one:

$$\begin{aligned} H(u,0) &= \underbrace{L(u) - L(s_{\text{in}})}_{f_1} = 0 \quad \Rightarrow L(u) = L(s_{\text{in}}), \\ H(u,1) &= \underbrace{A(u) - f(\mathbf{b})}_{f_2} = 0 \quad \Rightarrow A(u) = f(\mathbf{b}). \end{aligned}$$

Therefore, changing the parameter ε should allow the continuous transition from the initial solution to a solution of equation (1.21). The variation of the parameter ε from 0 to 1 results in the corresponding transformation of S from $u_{\text{in}}(r)$ to $u(r)$. If the embedding parameter ε ($0 < \varepsilon < 1$) is considered as a small parameter, the solution can be written as a power series in ε by applying the classical perturbation technique:

$$u = u(r) = \sum_{i=0}^{\infty} u_i(r)\varepsilon^i. \tag{1.26}$$

Hence, when ε is set to unity ($\varepsilon = 1$), it produces an approximate solution of Eq. (1.21)

$$S(r) = S = \lim_{\varepsilon \to 1} \sum_{i=0}^{\infty} u_i(r)\varepsilon^i = \sum_{i=0}^{\infty} u_i(r). \tag{1.27}$$

Typically, the series (1.26) converges and $\varepsilon = 1$ is inside the radius of convergence. For most cases, the general form of $u_i(r)$ is hard to find, so the solution $S(r) = \sum_{i=0}^{k} u_i(r)$ is called the k-th order HPM approximation of equation (1.21) [56].

1.4. Numerical modeling

In bioreactor models the chemical kinetics is often expressed by the non-linear Michaelis-Menten kinetics [12, 30]. The analytical solution of the concentration distribution in space and time is usually a hard task [67, 100]. The main issue is the non-linear reaction part. Only in some specific (usually stationary or limiting) cases analytical solutions can be found [13]. For example, under small concentration the limiting case occurs: $K_{\text{M}} \gg S(r,t), \forall r \in \Omega, t > 0$:

$$v(s) = \frac{V_{\max} S}{S + K_{\text{M}}} \approx \frac{V_{\max} S}{K_{\text{M}}}. \tag{1.28}$$

In such a case the reaction term (RMM-D) reduces to (Rt-D). Then the PDE system can be solved analytically and an analytical solution can be found (see Section 3.1).

To solve the problem of bioreactor modeling in general, numerical methods might be considered [5, 12]. One of the most extensive ways to solve problems defined by partial differential equations is to use the finite difference method [71].

Solving the bioreactor model using the finite difference method, firstly a differential equation should be transformed into simple linear equations defined by the finite difference method [40]. In practice the finite difference method can be implemented in multiple ways. The author chose to use the programming language C++ [91]. The explicit schemes as well as computation pipeline were implemented from scratch.

Let us consider a one-dimensional, mathematical model of a single-layer bioreactor. The variables r and t are defined in the area as follows:

$$\Omega_{\mathrm{h}} = \{0 \leqslant r \leqslant r_0, 0 \leqslant t \leqslant t_0\}. \tag{1.29}$$

The range of continuous variables Ω (theoretical) is replaced by a discrete set of points Ω_{h}. One of the simplest and most commonly used applications is the usage of two discrete domains [13, 71]:

$$r = ih, \quad i = 0,1,...,N, N = \frac{r_0}{h}; \tag{1.30}$$

$$t = j\tau, \quad j = 0,1,...,M, M = \frac{t_0}{\tau}. \tag{1.31}$$

These points divide the area Ω to uniform rectangles. The set of those points is also called the grid and intersections are called nodes [12, 40]. The constants h and τ represent the steps in space and in time, respectively. The grid and nodes give the discrete set Ω_{h}.

The nodes (i, j), when $i = 1,2,..,N-1$ and $j = 1,2,..,M$, are called the inner nodes. For each inner node the finite difference scheme equations are created. The boundary conditions are formulated at nodes at $i = 0$ and $i = N$ time boundaries are $j = 0$ and $j = M$.

The second derivative in space is replaced as follows:

$$\frac{\partial^2 s}{\partial r^2} \approx \frac{s_{i+1,j} - 2s_{i,j} + s_{i-1,j}}{h^2}. \tag{1.32}$$

The first derivative can be expressed as a left or right derivatives:

$$\frac{\partial s}{\partial r} \approx \frac{s_{i,j} - s_{i-1,j}}{h}, \tag{1.33}$$

$$\frac{\partial s}{\partial r} \approx \frac{s_{i+1,j} - s_{i,j}}{h}. \tag{1.34}$$

The explicit scheme allows to formulate the difference equation in such a order that each inner point depends only on the previous time values. Such a type of equations allows to apply the boundary conditions easily. After each iteration at fixed time t, the next step $t + \tau$ can be calculated.

The explicit scheme calculation algorithm is easily implemented in programming languages. However, in order to use the explicit scheme, the stability condition must be satisfied [13]:

$$\tau \leqslant \frac{h^2}{2D}. \tag{1.35}$$

This condition must be satisfied for every equation in the system of equations. In order to ensure the stability of the scheme, it may be necessary to take a very small step in time. This obviously slows down the computations.

Recently the team of R. Čiegis have developed efficient [34, 35] numerical schemes for tasks similar to that formulated in this thesis. However, those schemes were not used in this thesis since the main results had been already received at the time those papers were published.

1.5. Other modeling approaches

Differential equations, especially partial differential equations (PDEs), play a crucial role in many disciplines including the modeling of chemical kinetic processes. Traditionally, PDEs are solved mathematically or physically based on some basic principles, e.g., molecular dynamic models. However, many complex systems in modern applications (such as neuroscience, finance, biological science) including the Michaelis-Menten reaction equation still can not be solved, and the governing equations of these systems are commonly obtained by empirical formulas [27, 46]. The successful applications of using deep neural networks to modeling ODEs was presented [33]. It has even been suggested to create PDE based neural networks [97], but no significant practical applications have been delivered yet.

The stochastic approaches [120] to modeling chemical kinetics provide different challenges. While stochastic modeling can be used to the same task, the evaluation of system parameters without an experimental data is an issue [86].

1.6. Related Work

The mathematical models of spherical one and two layer microreactors are known and intensively analysed [44]. However, the substrate conversion is often studied only in the case were the enzyme kinetics approaches either first or zero order kinetics [44, 68, 96]. In bioreactors linear reaction appears on rare occasions. In practice the non-linear Michaelis-Menten reaction term leads to non-linear behaviour on internal and external diffusion impact. When modeling microbioreactors where the intraparticle and external diffusion resistance is considered, multi-compartment models are required to achieve a sufficient accuracy of the model [11, 102, 110]. Nevertheless, mono compartment models, in which the internal mass transport by diffusion and substrate conversion is considered, are still used in different applications due to the model simplicity [8]. The external diffusion is usually modeled by the mass flux boundary condition

involving the mass transfer rate of the boundary layer in the presence of diffusive and convective flows [1, 31, 83]. Adequate mass transfer is required in order to successfully model bioprocess experiments [101]. However, the mass transfer coefficient can only be estimated on the basis of rather sophisticated measurements [96].

One of the objectives of this thesis was to investigate in detail the influence of the physical and kinetic parameters on the effectiveness of the bioreactor system based on a porous spherical mircrobioreactors acting in the continuous flow mode.

For BSTR, a pseudo-homogeneous model to calculate the transient effectiveness factor in spherical porous catalyst particles in gradient less reactors, where the first-order reaction and intraparticle mass transfer are considered, has been recently developed [19, 21]. However, in practical systems, the microreactor response may be greatly affected by the mass transfer outside the catalyst region even when the medium is highly stirred [11, 25, 51, 52].

One of the objectives of this thesis was to develop a computational model for simulation and investigate the dynamics of BSTR based on an array of spherical microbioreactors until the steady-state is reached. Another objective was to investigate the influence of the physical and kinetic parameters on the transient effectiveness of bioreactor system.

A system of co-immobilized enzymes provides a practical method to increase their efficiency [77, 88]. Recently, artificial microcatalysts containing two conjugated enzymes have been investigated [93, 94]. The non-specific glucose dehydrogenase (GDH) and oxygen reducing laccase (LAC) have been wired via carbon nanotubes or gold nanoparticles. The systems demonstrated effective carbohydates conversion by oxygen in the absence of a mediator.

One of the objectives of this thesis was to propose a MR mathematical model, develop a computational model for a batch stirred tank reactor (BSTR) based on an array of spherical porous microbioreactors loaded with these enzymes, and investigate the influence of the physical and kinetic parameters on the transient effectiveness of the bioreactor.

Concluding remarks

Many different types of bioreactors have been created over the years. Bioreactors are commonly compared with each other by the efficiency and ability to produce product fast. The most important processes that occur in the bioreactors are chemical reactions and diffusion. Chemical kinetics in bioreactor models can be defined using the Michaelis-Menten kinetic equation and its variations, and the diffusion is defined using the laws of Fick. To increase accuracy the microbioreactor, the additional diffusion (Nernst) layer are to be considered. Because of the nonlinearity of equations, analytical solutions are known only case-by-case, so the problem is usually solved by numerical or symbolic methods.

The main conclusions from this Chapter:

1. The effectiveness factor should be analysed in order to investigate the influence of the physical and kinetic parameters of a bioreactor (CSTR) system,

2. The transient effectiveness of a bioreactor system should be analysed to investigate the influence of the physical and kinetic parameters of bioreactor (BSTR) system,

3. The recently proposed microreactor based on carbon nanotubes [93, 94] should be formulated and analysed in depth, since the current research is not sufficient.

2. Mathematical Models of Bioreactors Based on Microbioreactor Particles

In this Chapter three mathematical models of microbioreactors are considered. A generalization of existing mathematical models as well as a developed new mathematical model for microbioreactor based on carbon nanotubes are presented. The models are based on results of this Chapter published in articles [A1–A3] and conference proceedings [A7-A9].

2.1. Continuous-flow stirred tank reactor

Firstly, we introduce the domain homogenization, then all three models are presented.

2.1.1. Domain homogenization

The bioreactor system to be analized is rather complex. Simulating each particle individually futher increases the complexity of the system and requires a large number of computational resources. We consider the method of volume cover by polyhedrs. In particular, the hexahedral, hexagonal discretization techniques [61] are successfully used in modeling similar systems [10, 53].

A hexagonal distribution of unit cells containing microbioreactor particles is analysed. To simplify the complexity of a bioreactor, the entire volume was divided into hexahedral subvolumes, with a microbioreactor inside (see Figure 2.1). When the volume is significantly large in comparison with the microbioreactor particle, the hexahedral volume is approximately equal to the volume of the sphere. Such an assumption made possible to use the Laplace operator in shperical coordinates and to obtain analytical expressions.

2.1.2. Governing equations

The dynamics of the MR system includes changes over the time of the substrate consumption as well as the product production. Since the reaction product is produced at the same rate as the substrate is consumed, the dynamics of the MR operation can be qualitatively expressed by the dynamics of the substrate concentration alone [15, 44]. Assuming the symmetrical geometry

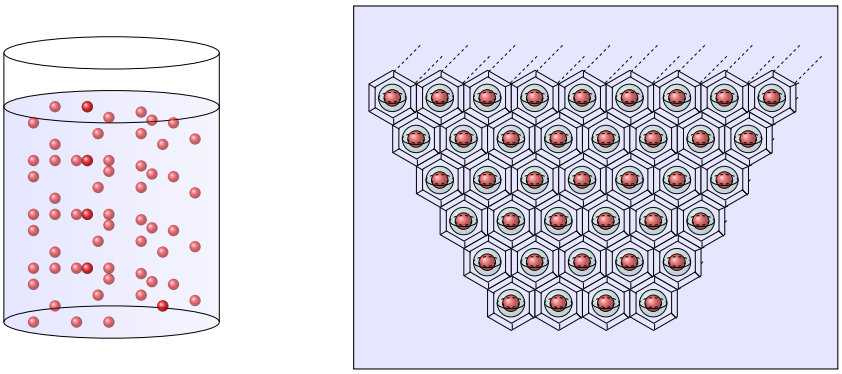

Figure 2.1: Hexagon type volume domain homogenization

of the spherical MR and homogenized distribution of the immobilized enzyme inside the MR, the mathematical model can be described in one-dimensional domain using the radial distance ($0 < r < r_0, t > 0$),

$$\frac{\partial s_{\mathrm{m}}}{\partial t} = \mathrm{D_m}\Delta s_{\mathrm{m}} - v(s_{\mathrm{m}}), \tag{2.1}$$

where $s_{\mathrm{m}} = s_{\mathrm{m}}(r,t)$ is the concentration of the substrate in the MR, Δ is the Laplace operator, r_0 is the radius of the MR and $\mathrm{D_m}$ is the effective diffusion coefficient [14, 102].

Assuming that the solution is permanently stirred and applying the Nernst approach, a thin spherical shell (the Nernst diffusion layer) adjacent to the MR surface remains stagnant in time ($r_0 < r < r_1, t > 0$),

$$\frac{\partial s_{\mathrm{d}}}{\partial t} = \mathrm{D_d}\Delta s_{\mathrm{d}}, \tag{2.2}$$

where $s_{\mathrm{d}} = s_{\mathrm{d}}(r,t)$ is the concentration of the substrate in the diffusion shell, $\mathrm{D_d}$ is the corresponding diffusion coefficient, and $h = r_1 - r_0$ is the thickness of the spherical diffusion shell [14, 29, 112].

2.1.3. Initial and boundary conditions

It was assumed that, initially, i.e., when $t = 0$, the MR is uniformly loaded with the enzyme and is free of the substrate,

$$s_{\mathrm{m}}(r,0) = 0, \quad 0 \le r \le r_0. \tag{2.3}$$

The reaction starts when the MR is poured into a container with some substrate distributed uniformly outside the MR,

$$s_{\mathrm{d}}(r,0) = s_0, \quad r_0 \le r \le r_1, \tag{2.4}$$

where s_0 is the substrate concentration in the bulk. More detailed analysis on impact of initial conditions are in [A8].

Due to the symmetry, the zero-flux boundary condition is defined for the centre of the spherical microbioreactor ($t > 0$, the initial condition at $t = 0$ was defined before),

$$\mathrm{D_m} \frac{\partial s_\mathrm{m}}{\partial r}\bigg|_{r=0} = 0. \tag{2.5}$$

Away from the diffusion shell ($r > r_1$), the solution is uniform throughout the outside of the shell and remains of constant concentration ($t > 0$) [39, 42, 98],

$$s_\mathrm{d}(r_1, t) = s_0. \tag{2.6}$$

The formal partition coefficient ϕ is used in the matching conditions to describe the specificity in the concentration distribution of the substrate between two neighboring regions ($t > 0$),

$$\mathrm{D_m} \frac{\partial s_\mathrm{m}}{\partial r}\bigg|_{r=r_0} = \mathrm{D_d} \frac{\partial s_\mathrm{d}}{\partial r}\bigg|_{r=r_0}, \tag{2.7}$$

$$s_\mathrm{m}(r_0, t) = \phi s_\mathrm{d}(r_0, t). \tag{2.8}$$

The partition coefficient ϕ is less than unity as the averaged concentration of the substrate in the MR becomes less than the concentration in the bulk solution due to the porous materials [38, 110]. The more detailed impact of partition coefficient is [A9].

We assume that the system approaches a steady state as $t \to \infty$,

$$s_{\mathrm{m,s}}(r) = \lim_{t\to\infty} s_\mathrm{m}(r, t), \quad s_{\mathrm{d,s}}(r) = \lim_{t\to\infty} s_\mathrm{d}(r, t). \tag{2.9}$$

2.1.4. Dimensionless model

In order to reduce the number of the model parameters, a dimensionless model was derived by introducing the following dimensionless variables [76, 110]:

$$\begin{aligned} &R = \frac{r}{r_0}, \quad R_1 = \frac{r_1}{r_0}, \quad H = \frac{r_1 - r_0}{r_0}, \quad T = \frac{\mathrm{D_m} t}{r_0^2}, \quad \theta = \frac{\mathrm{D_d}}{\mathrm{D_m}}, \\ &S_\mathrm{m} = \frac{s_\mathrm{m}}{K_\mathrm{M}}, \quad S_\mathrm{d} = \frac{s_\mathrm{d}}{K_\mathrm{M}}, \quad S_0 = \frac{s_0}{K_\mathrm{M}}, \quad S_{\mathrm{m,s}} = \frac{s_{\mathrm{m,s}}}{K_\mathrm{M}}, \quad S_{\mathrm{d,s}} = \frac{s_{\mathrm{d,s}}}{K_\mathrm{M}}. \end{aligned} \tag{2.10}$$

The governing equations (2.1) and (2.2) in the dimensionless form are then expressed as follows ($T > 0$):

$$\begin{aligned} \frac{\partial S_{\mathrm{m}}}{\partial T} &= \Delta S_{\mathrm{m}} - \sigma^2 \frac{S_{\mathrm{m}}}{1+S_{\mathrm{m}}}, \quad R \in (0,1), \\ \frac{\partial S_{\mathrm{d}}}{\partial T} &= \theta \Delta S_{\mathrm{d}}, \quad R \in (1, R_1). \end{aligned} \tag{2.11}$$

The initial conditions (2.3) and (2.4) are transformed to the following conditions:

$$\begin{aligned} S_{\mathrm{m}}(R,0) &= 0, \quad R \in [0,1], \\ S_{\mathrm{d}}(R,0) &= S_0, \quad R \in [1, R_1]. \end{aligned} \tag{2.12}$$

The boundary conditions (2.5)–(2.8) are rewritten as follows ($T > 0$):

$$\begin{aligned} \left.\frac{\partial S_{\mathrm{m}}}{\partial R}\right|_{R=0} &= 0, \quad S_{\mathrm{d}}(R_1, T) = S_0, \\ \left.\frac{\partial S_{\mathrm{m}}}{\partial R}\right|_{R=1} &= \theta \left.\frac{\partial S_{\mathrm{d}}}{\partial R}\right|_{R=1}, \quad S_{\mathrm{m}}(1,T) = \phi S_{\mathrm{d}}(1,T). \end{aligned} \tag{2.13}$$

2.2. Batch stirred tank reactor

2.2.1. Governing equations

Assuming the symmetrical geometry of the MR and homogenized distribution of the enzyme inside the porous MR, a mathematical model can be formalised in a one-dimensional domain using the radial coordinate alone [A3]. Since the reaction product is usually produced at the same rate as the substrate is consumed, the dynamics of the system operation can be qualitatively expressed by the dynamics of the substrate concentration only [15, 44]. Coupling the enzymatic reaction in a microbioreactor with the one-dimensional-in-space diffusion, described by the Fick's second law, leads to the following reaction-diffusion equation:

$$\frac{\partial s_{\mathrm{m}}}{\partial t} = \mathrm{D}_{\mathrm{m}} \Delta s_{\mathrm{m}} - V(s_{\mathrm{m}}), \quad 0 < r < r_0,\ t > 0, \tag{2.14}$$

where $s_{\mathrm{m}}(r,t)$ is the concentration of the substrate in the MR, r and t stand for the space and time, respectively, $\Delta = (1/r^2)\partial/\partial r(r^2 \partial/\partial r)$ is the Laplace operator, r_0 is the radius of the MR, and D_{m} is the effective diffusion coefficient [14].

No reaction takes place outside the MR, i.e., when $r > r_0$. Applying the Nernst approach [14, 112], a thin diffusion shell adjacent to the MR surface remains at a constant thickness $h_1 = r_1 - r_0$,

$$\frac{\partial s_\mathrm{d}}{\partial t} = \mathrm{D_d}\Delta s_\mathrm{d}, \quad r_0 < r < r_1,\, t > 0, \tag{2.15}$$

where $s_\mathrm{d}(r,t)$ is the concentration of the substrate in the diffusion shell, and $\mathrm{D_d}$ is the corresponding diffusion coefficient.

The diffusion shells of different particles do not influence each other [65]. The thickness h_1 of the diffusion shell depends upon the nature and intensity of the stirring of the buffer solution. The less intense stirring corresponds to the thicker diffusion shell (greater h_1) [14, 112]. Environmental diffusion resistance also increases with the molecular size of the substrate [65].

Due to the intensive agitation of the solution, the substrate is assumed to be uniformly distributed throughout the outside of the diffusion shell and its concentration depends only on time [42, 98]. The rate at which the substrate leaves the convective enclosure of volume $4\pi(r_2^3 - r_1^3)/3$ is always equal to that at which it enters the diffusion shell over the surface of the area $4\pi r_1^2$,

$$\frac{\mathrm{d}s_\mathrm{b}}{\mathrm{d}t} = -\frac{1}{q}\mathrm{D_d}\frac{\partial s_\mathrm{d}}{\partial r}\Big|_{r=r_1}, \quad t > 0, \tag{2.16}$$

where $s_\mathrm{b}(t)$ is the substrate concentrations in the bulk (convective shell, $r_1 \leq r \leq r_2$), q is the ratio of the volume of the convective enclosure ($r_1 \leq r \leq r_2$) to the area of the outer surface of the diffusion shell ($r = r_1$),

$$q = \frac{4\pi(r_2^3 - r_1^3)/3}{4\pi r_1^2} = \frac{r_2^3 - r_1^3}{3r_1^2}. \tag{2.17}$$

The value $1/q$ can be also considered as the adsorption capacity of the MR [18, 21]. Finally, $h_2 = r_2 - r_1$ is the thickness of the convective shell.

2.2.2. Initial and boundary conditions

The process starts ($t = 0$) when the substrate is injected into the bioreactor,

$$s_\mathrm{m}(r,0) = 0, \quad 0 \leq r \leq r_0, \tag{2.18}$$

$$s_\mathrm{d}(r,0) = 0, \quad r_0 \leq r \leq r_1, \tag{2.19}$$

$$s_\mathrm{b}(0) = s_0, \tag{2.20}$$

where s_0 is the initial concentration of the substrate in the bulk solution.

Due to symmetry, the zero-flux boundary condition is defined on the centre of the spherical microbioreactor ($t > 0$),

$$\mathrm{D_m}\frac{\partial s_\mathrm{m}}{\partial r}\Big|_{r=0} = 0. \tag{2.21}$$

The flux of the substrate through the stagnant external diffusion shell is assumed to be equal to the flux entering the MR surface. The formal partition coefficient ϕ is used in the matching conditions to describe the specificity in the concentration distribution of the substrate between two neighboring regions ($t > 0$) [51, 113],

$$\mathrm{D_m}\frac{\partial s_\mathrm{m}}{\partial r}\Big|_{r=r_0} = \mathrm{D_d}\frac{\partial s_\mathrm{d}}{\partial r}\Big|_{r=r_0}, \quad s_\mathrm{m}(r_0,t) = \phi s_\mathrm{d}(r_0,t). \tag{2.22}$$

The dimensionless partition coefficient ϕ is less than unity as the averaged concentration of the substrate in the MR becomes lower than the concentration in the bulk solution due to the insoluble MR carrier. The coefficient ϕ can also be interpreted as the porosity of the MR and defined as the ratio of the porous volume to the total volume of the microbioreactor [38, 110].

On the boundary between the diffusion and convective shells ($r = r_1$), the continuity of the substrate concentration is required ($t > 0$),

$$s_\mathrm{d}(r_1,t) = s_\mathrm{b}(t). \tag{2.23}$$

The boundary condition (2.23) and the governing equation (2.16) are only specific to the batch mode of the bioreactor operation (BSTR) [A3]. In the case of open system (CSTR), away from the diffusion shell ($r > r_1$) the concentration of the substrate remains constant at its initial value [41, 44, 112]. This difference appears at the steady state: in the case of BSTR, the substrate concentration in the bulk continuously decreases over the time and asymptotically approaches zero, while the continuous process can be operated for a long period under the steady state condition producing the target product.

2.2.3. Dimensionless model

In order to identify the main governing parameters of the mathematical model, a dimensionless model has been derived [A3]. The following dimensionless distance R, time T and concentration variables have been introduced in the system (2.14)–(2.23):

$$\begin{gathered} R = \frac{r}{r_0}, \quad R_1 = \frac{r_1}{r_0}, \quad \theta = \frac{q}{r_0}, \quad T = \frac{\mathrm{D_m}t}{r_0^2}, \\ S_\mathrm{m} = \frac{s_\mathrm{m}}{K_\mathrm{M}}, \quad S_\mathrm{d} = \frac{s_\mathrm{d}}{K_\mathrm{M}}, \quad S_\mathrm{b} = \frac{s_\mathrm{b}}{K_\mathrm{M}}, \quad S_0 = \frac{s_0}{K_\mathrm{M}}, \quad \alpha = \frac{\mathrm{D_d}}{\mathrm{D_m}}. \end{gathered} \tag{2.24}$$

The governing equations (2.14)–(2.16) reduce to the following dimensionless form ($T > 0$):

$$\begin{aligned}
&\frac{\partial S_{\mathrm{m}}}{\partial T} = \Delta S_{\mathrm{m}} - \sigma^2 \frac{S_{\mathrm{m}}}{1+S_{\mathrm{m}}}, \quad R \in (0,1),\\
&\frac{\partial S_{\mathrm{d}}}{\partial T} = \alpha \Delta S_{\mathrm{d}}, \quad R \in (1,R_1),\\
&\frac{\mathrm{d}S_{\mathrm{b}}}{\mathrm{d}T} = -\frac{\alpha}{\theta}\frac{\partial S_{\mathrm{d}}}{\partial R}\Big|_{R=R_1}.
\end{aligned} \tag{2.25}$$

If $\sigma \ll 1$, then enzyme kinetics controls the MR action, and the MR action is under diffusion control when $\sigma \gg 1$. In general even more layers can be considered, the results are provided in [A7].

The initial conditions (2.18)–(2.20) are transformed into the following conditions:

$$\begin{aligned}
&S_{\mathrm{m}}(R,0) = 0, \quad R \in [0,1],\\
&S_{\mathrm{d}}(R,0) = 0, \quad R \in [1,R_1),\\
&S_{\mathrm{b}}(0) = S_0.
\end{aligned} \tag{2.26}$$

The boundary conditions (2.21)–(2.23) are rewritten as follows ($\tau > 0$):

$$\begin{aligned}
&\frac{\partial S_{\mathrm{m}}}{\partial R}\Big|_{R=0} = 0, \quad \frac{\partial S_{\mathrm{m}}}{\partial R}\Big|_{R=1} = \alpha \frac{\partial S_{\mathrm{d}}}{\partial R}\Big|_{R=1},\\
&S_{\mathrm{m}}(1,T) = \phi S_{\mathrm{d}}(1,T), \quad S_{\mathrm{d}}(R_1,T) = S_{\mathrm{b}}(T).
\end{aligned} \tag{2.27}$$

The Biot number is another widely used dimensionless parameter that compares the external and internal mass transfer resistances [1],

$$\beta = \frac{\mathrm{D_d} r_1}{\mathrm{D_m}(r_1 - r_0)} = \frac{\alpha R_1}{R_1 - R_0}. \tag{2.28}$$

A low Biot number means strong external mass transfer resistance, hence both the internal and external mass transfer resistances are important for determination of the substrate conversion. As the Biot number increases, the importance of the external mass transfer resistance decreases [1].

The diffusion module σ and the Biot number β as the most important parameters for the bioreactor effectiveness are widely used in analysis and design of different bioreactors [25, 65, 95].

2.3. Microbioreactor with carbon nanotubes

In this section a novel mathematical model is formulated for a microbioreactor based on carbon nanotubes.

2.3.1. Model domain

We consider an array of identical spherical microbioreactors placed in an aqueous solution containing lactose and oxygen. The microbioreactors are assumed to be uniformly distributed in a container filled with the described solution. Due to the idealised uniform distribution of the microbioreactors, the container can be divided into space-filling convex polyhedrons of the same volume containing only one MR. For simplicity, it is reasonable to consider a sphere, the volume of which equals to that of the polyhedron and to regard one of the spheres as a unit cell to be considered [A1,A3]. The spherical unit cell includes the enzyme-loaded MR placed at the center.

If V_S is the volume of an entire container containing N identical spherical microbioreactors of radius R_0 uniformly distributed in the container, then the volume of the unit cell equals V_S/N and the radius R of the unit cell is equal to $\sqrt[3]{3V/(4N\pi)}$. In our experimental system, $V_S = 2.4\,\mathrm{cm}^3$, $R_0 = 0.25\,\mathrm{mm}$, $N = 981$, and $R \approx 0.84\,\mathrm{mm}$.

The porous microbioreactors were prepared from the silica carrier and were loaded with the bienzyme. Having the total density ρ_r of microrectors and the silica carier density ρ_c, the porosity [1] can be calculated as follows [9, 115]: $\phi = 1 - \rho_r/\rho_c$. In our case, $\rho_r = 0.96\,\mathrm{g/cm}^3$, $\rho_c = 2.2\,\mathrm{g/cm}^3$, and $\phi \approx 0.56$.

Principal structure of the cross section of the modeled unit cell is presented in Fig. 2.2. Assuming the symmetrical geometry of the MR and homogeneous distribution of the immobilized enzyme inside the MR, it's mathematical model can be formalised in one-dimensional domain using the radial distance.

2.3.2. Governing equations

In the bioelectrochemical process (1.1a)–(1.1b) presented in Section 1.1.3, electrons are released, while in the following process (1.1c)–(1.1d) those electrons are immediately accepted. Moreover, the reaction (1.1b) is only the source of electrons being accepted in the reaction (1.1c). On the other hand, the acceptance of electrons in the reaction (1.1c) is the prerequisite for the process (1.1a)–(1.1b).

[1] Porosity or void fraction is a measure of the empty spaces in a material, and is a fraction of the volume of emptyness over the total volume.

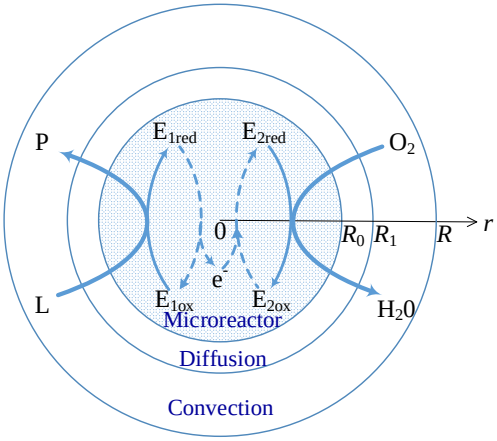

Figure 2.2: Schematic view of the cross section of a modeled unit cell

Assuming the quasi-steady-state approximation [14, 112], when the concentrations of both forms of both enzymes do not change over the time and all the electrons released in the ET reaction (1.1b) are immediately accepted in the reaction (1.1c), leads to reaction expression relationship:

$$V_1 = 2V_2, \tag{2.29}$$

where V_1 and V_2 are the quasi-steady-state reaction rates of the corresponding mono-enzyme catalyzed processes (1.1a)–(1.1b) and (1.1c)–(1.1d), respectively. A number 2 in (2.29) is associated with the electrons stoichiometry of the reactions.

The quasi-steady-state reaction rate V of a conjugated two-enzyme catalyzed process (1.1a)–(1.1d) and the rates V_1 and V_2 of a partial one enzyme catalyzed processes hold the following relationship [14, 112]:

$$\frac{1}{V} = \frac{1}{V_1} + \frac{1}{2V_2}. \tag{2.30}$$

Assuming that both enzyme catalyzed processes (1.1a)–(1.1b) and (1.1c)–(1.1d) obey the Michaelis–Menten kinetics leads to the following:

$$\begin{aligned} V_1 &= V_1(L_\mathrm{m}) = \frac{V_\mathrm{L} L_\mathrm{m}}{K_L + L_\mathrm{m}}, \\ V_2 &= V_2(O_\mathrm{m}) = \frac{V_\mathrm{O} O_\mathrm{m}}{K_O + O_\mathrm{m}}, \quad 0 < r < R_0,\ t > 0, \end{aligned} \tag{2.31}$$

where r and t stand for space and time, $L_\mathrm{m}(r,t)$ and $O_\mathrm{m}(r,t)$ are the volumetric concentrations of lactose and oxygen, in the MR, $V_\mathrm{L} = 2k_2E_{10}$ and $V_\mathrm{O} = 4k_3E_{20}$ are the maximal enzymatic rates for LAC and GDH, $K_L = 2k_2/k_1$ and $K_O =$

$4k_3/k_4$ are the Michaelis constants, E_{10} and E_{20} are the total concentrations of the enzymes, and R_0 is the radius of the enzyme-loaded MR.

The quasi-steady-state volumetric reaction rate V can be expressed as a function of the lactose and oxygen by putting (2.31) into (2.30),

$$\begin{aligned} V &= V(L_{\mathrm{m}}, O_{\mathrm{m}}) = \frac{2V_1V_2}{V_1+2V_2} \\ &= \frac{V_{\max,1}V_{\max,2}L_{\mathrm{m}}O_{2,m}}{V_{\max,1}\mathrm{K}_{\mathrm{M},2}L_{\mathrm{m}} + (V_{\max,1}+2V_{\max,2})L_{\mathrm{m}}O_{2,m} + V_{\max,2}\mathrm{K}_{\mathrm{M},1}O_{2,m}}. \end{aligned} \tag{2.32}$$

Taking into account (2.33) and the coupling reactions (1.1) with the one-dimensional-in-space diffusion described by the Fick's second law leads us to the following reaction-diffusion equations ($0 < r < R_0$, $t > 0$) [8,A1]:

$$\begin{aligned} \frac{\partial L_{\mathrm{m}}}{\partial t} &= \mathrm{D}_{L,\mathrm{m}}\Delta L_{\mathrm{m}} - V, \\ \frac{\partial P_{\mathrm{m}}}{\partial t} &= \mathrm{D}_{P,\mathrm{m}}\Delta P_{\mathrm{m}} + V, \\ \frac{\partial O_{\mathrm{m}}}{\partial t} &= \mathrm{D}_{O,\mathrm{m}}\Delta O_{\mathrm{m}} - \frac{V}{2}, \end{aligned} \tag{2.33}$$

where $P_{\mathrm{m}}(r,t)$ is the concentration of the reaction product in the MR, $\Delta = (1/r^2)\partial/\partial r(r^2\partial/\partial r)$ is the Laplace operator in the spherical coordinate r, $\mathrm{D}_{L,\mathrm{m}}$, $\mathrm{D}_{P,\mathrm{m}}$ and $\mathrm{D}_{O,\mathrm{m}}$ are the effective diffusion coefficients [24, 104].

No enzymatic as well as ET reaction takes place outside the MR ($R_0 < r < R$). Assuming that the solution is permanently stirred and applying the Nernst approach, a thin spherical shell (the Nernst diffusion layer) adjacent to the MR surface remains stagnant in time [113]. So, only the mass transport by the diffusion takes place in the shell surrounding the MR ($R_0 < r < R_1$, $t > 0$),

$$\frac{\partial C_{\mathrm{d}}}{\partial t} = \mathrm{D}_{C,\mathrm{d}}\Delta C_{\mathrm{d}}, \quad C = L, P, O, \tag{2.34}$$

where $L_{\mathrm{d}}(r,t)$, $P_{\mathrm{d}}(r,t)$ and $O_{\mathrm{d}}(r,t)$ are the concentrations of the lactose, reaction product and oxygen, in the diffusion shell, $\mathrm{D}_{L,\mathrm{d}}$, $\mathrm{D}_{P,\mathrm{d}}$ and $\mathrm{D}_{O,\mathrm{d}}$ are the corresponding diffusion coefficients, and $R_1 - R_0$ is the thickness of the spherical shell corresponding to the Nernst diffusion layer.

Away from the diffusion shell the solution is in motion, and the concentrations of all the soluble species are uniform throughout the outside of the shell and depend only on the time [19, 99]. The rate at which solute leaves (enters) the enclosure of volume $4\pi(R^3 - R_1^3)/3$ is always equal to that at which it enters (leaves) the diffusion shell over the surface of the area $4\pi R_1^2$, i.e.,

$$\frac{\mathrm{d}C_{\mathrm{b}}}{\mathrm{d}t} = -\frac{1}{q}\mathrm{D}_{C,\mathrm{d}}\frac{\partial C_{\mathrm{d}}}{\partial r}\Big|_{r=R_1}, \quad C = L, P, O, \tag{2.35}$$

where $L_{\mathrm{b}}(t)$, $P_{\mathrm{b}}(t)$ and $O_{\mathrm{b}}(t)$ are the concentrations of the lactose, reaction product and oxygen, respectively, in the bulk ($R_1 \leq r \leq R$), q is the ratio of the volume of the enclosure ($R_1 \leq r \leq R$) of the diffusion shell to the area of the outer surface of the shell ($r = R_1$) [A1], defined as:

$$q = \frac{4\pi(R^3 - R_1^3)/3}{4\pi R_1^2} = \frac{R^3 - R_1^3}{3R_1^2}. \tag{2.36}$$

The value $1/q$ can be also considered as the adsorption capacity of the MR [18, 21].

2.3.3. Initial conditions

It was assumed that, initially, the dissolved oxygen is uniformly distributed in the MR, while it is free of lactose as well as of the reaction product ($0 \leq r \leq R_0$),

$$L_{\mathrm{m}}(r,0) = 0, \quad P_{\mathrm{m}}(r,0) = 0, \quad O_{\mathrm{m}}(r,0) = \phi O_0, \tag{2.37}$$

where O_0 is the initial concentration of oxygen, and ϕ is the formal partition coefficient [64, 110]. The coefficient ϕ is less than unity as the averaged concentrations of all the compounds in the MR becomes less than the concentration in the bulk due to the insoluble MR carrier.

The reaction (1.1) starts when lactose is pouring into a buffer solution containing the MR. All the soluble compounds were assumed to be distributed uniformly outside the MR,

$$\begin{aligned} &L_{\mathrm{d}}(r,0) = 0, \quad P_{\mathrm{d}}(r,0) = 0, \quad O_{\mathrm{d}}(r,0) = O_0, \quad R_0 \leq r \leq R_1, \\ &L_{\mathrm{b}}(0) = L_0, \quad P_{\mathrm{b}}(0) = 0, \quad O_{\mathrm{b}}(0) = O_0. \end{aligned} \tag{2.38}$$

2.3.4. Boundary conditions

Due to the symmetry, the zero-flux boundary conditions are defined on the center of the MR ($r = 0, t > 0$),

$$\mathrm{D}_{C,\mathrm{m}} \frac{\partial C_{\mathrm{m}}}{\partial r}\bigg|_{r=0} = 0, \quad C = L, P, O. \tag{2.39}$$

Under the circumstances where both external and internal diffusion gradients are found, the flux of the compounds through the diffusion shell must equal the flux entering the surface of the MR. The formal partition coefficient ϕ is used in the matching conditions to describe the specificity in concentration distribution of the compounds between two neighboring regions ($t > 0$),

$$\begin{aligned} &\mathrm{D}_{C,\mathrm{m}} \frac{\partial C_{\mathrm{m}}}{\partial r}\bigg|_{r=R_0} = \mathrm{D}_{C,\mathrm{d}} \frac{\partial C_{\mathrm{d}}}{\partial r}\bigg|_{r=R_0}, \\ &C_{\mathrm{m}}(R_0,t) = \phi C_{\mathrm{d}}(R_0,t), \quad C = L, P, O. \end{aligned} \tag{2.40}$$

The same partition coefficient ϕ was applied for all the soluble compounds as the ratio of the insoluble carrier volume to the total volume of the MR [64, 110].

On the boundary between the diffusion and convective shells ($r = R_1$), the continuity of the concentrations is required ($t > 0$),

$$C_{\mathrm{d}}(R_1, t) = C_{\mathrm{b}}(t), \quad C = L, P, O. \tag{2.41}$$

The boundary condition (2.41) and the governing equations (2.35) are only specific to the batch mode of the bioreactor operation (BSTR) [A1]. In the case of open system (CSTR), away from the diffusion shell ($r > R_1$) the concentration of the soluble compounds remains constant at its initial value [44, 77, 88, 112].

2.3.5. Dimensionless governing parameters

In order to define the main governing parameters of the mathematical model, a dimensionless mathematical model has to be derived [110]. The following main dimensionless parameters have been introduced for the system (2.33)–(2.23) [A1–A3]:

$$\Phi_{\mathrm{C}}^2 = \frac{R_0^2 V_{\mathrm{C}}}{\mathrm{D}_{C,\mathrm{m}} K_{\mathrm{C}}}, \quad \beta_{\mathrm{C}} = \frac{\mathrm{D}_{C,\mathrm{d}} R_1}{\mathrm{D}_{C,\mathrm{m}}(R_1 - R_0)}, \quad C = L, O, \tag{2.42}$$

where Φ_L^2 and Φ_O^2 are known as the Thiele modulus or the diffusion module or the Damköhler number [41, 44], while β_L and β_O are the Biot numbers corresponding to lactose and oxygen, respectively [1, 24, 104].

The Thiele modulus essentially define internal characteristics of the enzyme-catalized systems [69]. The enzyme-catalized system is known to be under diffusion control when the corresponding Thiele modulus is much greater than unity. In the opposite case, when the Thiele modulus is significantly less than unity, the enzyme kinetics controls the system action.

The Biot number compares the external and internal mass transfer resistances [A3][1, 104]. As the Biot number increases, the importance of the external mass transfer resistance decreases [1, 24]. Since $\mathrm{D}_{L,\mathrm{m}} \leq \mathrm{D}_{L,\mathrm{d}}$, $\mathrm{D}_{O,\mathrm{m}} \leq \mathrm{D}_{O,\mathrm{d}}$ and $R_1 \geq R_0$, the Biot numbers defined in (2.42) can not be less than unity, $\beta_L \geq 1$, $\beta_O \geq 1$ [A1].

The Thiele modulus and the Biot number as the most important parameters for the bioreactor effectiveness are widely used in analysis and design of different bioreactors [24, 77, 88, 104, 118].

Conclusions

A typical microbioreactor model is based on separation of the domains. Firstly, the microbioreactor domain, where reactions take place, is defined. Then the Nernst diffusion layer occurs to incorporate particle interactions with the solution. Thirdly, the different boundary conditions are assigned depending does concentration is constant (open system), or changing (closed system) within the bulk. Since microbioreactors considered a porous, it is common to use discontinuities at the domain boundaries. A microbioreactor might also be multi-layer system [A7].

The main conclusion from this Chapter:

1. The proposed model 2.1 is generalization of continuous stirred tank reactors considering that CSTR are based on microbioreactors.

2. The proposed model 2.2 is generalization of batch stirred tank reactors considering that BSTR are based on microbioreactors.

3. The proposed model 2.3 is novel model based on experiments proposed by [93, 94].

In this Chapter the generalization of bioreactor models is presented. The third mathematical model is a novel model of microbioreactor with carbon nanotubes, which includes a combination of multiple separately independent reactions by electrons wiring.

3. Symbolic and Numerical Computational Models

In this Chapter the analytical, symbolic and numerical solutions for the mathematical models of Chapter 2 are presented. The analytical solutions and analytical approximations are provided for the limiting cases of those models and the numerical methods used for simulations. This Chapter also includes the formulation for multi-objective bioreactor optimization. The main results of this Chapter were presented in articles [A3,A4] and conference proceedings [A6].

3.1. Analytical solutions

Let us consider the continuous stirred-tank reactor model based on microbioreactors that was defined in Section 2.1. In this case, the system usually works for a long time, and commonly reaches a steady state quickly. In such case reaction term is equivalent to equation (RMM-D) with $\tau = 0$. Under such limitations, some analytical solutions can be found. These analytical solutions (and analytical approximations) allow us not only to check the numerical simulation results, but also to solve analytically the expressions of various characteristics like microbioreactor efficiency. In this Section we will obtain such analytical solutions under limiting cases.

3.1.1. First-order steady-state solution

At low concentration of the substrate ($s_0 \ll K_\mathrm{M}$), the Michaelis-Menten kinetics approaches the first-order kinetics, i.e., $v(s_\mathrm{m}) \approx V_\mathrm{max} s_\mathrm{m}/K_\mathrm{M}$. Then, assuming a steady-state approximation, the governing equation (2.14) for substrate reduces to the following one:

$$\mathrm{D_m} \frac{\partial}{\partial r}\left(r^2 \frac{\partial s_\mathrm{m,s}}{\partial r} \right) = \frac{V_\mathrm{max} s_\mathrm{m,s}}{K_\mathrm{M}} r^2. \tag{3.1}$$

The linear second order differential equation (3.1) can be easily solved [15],

$$s_\mathrm{m,s}(r) = \frac{c_1}{r} \sinh\left(r\sqrt{\frac{V_\mathrm{max}}{K_\mathrm{M}\mathrm{D_m}}} \right) + \frac{c_2}{r} \cosh\left(r\sqrt{\frac{V_\mathrm{max}}{K_\mathrm{M}\mathrm{D_m}}} \right), \quad 0 < r < r_0, \tag{3.2}$$

where c_1 and c_2 are the constants of integration.

At the steady-state conditions, it is also no problem to integrate the classical diffusion equation (2.15) in a spherical shell, i.e.,

$$s_{\mathrm{d,s}}(r) = \frac{d_1}{r} + d_2, \quad r_0 < r < r_1, \tag{3.3}$$

where d_1 and d_2 are the constants of integration.

By evaluating c_1, c_2, d_1 and d_2 from the boundary conditions, we get the following solution of the problem:

$$s_{\mathrm{m,s}}(r) = \frac{\phi s_0 r_1}{r} \times \frac{\theta r_0 \sinh(\sigma r/r_0)}{\theta r_1 \sinh\sigma + \phi(r_1 - r_0)(\sigma\cosh\sigma - \sinh\sigma)}, \quad 0 \le r \le r_0, \tag{3.4}$$

$$s_{\mathrm{d,s}}(r) = \frac{s_0 r_1}{r} \times \frac{\theta r \sinh\sigma + \phi(r - r_0)(\sigma\cosh\sigma - \sinh\sigma)}{\theta r_1 \sinh\sigma + \phi(r_1 - r_0)(\sigma\cosh\sigma - \sinh\sigma)}, \quad r_0 \le r \le r_1. \tag{3.5}$$

The analytical expressions (3.4)–(3.5), obtained for the substrate concentration at the steady-state, can be applied to evaluating the effectiveness factors, i.e.,

$$\eta_{\mathrm{i}} = \frac{3}{\sigma^2}(\sigma\coth\sigma - 1), \tag{3.6}$$

$$\eta_{\mathrm{e}} = \frac{\beta}{\beta + \phi(\sigma\coth\sigma - 1)}, \tag{3.7}$$

$$\eta_{\mathrm{p}} = \phi, \tag{3.8}$$

$$\eta_{\mathrm{o}} = \frac{3\beta\phi(\sigma\coth\sigma - 1)}{\sigma^2(\beta + \phi(\sigma\coth\sigma - 1))}, \tag{3.9}$$

where

$$\beta = \frac{\theta r_1}{r_1 - r_0} = \frac{\mathrm{D_d} r_1}{\mathrm{D_m}(r_1 - r_0)} = \frac{\mathrm{D_d}(r_0 + h)}{\mathrm{D_m} h}. \tag{3.10}$$

The dimensionless factor β can be considered as the effective Biot number or dimensionless mass transfer coefficient that quantifies the relative preponderance of internal or external diffusion [6]. The expression (3.10) of the Biot number β was deduced by substituting the expressions (3.4) and (3.5) into the boundary condition (2.7) and rewriting it in the dimensionless form as the flux condition [73],

$$\left.\frac{\partial S_{\mathrm{m,s}}}{\partial R}\right|_{R=1} = \beta\,(1 - S_{\mathrm{d,s}}(1))\,. \tag{3.11}$$

The mass transfer coefficient is dependent on the system geometry, the physical properties of medium and flow dynamics, and it is hard to evaluate the mass transfer resistance between biocatalytic bioreactors and liquids [3, 41, 96].

That is why the effectiveness factors are sometimes estimated without external mass transfer resistance [83, 113]. The Biot number β defined in (3.10) depends only on the geometry of the diffusion shell and diffusivity of the substrate.

A low Biot number means the strong external mass transfer resistance and hence both internal and external mass transfer resistances are important for the determination of substrate conversion. As the Biot number increases, the importance of the external mass transfer resistance decreases [1]. When $r_0 \leq r_1$, the effective Biot number β ranges from $\theta = \mathrm{D_d}/\mathrm{D_m}$ ($r_1 \gg r_0$, $h \gg r_0$) to ∞ ($r_1 \to r_0$, $h \to 0$), and when $\mathrm{D_m} \leq \mathrm{D_d}$, the Biot number $\beta \geq 1$ [113]. As the thickness h of the external diffusion shell depends upon the nature and intensity of the stirring of the buffer solution, the less intense stirring corresponds to lower β and, correspondingly, greater h, more intense stirring corresponds to greater β (lower h). The diffusion module and the Biot number are widely used in analysis and design of different bioreactors [31, 68, 109].

The expression (3.6) of the internal effectiveness factor is invariant to the external mass transfer and is equivalent to another already known expression called the Thiele modulus [44, 63, 109].

Both internal and external effectiveness factors are monotonously decreasing functions of the diffusion module σ. Moreover $\eta_\mathrm{i} \to 0$ and $\eta_\mathrm{e} \to 0$ as $\sigma \to \infty$, and $\eta_\mathrm{i} \to 1$ and $\eta_\mathrm{e} \to 1$ as $\sigma \to 0$. In addition, the external effectiveness factor is an monotonously increasing function of the Biot number. Moreover $\eta_\mathrm{e} \to 1$ as $\beta \to \infty$ and $\eta_\mathrm{e} \to 0$ as $\beta \to 1$. Since β decreases while increasing the thickness $h = r_1 - r_0$ of the external diffusion layer, the external effectiveness factor η_e monotonously decreases with increasing the thickness h.

After calculating the Biot number β, the expression (3.4) of the substrate concentration inside the MR reduces to the following:

$$s_{\mathrm{m,s}}(r) = \frac{\phi s_0}{r} \times \frac{\beta r_0 \sinh(\sigma r/r_0)}{\beta \sinh\sigma + \phi(\sigma\cosh\sigma - \sinh\sigma)}, \quad 0 \leq r \leq r_0\,. \tag{3.12}$$

Similarly, the dimensionless substrate concentration $S_{\mathrm{m,s}}$ depends on the dimensionless concentration S_0, diffusion module σ, Biot number β, partition coefficient ϕ and space coordinate R, while $S_{\mathrm{d,s}}$ additionally depends on the dimensionless radius R_1, i.e.,

$$S_{\mathrm{m,s}}(R) = \frac{\phi S_0}{R} \times \frac{\beta \sinh(\sigma R)}{\beta \sinh\sigma + \phi(\sigma\cosh\sigma - \sinh\sigma)}, \quad 0 \leq R \leq 1. \tag{3.13}$$

$$\begin{aligned} S_{\mathrm{d,s}}(R) \quad &= \quad \frac{S_0}{R} \times \frac{\beta R \sinh\sigma + \phi R_1(\sigma\cosh\sigma - \sinh\sigma)(R-1)/(R_1-1)}{\beta \sinh\sigma + \phi(\sigma\cosh\sigma - \sinh\sigma)}, \\ &\qquad 1 \leq R \leq R_1. \end{aligned} \tag{3.14}$$

When the external mass transfer by diffusion is ignored ($h \to 0$, $\beta \to \infty$), the concentration expressions (3.4) and (3.12) reduces to a known formulae

[15, 44, 63, 109], as follows:

$$s_{\mathrm{m,s}} = \frac{\phi s_0 r_0 \sinh(\sigma r/r_0)}{r \sinh \sigma}, \quad 0 \le r \le r_0,\ r_1 = r_0, \tag{3.15}$$

where ϕs_0 is the substrate concentration at the inner surface of the MR.

3.1.2. Zero-order steady-state solution

At high concentration of the substrate ($s_0 \gg K_{\mathrm{M}}$), the Michaelis-Menten kinetics approaches the zero-order kinetics, i.e., $v(s_{\mathrm{m}}) \approx V_{\max}$. The governing equation (2.14) at a steady-state reduces to the following one:

$$\mathrm{D_m} \frac{\partial}{\partial r} \left(r^2 \frac{\partial s_{\mathrm{m,s}}}{\partial r} \right) = V_{\max} r^2. \tag{3.16}$$

Solution of (3.16) with (3.3) and the boundary conditions (2.5)–(2.8) gives the following expressions:

$$s_{\mathrm{m,s}}(r) = \phi s_0 - \frac{V_{\max}}{6\mathrm{D_m}} \left(r_0^2 - r^2 + \frac{2\phi r_0^2}{\beta} \right), \quad 0 \le r \le r_0, \tag{3.17}$$

$$s_{\mathrm{d,s}}(r) = s_0 - \frac{V_{\max} r_0^3}{3\mathrm{D_d}} \left(\frac{1}{r} - \frac{1}{r_1} \right), \quad r_0 \le r \le r_1. \tag{3.18}$$

Since the reaction term in the governing equation (3.16) is independent of the substrate concentration, its solution can produce a negative concentration of the substrate. The maximal MR radius r_0, for which expression (3.17) can be used is,

$$r_{\max} = \sqrt{\frac{6\mathrm{D_m}\phi s_0}{V_{\max}(1 + 2\phi/\beta)}}. \tag{3.19}$$

Since, in the case of zero-order reactions, the reaction rate is independent of the substrate concentration, the effectiveness factors approaches their maximal values, $\eta_{\mathrm{i}} = \eta_{\mathrm{e}} = \eta_{\mathrm{p}} = 1$, $\eta_{\mathrm{o}} = 1$, if only $r_0 \le r_{\max}$.

The derived expression (3.17) generalises a known expression of the substrate concentration inside the spherical bioreactor when the external mass transfer is ignored and $r_0^2 \le 6\mathrm{D_m}\phi s_0 / V_{\max}$ [44], i.e.,

$$s_{\mathrm{m,s}}(r) = \phi s_0 - \frac{V_{\max}}{6\mathrm{D_m}} \left(r_0^2 - r^2 \right), \quad 0 \le r \le r_0, \quad r_1 = r_0\,. \tag{3.20}$$

3.2. Approximations using homotopy perturbation method

Let us consider the bioreactor at a steady state [A3,63,113]. Let us also define the inner layer where the reaction and diffusion take place: $0 < r < r_{\mathrm{m}}$, and external layer where only diffusion takes place: $r_{\mathrm{m}} < r < r_{\mathrm{n}}$. It is common to model the substrate concentration in the domain $0 < r < r_{\mathrm{n}}$ by the following non-linear second order differential equation:

$$D(r)\Delta S(r) \quad = \quad a(r)\frac{V_{\max}S(r)}{K_{\mathrm{M}}+S(r)}, \tag{3.21}$$

where $\Delta = r^{-2}\frac{\mathrm{d}}{\mathrm{d}r}(r^2\frac{\mathrm{d}}{\mathrm{d}r})$ is the Laplace operator, while the diffusion $D(r)$ and reaction term $a(r)$ are defined as follows:

$$D(r) \quad = \quad \begin{cases} \mathrm{D}_{S,\mathrm{m}}, & 0 < r < r_{\mathrm{m}}, \\ \mathrm{D}_{S,\mathrm{n}}, & r_{\mathrm{m}} < r < r_{\mathrm{n}}, \end{cases} \tag{3.22}$$

$$a(r) \quad = \quad \begin{cases} 1, & 0 < r < r_{\mathrm{m}}, \\ 0, & r_{\mathrm{m}} < r < r_{\mathrm{n}}, \end{cases} \tag{3.23}$$

where $\mathrm{D}_{S,\mathrm{m}}$ and $\mathrm{D}_{S,\mathrm{n}}$ are the diffusion coefficients in the bioreactor and diffusion layers, $V_{\max}$ the maximal enzyme reaction rate, and K_{M} is the Michael constant.

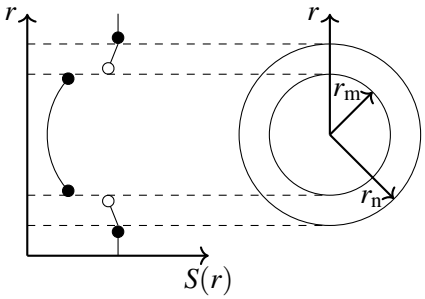

Figure 3.1: The profile of concentrations in the bioreactor

Boundary conditions. We assume that on the boundary between r_{m}^- and r_{m}^+, the fluxes between the adjacent areas are equal:

$$\mathrm{D}_{S,\mathrm{m}}\frac{dS(r)}{dr}\Big|_{r=r_{\mathrm{m}}^-} \quad = \quad \mathrm{D}_{S,\mathrm{n}}\frac{dS(r)}{dr}\Big|_{r=r_{\mathrm{m}}^+}. \tag{3.24}$$

Due to different materials, the layers usually have different properties, and the concentration along the boundary r_{m} is discontinuous. This is formalized by using the partition coefficient ϕ [43] (see. Figure 3.1):

$$S(r_{\mathrm{m}}^{-}) \quad = \quad \phi S(r_{\mathrm{m}}^{+}). \tag{3.25}$$

We assume that the bioreactor is relatively small in contrast to the total volume of the solution, and the substrate r_{m} that the concentration remains the same on the boundary:

$$\mathrm{D}_{S,\mathrm{m}} \frac{dS(r)}{dr}\Big|_{r=0} = 0, \;\; S(r_{\mathrm{n}}) = S_0. \tag{3.26}$$

Dimensionless model. We transform (3.21)–(3.26) equations to a dimensionless model, by transforming the space variable r and concentration $S(r)$ as follows:

$$\widetilde{r} = \frac{r_{\mathrm{n}} - r_{\mathrm{m}}}{r_{\mathrm{m}}}, \;\; \widetilde{S} = \frac{S}{K_{\mathrm{M}}}, \;\; \widetilde{\nu} = \frac{\nu}{r_{\mathrm{m}}}, \;\; \widetilde{S}_0 = \frac{S_0}{K_{\mathrm{M}}}, \tag{3.27}$$

where $\widetilde{r}$ is the dimensionless radius from the bioreactor center, $\widetilde{S}(\widetilde{r})$ is the dimensionless concentration, $\widetilde{\nu}$ is the dimensionless Nernst layer thickness, and $\widetilde{S}_0$ is the concentration in Nernst layer. The governing equations (3.21)–(3.23) then become:

$$D^*(\widetilde{r})\Delta\widetilde{S}(\widetilde{r}) \quad = \quad a^*(\widetilde{r})\frac{\sigma^2\widetilde{S}(\widetilde{r})}{1+\widetilde{S}(\widetilde{r})}, \tag{3.28}$$

$$D^*(\widetilde{r}) \quad = \quad \begin{cases} 1, & 0 < r < 1, \\ \gamma = \mathrm{D}_{S,\mathrm{n}}/\mathrm{D}_{S,\mathrm{m}}, & 1 < \widetilde{r} < 1+\widetilde{\nu}, \end{cases} \tag{3.29}$$

$$a^*(\widetilde{r}) \quad = \quad \begin{cases} 1, & 0 < \widetilde{r} < 1, \\ 0, & 1 < \widetilde{r} < 1+\widetilde{\nu}, \end{cases} \tag{3.30}$$

where σ is the Thiele module, also known as the Damkohler number [49, 84, 103]:

$$\sigma^2 = \frac{V_{\max} r_{\mathrm{m}}^2}{K_{\mathrm{M}}\mathrm{D}_{S,\mathrm{m}}}. \tag{3.31}$$

The boundary conditions (3.24)–(3.26) become:

$$\frac{\partial\widetilde{S}}{\partial\widetilde{r}}\Big|_{\widetilde{r}=1^-} \quad = \quad \frac{\mathrm{D}_{S,\mathrm{n}}}{\mathrm{D}_{S,\mathrm{m}}}\frac{\partial\widetilde{S}}{\partial\widetilde{r}}\Big|_{\widetilde{r}=1^+}, \tag{3.32}$$

$$\widetilde{S}(1^-) \quad = \quad \phi\widetilde{S}(1^+), \frac{\partial\widetilde{S}}{\partial\widetilde{r}}\Big|_{\widetilde{r}=0} = 0, \widetilde{S}(1+\widetilde{\nu}) = \widetilde{S}_0. \tag{3.33}$$

3.2.1. Algorithm of homotopy perturbation method

As provided in Section 1.3 the k-th order aproximation $S^k(r)$ is consider of the solution $S(r)$. Authors [47, 79] provide the solutions to more simplex systems. Now let us construct the algorithm to perform the HPM see Algorithm 1.

Algorithm 1: Algorithm of Homotopy perturbation method for two layers model

Result: The k-th order aproximation $\tilde{S} = S^0 + S^1 + ... + S^k$
Initialization: we select initial equation by introducing ε. Set the $\varepsilon = 0$, and receive the initial equation $[L(u) - L(u_{\text{in}})]$ see equation (1.25). Set $i = 1$
while $i \leqslant k$ **do**
  Calculating $\widetilde{S}_i(\widetilde{r}) = \frac{1}{i!}\frac{d^i\widetilde{S}(\widetilde{r},\varepsilon)}{d\varepsilon^i}\Big|_{\varepsilon=0}$, and selecting expresions near ε;
  Change the boundary condition to zero, for improving the equation error.
  Solve the equation by placing the calculated expression $\widetilde{S}_{i-1}(\widetilde{r})$
  Solve the equation and receive the i-th order solution $\widetilde{S}_i(\widetilde{r})$
  Solve the i-th order equation in additional layers
end

3.2.2. Approximation of solution

The equations (3.28)–(3.33) have been also considered by Radžendran [47, 79], where they suggest to use the (so called) small parameter ε, and provide the first order approximations of non-linear PDE. However, in this Section we will demonstrate that different formulation of the small parameter within the equation gives different results.

Let us consider a solution $\widetilde{S}(\widetilde{r})$ as expression perturbation series [16]:

$$\widetilde{S}(\widetilde{r},\varepsilon) = \widetilde{S}_0(\widetilde{r}) + \sum_{n=1}^{\infty}\widetilde{S}_{\text{n}}(\widetilde{r})\varepsilon^n. \tag{3.34}$$

When $\varepsilon = 0$ is used, we get the initial solution of a simpler equation, while taking limit $\varepsilon = 1$, we get the approximation of PDE defined in (3.28)-(3.33).

In the domain $0 < \widetilde{r} < 1$, we differently put the small parameter ε into equation [16]. Let us consider a different initial equation as separate models:

$$\left(\widetilde{S}''(\widetilde{r}) + \frac{2}{\widetilde{r}}\widetilde{S}'(\widetilde{r})\right) - \varepsilon\frac{\sigma^2\widetilde{S}(\widetilde{r})}{1+\widetilde{S}(\widetilde{r})} = 0, \tag{M1}$$

$$\left(\widetilde{S}''(\widetilde{r})+\frac{2}{\widetilde{r}}\widetilde{S}'(\widetilde{r})\right)\left(1+\widetilde{S}(\widetilde{r})\right)-\varepsilon\sigma^2\widetilde{S}(\widetilde{r})=0, \tag{M2}$$

$$\widetilde{S}''(\widetilde{r})+\frac{2}{\widetilde{r}}\widetilde{S}'(\widetilde{r})-\sigma^2\widetilde{S}(\widetilde{r})+\widetilde{S}^{\varepsilon}(\widetilde{r})\left(\widetilde{S}''(\widetilde{r})+\frac{2}{\widetilde{r}}\widetilde{S}'(\widetilde{r})\right)=0, \tag{M3}$$

$$\left(\widetilde{S}''(\widetilde{r})+\frac{2}{\widetilde{r}}\widetilde{S}'(\widetilde{r})\right)-\sigma^2+\varepsilon\frac{\sigma^2}{1+\widetilde{S}(\widetilde{r})}=0, \tag{M4}$$

$$\left(\widetilde{S}''(\widetilde{r})+\frac{2}{\widetilde{r}}\widetilde{S}'(\widetilde{r})\right)\left(1+\varepsilon\widetilde{S}(\widetilde{r})\right)-\sigma^2\widetilde{S}(\widetilde{r})=0, \tag{M5}$$

Even though the introduction of the small parameter into the equations (M2) and (M5) can be found in literature [47, 79], the models (M1), (M3), (M4) have not been considered yet.

Let us now take a look at $\widetilde{S}_n(\widetilde{r})=\frac{1}{n!}\frac{d^n\widetilde{S}(\widetilde{r},\varepsilon)}{d\varepsilon^n}\Big|_{\varepsilon=0}$, $n=0,1,2,\ldots$. By insert the expression (3.34) to (M1)–(M5) and with the collected members near power of ε , we solve the differential equations (3.28)–(3.33) [16].

In the case of (M1) we get:

$$\begin{aligned}
\varepsilon^0 \quad &: \quad \left(\widetilde{S}_0''(\widetilde{r})+\frac{2}{\widetilde{r}}\widetilde{S}_0'(\widetilde{r})\right)=0,\\
\widetilde{S}_{\mathrm{M1},0}(\widetilde{r}) \quad &= \quad \begin{cases}\phi S_0, & 0<\widetilde{r}<1,\\ S_0, & 1<\widetilde{r}<1+\widetilde{\nu},\end{cases}\\
\varepsilon^1 \quad &: \quad \left(\widetilde{S}_1''(\widetilde{r})+\frac{2}{\widetilde{r}}\widetilde{S}_1'(\widetilde{r})\right)-\frac{\sigma^2\widetilde{S}_0(\widetilde{r})}{1+\widetilde{S}_0(\widetilde{r})}=0,
\end{aligned} \tag{3.35}$$

$$\widetilde{S}_{\mathrm{M1},1}(\widetilde{r}) \quad = \quad \begin{cases}\frac{1}{6}\frac{\sigma\phi S_0}{\gamma(1+\widetilde{\nu})(\phi S_0+1)}((1+\widetilde{\nu})\gamma\widetilde{r}^2-2r_N\phi-r_N\gamma+2\phi),\\ \frac{1}{3}\frac{\sigma\phi S_0}{\gamma(1+\widetilde{\nu})(\phi S_0+1)}(1-\frac{(1+\widetilde{\nu})}{\widetilde{r}}),\end{cases} \tag{3.36}$$

$$\begin{aligned}
\varepsilon^2 \quad &: \quad \left(\widetilde{S}_2''(\widetilde{r})+\frac{2}{\widetilde{r}}\widetilde{S}_2'(\widetilde{r})\right)-\frac{\sigma^2\widetilde{S}_1(\widetilde{r})}{1+\widetilde{S}_0(\widetilde{r})}\\
&\quad +\frac{\sigma^2\widetilde{S}_0(\widetilde{r})\widetilde{S}_1(\widetilde{r})}{(1+\widetilde{S}_0(\widetilde{r}))^2}=0,
\end{aligned}$$

$$\widetilde{S}_{\mathrm{M1},2}(\widetilde{r}) \quad = \quad \begin{cases}\frac{1}{8\cdot45}\frac{1}{\gamma^2(1+\widetilde{\nu})^2(\phi^3S_0^3+3\phi^2S_0^2+3\phi S_0+1)}\Big(\phi S_0\sigma^2(3\gamma^2(1+\widetilde{\nu})^2\widetilde{r}^4,\\ -20\gamma(1+\widetilde{\nu})^2\phi\widetilde{r}^2+40(1+\widetilde{\nu})^2\phi^2-10\gamma^2(1+\widetilde{\nu})^2\widetilde{r}^2\\ +20\gamma(1+\widetilde{\nu})\phi\widetilde{r}^2+28\gamma(1+\widetilde{\nu})^2\phi\\ -80(1+\widetilde{\nu})\phi^2+7\gamma^2(1+\widetilde{\nu})^2-28\gamma(1+\widetilde{\nu})\phi+40\phi^2)\Big)\\ \frac{1}{45}\frac{\phi S_0\sigma^2(5(1+\widetilde{\nu})\phi+(1+\widetilde{\nu})\gamma-5\phi)}{\gamma^2(1+\widetilde{\nu})^2(\phi^3S_0^3+3\phi^2S_0^2+3\phi S_0+1)}(\frac{(1+\widetilde{\nu})}{\widetilde{r}}-1),\end{cases} \tag{3.37}$$

$$
\begin{aligned}
\varepsilon^3 \quad : \quad & \left(\widetilde{S}_3''(\widetilde{r})+\frac{2}{\widetilde{r}}\widetilde{S}_3'(\widetilde{r})\right)-\frac{\sigma^2\widetilde{S}_2(\widetilde{r})}{1+\widetilde{S}_0(\widetilde{r})} \\
& +\frac{\sigma^2\widetilde{S}_0(\widetilde{r})\widetilde{S}_2(\widetilde{r})}{(1+\widetilde{S}_0(\widetilde{r}))^2}+\frac{\sigma^2\widetilde{S}_1^2(\widetilde{r})}{(1+\widetilde{S}_0(\widetilde{r}))^2}-\frac{\sigma^2\widetilde{S}_0(\widetilde{r})\widetilde{S}_1^2(\widetilde{r})}{(1+\widetilde{S}_0(\widetilde{r}))^3}=0, \\
.. & \\
\varepsilon^n \quad : \quad & \left(\widetilde{S}_n''(\widetilde{r})+\frac{2}{\widetilde{r}}\widetilde{S}_n'(\widetilde{r})\right)-\frac{\sigma^2\widetilde{S}_n(\widetilde{r})}{1+\widetilde{S}_0(\widetilde{r})}+\frac{\sigma^2\sum_{i,j\in I_1}\widetilde{S}_j(\widetilde{r})\widetilde{S}_i(\widetilde{r})}{(1+\widetilde{S}_0(\widetilde{r}))^2}+ \\
& +\sigma^2\sum_{i=3}^{n-1}(-1)^n\frac{\sum_{i,j\in I_2}\widetilde{S}_j(\widetilde{r})\widetilde{S}_i(\widetilde{r})}{(1+\widetilde{S}_0(\widetilde{r}))^i} \\
& +\frac{(-1)^n\sigma^2\widetilde{S}_0(\widetilde{r})\widetilde{S}_1^{n-1}(\widetilde{r})}{(1+\widetilde{S}_0(\widetilde{r}))^n}=0,
\end{aligned}
$$

$$
\widetilde{S}_{\mathrm{M1},n}(\widetilde{r})=\begin{cases}\sum_{i=0}^{n}C_i\widetilde{r}^{2i}, & 0<\widetilde{r}<1,\\ C_{n+1}+C_{n+2}\frac{1}{\widetilde{r}}, & 1<\widetilde{r}<1+\widetilde{\nu},\end{cases} \tag{3.38}
$$

Analogously, for (M2) - (M5) we get:

$$
\widetilde{S}_{\mathrm{M2},0}(\widetilde{r}) = \begin{cases}\phi S_0,\\ S_0,\end{cases} \tag{3.39}
$$

$$
\widetilde{S}_{\mathrm{M2},1}(\widetilde{r}) = \begin{cases}\sigma^2\phi S_0\Big((1+\widetilde{\nu})\gamma\widetilde{r}^2-2(1+\widetilde{\nu})\phi-(1+\widetilde{\nu})\gamma+2\phi\Big)/\\ \Big(6\gamma(1+\widetilde{\nu})(\phi S_0+1)\Big)\\ -\sigma^2\phi S_0((1+\widetilde{\nu})-\widetilde{r})/(3\gamma(1+\widetilde{\nu})(\phi S_0+1)\widetilde{r}),\end{cases} \tag{3.40}
$$

$$
\widetilde{S}_{\mathrm{M3},0}(\widetilde{r}) = \begin{cases}\frac{C_1\sinh((1/2)\sqrt{2}\widetilde{r})}{\widetilde{r}}\\ C_2+\frac{C_3}{\widetilde{r}},\end{cases} \tag{3.41}
$$

$$
\tag{3.42}
$$

$$
\widetilde{S}_{\mathrm{M4},0}(\widetilde{r}) = \begin{cases}\frac{((1+\widetilde{\nu})\gamma\widetilde{r}^2\sigma^2+6(1+\widetilde{\nu})\gamma S_0+2\sigma^2)}{(6\gamma(1+\widetilde{\nu}))},\\ C_5+\frac{C_6}{\widetilde{r}},\end{cases} \tag{3.43}
$$

$$
\widetilde{S}_{\mathrm{M5},0}(\widetilde{r}) = \begin{cases}\frac{C_4\sinh(\sigma^2\widetilde{r})}{\widetilde{r}},\\ C_7+\frac{C_8}{\widetilde{r}},\end{cases} \tag{3.44}
$$

where $C_i, i=1,\ldots,8$ are the constants that were found by applying the boundary conditions. The constants are not provided here due the large expressions of revelation.

By looking to (M1) n-th part of the solution, in the domain $0 < \widetilde{r} < 1$ we are looking for the following solution:

$$\widetilde{S}^m_{\mathrm{M6}}(\widetilde{r}) = \sum_{n=0}^{m} a_n \widetilde{r}^{2n}. \tag{M6}$$

By inserting (M6) to (3.28), we get that a_n is of the following form:

$$a_n = \frac{1}{n!} \frac{a_0 \varepsilon^n \sum_{i=0}^{n} b_i a_0^i}{\sum_{j=0}^{2n+1} \binom{2n+1}{j} a_0^j}. \tag{3.45}$$

By solving the differential equations (3.28)–(3.33), we found:

$$\begin{aligned} a_0 &= \phi\widetilde{S}_0 - \frac{1}{6}\sigma^2\phi\widetilde{S}_0 \frac{2(1+\widetilde{\nu})\phi + (1+\widetilde{\nu})\gamma - 2\phi}{(1+\widetilde{\nu})\gamma(\phi\widetilde{S}_0+1)}, \\ a_1 &= \frac{1}{6}\cdot\frac{\varepsilon a_0}{1+a_0},\ a_2 = \frac{1}{120}\cdot\frac{\varepsilon^2 a_0}{a_0^3+3a_0^2+3a_0+1}, .. \end{aligned}$$

The HPM allows to introduce the small parameter to the non-liner PDE and find the recursive approximations in an analytical form.

3.2.3. Nonlinear steady-state solution

Analogously, an application of the HPM to the stationary case of the nonlinear reaction-diffusion problem (2.14)–(2.8) results in the following approximate analytical expressions of the substrate concentration inside ($s_{\mathrm{m,H}}$) and outside ($s_{\mathrm{d,H}}$) of the MR:

$$\begin{aligned} s_{m,s}(r) &\approx s_{\mathrm{m,H}}(r) = s_0\phi - \frac{P\sigma^2\phi s_0}{2}\left(1 - \frac{r^2}{r_0^2} + \frac{2\phi}{\beta}\right. \\ &+ \left.\frac{3P^2\sigma^2}{20}\left(8\frac{\phi}{\beta}\left(1+5\frac{\phi}{\beta}\right) - 3\left(1-\frac{r^4}{r_0^4}\right) + 10\left(1+2\frac{\phi}{\beta}\right)\left(1-\frac{r^2}{r_0^2}\right)\right)\right), \end{aligned} \tag{3.46}$$

$$s_{\mathrm{d,s}}(r) \approx s_{\mathrm{d,H}}(r) = s_0 - \frac{P\sigma^2\phi s_0 r_0}{\theta}\left(\frac{1}{r} - \frac{1}{r_1}\right)\left(1 + \frac{3P^2\sigma^2}{5}\left(1+5\frac{\phi}{\beta}\right)\right), \tag{3.47}$$

where $P = K_{\mathrm{M}}/(3(\phi s_0 + K_{\mathrm{M}})) = 1/(3(\phi S_0 + 1))$.

The substrate concentrations (3.46) and (3.47) in the dimensionless form are expressed in a more compact form,

$$S_{m,s}(R) \approx S_{\mathrm{m,H}}(R) = \phi - \frac{P\sigma^2\phi}{2}\left(1-R^2+\frac{2\phi}{\beta}\right. \tag{3.48}$$
$$\left. + \frac{3P^2\sigma^2}{20}\left(8\frac{\phi}{\beta}\left(1+5\frac{\phi}{\beta}\right)-3\left(1-R^4\right)+10\left(1+2\frac{\phi}{\beta}\right)\left(1-R^2\right)\right)\right),$$

$$S_{\mathrm{d,s}}(R) \approx S_{\mathrm{d,H}}(r) = 1-\frac{P\sigma^2\phi}{\theta}\left(\frac{1}{R}-\frac{1}{R_1}\right)\left(1+\frac{3P^2\sigma^2}{5}\left(1+5\frac{\phi}{\beta}\right)\right). \tag{3.49}$$

Although, the form of expressions (3.46)–(3.49) is rather complicated, but, nevertheless, their accuracy is not good enough. In next paragraphs we analyse the quality of approximations.

Table 3.1 present values of concentrations the points $R = 0$ and $R = 1$, for both HPM approximation and calculated by finite difference. The percentage error is $e(R) = |S_{\mathrm{m,s}}(R) - S_{\mathrm{m,H}}(R)|/S_{\mathrm{m,s}}(R) \times 100\%$, where $S_{m,s}$ is the concentration calculated by FD, $S_{\mathrm{m,H}}$ is the concentration calculated with HPM.

Table 3.1: Concentration values calculated by the finite difference method (FD) and the homotopy perturbation method (HPM)

S_0	β	σ^2	$S_{\mathrm{m,s}}(0)$	$S_{\mathrm{m,H}}(0)$	$e(0)$	$S_{m,s}(1)$	$S_{\mathrm{m,H}}(1)$	$e(1)$
10	10	0.1	4.99	4.98	0.13	5.00	5.00	0.02
0.1	10	0.1	0.05	0.05	0.72	0.05	0.05	0.10
10	0.1	0.1	4.94	4.85	1.85	4.95	4.86	1.74
0.1	0.1	0.1	0.05	0.04	8.75	0.05	0.04	8.22
1	1	1	0.45	0.40	10.41	0.48	0.45	6.21
10	10	10	4.13	3.53	14.56	4.95	4.86	1.70
0.1	10	10	0.02	0.06	223	0.05	0.05	0.65
10	0.1	10	0.95	-2.90	406	1.48	-2.20	248
0.1	0.1	10	0.00	12.94	366162	0.01	11.73	136349

The expressions of the substrate concentration obtained by HPM are of low precision when the enzyme kinetics controls the MR action, i.e., when $\sigma < 1$, regardless of the Biot number β and the substrate concentration S_0. However, these expressions are practically useless for bioreactor configurations when the MR acts under diffusion control, especially at low values of β. Nevertheless, since typically the designers seek for bioreactors working in the reaction-limited regime ($\sigma \ll 1$) [45], the expressions of the substrate concentration obtained by HPM have a practical value.

Using, the analytical expressions (3.46)–(3.49), all the effectiveness factors can be also analytically expressed. However, due to limited use of the substrate expressions and their unclosed form, the analytical expressions of the

effectiveness factors are not presented. The numerical solution of PDE is more accurate than the solution obtained by HPM, and because of this, the influence of the model parameter to the effectiveness factors was mainly investigated by numerical simulation of the MR action.

3.2.4. Results and discussion

When we found the approximation $\widetilde{S}^*(\widetilde{r})$ of the solution (1.21), we would like to evaluate the quality of approximation, not only the errors at given space points. Let us consider this quadratic error function $\mathscr{E}$:

$$\begin{aligned} \mathscr{E} &= \mathscr{E}(\widetilde{S}^*) \\ &= \int_0^1 \left(D^*(\widetilde{r})\Delta\widetilde{S}^*(\widetilde{r}) - a^*(\widetilde{r})\frac{\sigma^2\widetilde{S}^*(\widetilde{r})}{1+\widetilde{S}^*(\widetilde{r})}\right)^2 \mathrm{d}r. \end{aligned} \tag{3.50}$$

Since we know that true solution must meet the conditions $A(S) - f(\mathbf{b}) = 0$, we can define the quadratic error of the solution, by integrating over the domain of interest. To illustrate the case, we consider (3.28).

The loss function $\mathscr{E}$ depends not only on the system variable $\widetilde{S}^*(\widetilde{r})$, but also on additional system parameters $\mathscr{E}(\widetilde{S}_0, \phi, \widetilde{\nu}, \gamma, \sigma^2)$. If we fix the range of system parameters, then we can calculate the total error of the approximation, as follows:

$$\begin{aligned} \mathscr{E}_{\mathrm{T}} &= \mathscr{E}_{\mathrm{T}}(\widetilde{S}^*, \phi, \widetilde{\nu}, \gamma, \sigma^2) \\ &= \int_0^{\widetilde{S}_{0,v}} \int_0^{\phi_v} \int_0^{\widetilde{\nu}_v} \int_0^{\gamma_v} \int_0^{\sigma_v^2} \mathscr{E}\mathrm{d}\widetilde{\nu}\mathrm{d}\gamma\mathrm{d}\sigma^2\mathrm{d}\phi\mathrm{d}\widetilde{S}_0. \end{aligned} \tag{3.51}$$

Let us fix the parameters of a bioreactor system by values having practical interpretations $\widetilde{S}_{0,v} = 10, \phi_v = 1, \widetilde{\nu}_v = 1, \gamma_v = 10, \sigma_v^2 = 10$. The error of approximations obtained for the considered models (M1)–(M6) is presented in Table 3.2 and 3.3. The cases marked by `'-'` were not provided due to extremely complicated integration of the loss expressions. The bolded cases show the best approximations.

One can see in Table 3.2 that errors of different models vary by a few orders of magnitude. If approximation gave the error 0 we would have the true analytical solution. First, it is worth to mention that the models (M3) and (M4) give the significantly worse errors up to magnitude of order 10^5. If we look at the model (M5), it provides the best error at the first order approximation among analysed. However, the complexity of this model is very high and the first order approximation can not be easily evaluated. On the other hand, since the model (M6) have the general form of approximation (3.45), k-th order approximations can be computed. In general, the error results show that for different bioreactor

Table 3.2: The errors $\mathscr{E}_{\mathrm{T}}$ of approximations of the models (M1) – (M6).

Model	0-order	1-order	2-order
(M1)	$3.7 \cdot 10^4$	$\mathbf{3.8 \cdot 10^3}$	$8.12 \cdot 10^2$
(M2)	$3.7 \cdot 10^4$	$\mathbf{3.8 \cdot 10^3}$	–
(M3)	$3.2 \cdot 10^5$	–	–
(M4)	$3.3 \cdot 10^3$	$8.8 \cdot 10^5$	–
(M5)	$\mathbf{2.24 \cdot 10^2}$	–	–
(M6)	$7.9 \cdot 10^4$	$2.1 \cdot 10^4$	$\mathbf{2.7 \cdot 10^2}$

configuration different small parameter ε introduction should be used. The HPM model produces worse results, when the linearization is made by a part of the non-linear equation.

Table 3.3: The errors of the approximations the models (M1)–(M6) at fixed parameters: $S_0 = 1, \phi = 0.5, \sigma^2 = \gamma = \widehat{\nu} = 1$.

Model	0-order	1-order	2-order
(M1)	$1.1 \cdot 10^{-1}$	$3.5 \cdot 10^{-4}$	$1.19 \cdot 10^{-7}$
(M2)	$1.1 \cdot 10^{-1}$	$3.5 \cdot 10^{-4}$	$1.19 \cdot 10^{-7}$
(M3)	$\mathbf{7.3 \cdot 10^{-3}}$	$\mathbf{4.3 \cdot 10^{-5}}$	–
(M4)	$1.7 \cdot 10^{-1}$	$7 \cdot 10^{-1}$	–
(M5)	$1.2 \cdot 10^{-2}$	–	–
(M6)	$9.4 \cdot 10^{-2}$	$1.1 \cdot 10^{-4}$	$\mathbf{9.4 \cdot 10^{-9}}$

Table 3.4: The errors of the approximations models (M1) – (M6) at fixed parameters: $S_0 = 100, \phi = 0.5, \sigma^2 = \gamma = \widehat{\nu} = 1$

Model	0-order	1-order	2-order
(M1)	$9.6 \cdot 10^{-1}$	$2.12 \cdot 10^{-9}$	$5 \cdot 10^{-10}$
(M2)	$9.6 \cdot 10^{-1}$	$2.12 \cdot 10^{-9}$	$\mathbf{1.6 \cdot 10^{-14}}$
(M3)	$4.4 \cdot 10^2$	$1.59 \cdot 10^2$	-
(M4)	$\mathbf{9.7 \cdot 10^{-5}}$	$9.7 \cdot 10^{-1}$	-
(M5)	$1.46 \cdot 10^3$	-	-
(M6)	$9.6 \cdot 10^{-1}$	$\mathbf{1 \cdot 10^{-9}}$	$\mathbf{4 \cdot 10^{-10}}$

One can see in Tables 3.3–3.4 that, when we have the fixed system parameters $\widetilde{S}_0, \phi, \widetilde{\nu}, \gamma, \sigma^2$, the error $\mathscr{E}$ varies a lot. In numerical analysis the approximations are considered good if the order of magnitude for an error is 10^{-6} or less [40]. By different introduction of the small parameter ε, the zero or first order approximations could have the error order of a different magnitude. By looking at the models (M3) and (M4), we see that the zero order approximation

works fine, while the first order approximation provides worse results. Such behavior implicates that the convergence regions of the small parameter ε is small and the value $\varepsilon = 1$ is not in the convergence region. In model (M5) we actually get that the considered equation reduces to zero order kinetics. In such a case we clearly see that our approximation works very well when the concentration $\widetilde{S}$ is small, i.e., reactions behave as zero order kinetics. But under larger concentrations the approximation does not work at all (error of magnitude becomes 10^3). Also, it is evident that the models (M1), (M2) and (M6) give proper approximation under the given fixed system parameters.

3.3. Numerical analysis

3.3.1. Explicit scheme

The diffusion is formalized as the Laplace operator, which in spherical coordinates is defined as follows:

$$\Delta = \frac{1}{r^2}\frac{\partial}{\partial r}\left(r^2\frac{\partial}{\partial r}\right) = \frac{\partial^2}{\partial r^2} + \frac{2}{r}\frac{\partial}{\partial r}.$$

As described in Section 1.29 for numerical modeling we used finite difference methods. Then then explicit scheme (3.21) becomes:

$$\begin{aligned}
\frac{G_{\mathrm{p,m}}^{(t+1)} - G_{\mathrm{p,m}}^{(t)}}{\Delta t} &= \mathrm{D}_{G,\mathrm{m}}\left(\frac{G_{\mathrm{p+1,m}}^{(t)} - 2G_{\mathrm{p,m}}^{(t)} + G_{\mathrm{p\text{-}1,m}}^{(t)}}{(\Delta r)^2}\right. \\
&\quad \left. + \frac{2}{r\cdot\Delta r}\frac{G_{\mathrm{p+1,m}}^{(t)} - G_{\mathrm{p\text{-}1,m}}^{(t)}}{2\Delta r}\right) - \frac{V_{\max} G_{\mathrm{p,m}}^{(t)}}{K_{\mathrm{M}} + G_{\mathrm{p,m}}^{(t)}}, \\
G_{\mathrm{p,m}}^{(t+1)} &= G_{\mathrm{p,m}}^{(t)} \\
&\quad + \Delta t \cdot \left(\mathrm{D}_{G,\mathrm{m}}\left(\frac{G_{\mathrm{p+1,m}}^{(t)} - 2G_{\mathrm{p,m}}^{(t)} + G_{\mathrm{p\text{-}1,m}}^{(t)}}{(\Delta r)^2}\right.\right. \\
&\quad \left.\left. + \frac{2}{r\cdot\Delta r}\frac{G_{\mathrm{p+1,m}}^{(t)} - G_{\mathrm{p,m}}^{(t)}}{\Delta r}\right) - \frac{V_{\max} G_{\mathrm{p,m}}^{(t)}}{K_{\mathrm{M}} + G_{\mathrm{p,m}}^{(t)}}\right),
\end{aligned}$$

where $G = P, S$.

The boundary condition at $r = 0$ (center of bioreactor), is as follows:

$$\frac{\partial^2}{\partial r^2} + \frac{2}{r}\frac{\partial}{\partial r} = 2\frac{\partial^2}{\partial r^2}.$$

After considering the boundary condition (3.26), we calculate:

$$G_{0,\mathrm{m}}^{(t+1)} = G_{0,\mathrm{m}}^{(t)} - \Delta t \cdot \mathrm{D}_{G,\mathrm{m}} \left(2 \frac{G_{1,\mathrm{m}}^{(t)} - G_{0,\mathrm{m}}^{(t)}}{(\Delta r)^2} \right) - \Delta t \frac{V_{\max} G_{0,\mathrm{m}}^{(t)}}{K_{\mathrm{M}} + G_{0,\mathrm{m}}^{(t)}},$$

$$G_{R_1,\mathrm{d}}^{(t+1)} \quad = \quad G_{R_1,\mathrm{d}}^{(t)} - \Delta t \cdot \frac{1}{\delta} \mathrm{D}_{G,\mathrm{m}} \left(\frac{G_{R_1,\mathrm{d}}^{(t)} - G_{R_1-1,\mathrm{d}}^{(t)}}{\Delta r} \right)$$

Table 3.5: Explicit scheme for the boundary conditions

Explicit scheme
r=0:
$G_{0,m}^{(t+1)} = G_{0,m}^{(t)} + \Delta t \cdot \left(\mathrm{D}_{G,\mathrm{m}} \left(2 \frac{G_{1,m}^{(t)} - G_{0,m}^{(t)}}{(\Delta r)^2} \right) - \frac{V_{\max} G_{0,m}^{(t)}}{K_{\mathrm{M}} + G_{0,m}^{(t)}} \right)$
$0 < r < R_0$:
$G_{\mathrm{p,m}}^{(t+1)} = G_{\mathrm{p,m}}^{(t)} + \Delta t \cdot \left(\mathrm{D}_{G,m} \left(\frac{G_{\mathrm{p+1},m}^{(t)} - 2G_{\mathrm{p,m}}^{(t)} + G_{\mathrm{p\text{-}1},m}^{(t)}}{(\Delta r)^2} + \frac{2}{r \cdot \Delta r} \frac{G_{\mathrm{p+1},m}^{(t)} - G_{\mathrm{p,m}}^{(t)}}{\Delta r} \right) - \frac{V_{\max} G_{\mathrm{p,m}}^{(t)}}{K_{\mathrm{M}} + G_{\mathrm{p,m}}^{(t)}} \right)$
$r = R_0$:
$G_{R_0,\mathrm{d}}^{(t+1)} = (\mathrm{D}_{G,\mathrm{d}} \Delta_{\mathrm{m}} G_{R_0+1,\mathrm{d}}^{(t)} + \mathrm{D}_{G,m\mathrm{m}} \Delta_{\mathrm{d}} G_{R_0-1,\mathrm{d}}^{(t)}) / (\mathrm{D}_{G,\mathrm{d}} \Delta_{\mathrm{m}} + D_{G,m} \Delta_{\mathrm{d}})$
$R_0 < r < R_1$:
$G_{\mathrm{p,d}}^{(t+1)} = G_{\mathrm{p,d}}^{(t)} + \Delta t \cdot \left(\mathrm{D}_{G,\mathrm{d}} \left(\frac{G_{\mathrm{p+1,d}}^{(t)} - 2G_{\mathrm{p,}d}^{(t)} + G_{\mathrm{p\text{-}1},d}^{(t)}}{(\Delta r)^2} + \frac{2}{r \cdot \Delta r} \frac{G_{\mathrm{p+1,d}}^{(t)} - G_{\mathrm{p,d}}^{(t)}}{\Delta r} \right) \right.$
$r = R_1$:
$G_{R_1,\mathrm{d}}^{(t+1)} = G_0^{(t)}$

3.3.2. Explicit scheme in stationary case

The equations (3.21)–(3.25) can be approximated as:

$$\mathrm{D}_{G,\mathrm{m}} \left(\frac{G_{p+1,m}^{(t)} - 2G_{\mathrm{p,m}}^{(t)} + G_{\mathrm{p\text{-}1,m}}^{(t)}}{(\Delta r)^2} + \frac{2}{r \cdot \Delta r} \frac{G_{\mathrm{p+1,m}}^{(t)} - G_{\mathrm{p,m}}^{(t)}}{\Delta r} \right) - \frac{V_{\max} G_{\mathrm{p,m}}^{(t)}}{K_{\mathrm{M}} + G_{\mathrm{p,m}}^{(t)}} = 0. \tag{3.52}$$

3.4. Software architecture

When modeling computer systems, it is common first to examine a mathematical model of a bioreactor system. Then the numerical model is constructed

(differential scheme) and implemented. The software covers the finite difference method implementation to solve a system of partial differential equations. For each simulation in time, the one realization of bioreactors was obtained. The experiments are repeated for different parameter values. The literature review indicated that there is no open-source software for bioreactors with multiple layers modeling. Therefore, appropriate software was developed in the dissertation. This section the architecture and basic algorithms of the developed software are presented. The components are divided into several areas according to their responsibilities. In the diagram in Figure 3.2, they are represented by UML packages. We employ the language R for visualization of the results of simulations as well as for running the parallelization of simulations. R, as an open-source language, has several parallel computing packages created by the open-source community. As shown in this diagram, the R package was the main block which provided the user interface. The code wrapper between the R and C++ was implemented as a separate component, which are the bridge between the solver and the R package. The explict_solver and Rcpp components are implemented as software libraries in `C++`. In order for a user to have the easy manipulation and visualization of simulations outputs the features provided by him, programs we implement in the user interface.

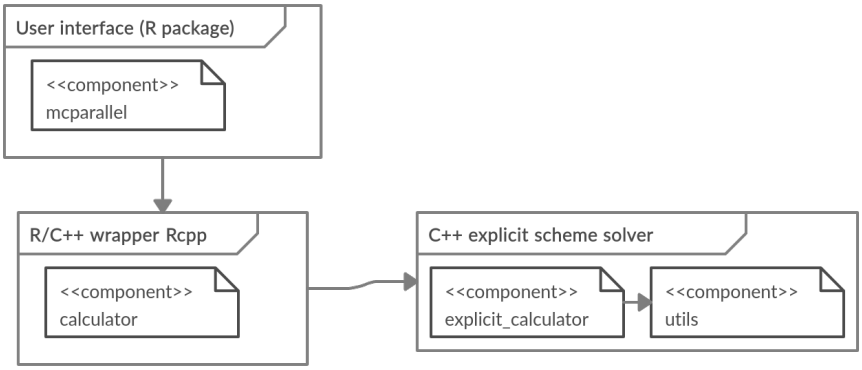

Figure 3.2: The structure of bioreactor model system. The UML diagram present aggregated scheme.

The output of the simulation results in the system is performed at a certain time events. Some results are to be reported periodically as for example, changes in concentration by the biosensor over time, others at the end of it or at some point in its execution. Such systems usage scenarios created a system data output subsystem that relies on the main R package control mechanism for announcing events. In addition, explicit_scheme component is implemented that have specific non-stability checking procedures. Such composite components allow invalid simulations due to stability issues to be reported time or frequency

of withdrawal.

3.5. Parallel computations

The numerical computations take some time to find a solution. However, even a small required time for a single computation can add up to huge total time if a large number of computations are performed sequentially. One of the most important strategies to achieve the required performance when solving the numerical models is to take advantage of parallel computing. Nowadays, even basic computers come with multiple cores (physical or virtual), and commonly with several central processing units (CPUs).

We only use the widely used `parallel` package, although there are other alternatives, such as the packages `foreach` and `doParallel`. The main function in the `parallel` package for parallel computing is the `mclapply` function, which performs the same task as `lapply`[1] but in parallel. The `lapply` method applies function $f(.)$ for the given (argument) parameter list $p = (p_1, p_2, ..., p_N)$ and produces the list $y = (f(p_1), f(p_2), ..., f(p_N))$. Since tasks are independent, calculations are parallelizable.

R offers relatively poor performance of running R code in comparison of (relatively) low level programming languages like `C++`. Fortunately, the `Rcpp` package in R allows the user to create and call functions in `C++`. Author used R versions 3.2-3.4.4.

Figure 3.3 demonstrates the characteristics of the simulation parallelization. The speed up for 2–4 cores in comparison to 1 core (see Figure 3.3). It is worth to mention that personal PC (3rd generation i5) with 4 cores was used for simulations. As can be seen from the given tasks, if the number of cores is larger than 4, the speed up becomes insignificant due to the employed hardware.

3.6. Formulation of optimal configuration search

For each fixed set of system configuration parameters (hyper-parameters), for example, concentration s_0, radius e_0, ect., we get a different physical representation of a real microbioreactor construction. If we would like to find preferable configurations of a microbioreactor which have some desired properties, or we would like to find the unknown optimal parameters (configuration) of the system, we should solve the optimization task. Since there are multiple hyper-parameters, we would have the multi-objective optimization task [119]. In this Section we will show how we can formulate the optimization task to find preferable configurations of a microbioreactors system.

[1] lapply is package R function which applies given function g to given data points independently.

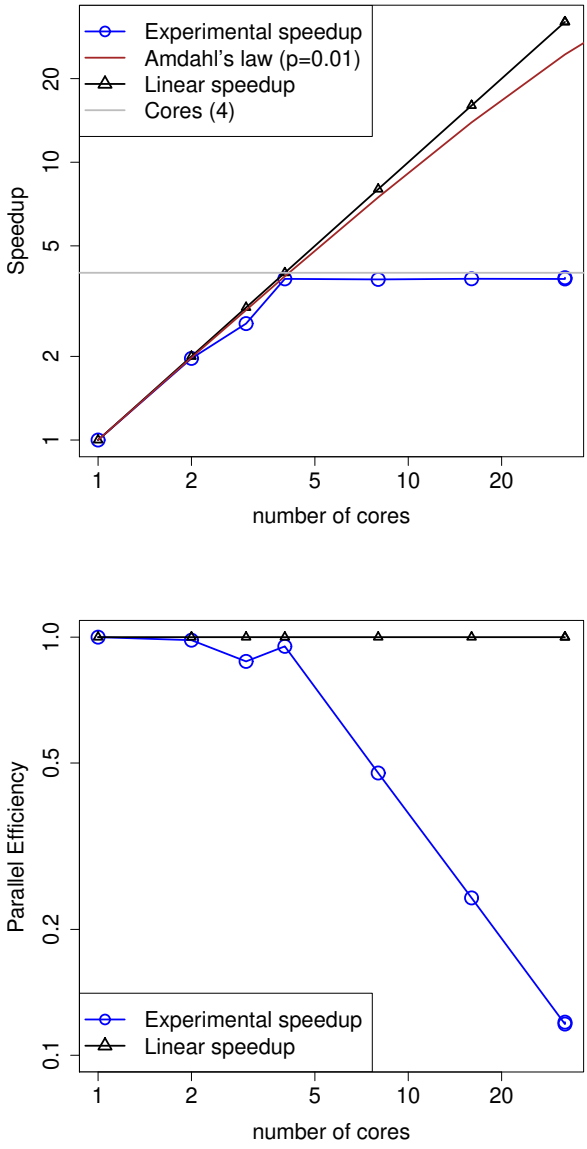

Figure 3.3: Speed up and parallel efficiency of the R parallel package.

A minimization of time-cost is often sought by the designers of biotechnological processes [59, 105]. The batch time required to achieve a certain conversion of the reactants is usually assumed as the main characteristic of the process duration [44]. The bioreactor should convert as much substrate as possible within the shortest possible time. In some applications of bioreactors,

enzymes are available only in microgram to milligram quantities and are very expensive [44, 112]. In such applications, the minimization of the enzyme usage is of crucial importance.

3.6.1. Formulation of three-objective optimization problem

In the case of a biocatalytic microbioreactor described in Section 2.2 and shown in Figure 1.1, the amount of the enzyme loaded into the MR is equal to the product of the initial enzyme concentration e_0 and the microbioreactor volume ($V_r = 4\pi r_0^3/3$). $V_{max} = k_{cat} e_0$, where and k_{cat} is the turnover number. The amount of enzyme loaded into all the microbioreactors placed into the container equals to $e_0 V_r N$, where N is the number of microbioreactors.

For the optimization task, without losing generality, the volumetric density N_V of microreators placed in the container ($N_V = N/V$) can be used instead of the total number $N = 3V/(4\pi r_2^3)$ of microbioreactors. Thus, the amount of enzyme used in N_V microbioreactors (used per volume unit of the container) equals to $e_0 V_r NV = e_0 V_r N/V = e_0 4\pi r_0^3/3 \times 3/(4\pi r_2^3) = e_0 r_0^3/r_2^3$. Accordingly, the amount of the substrate in the bulk per volume unit of the container can be expressed as follows: $s_b \times 4\pi(r_2^3 - r_1^3)/3 \times 3/(4\pi r_2^3) = s_b(r_2^3 - r_1^3)/r_2^3$.

The optimal design of the batch reactor mathematically is stated as a multi-objective optimization problem with three objective functions:

$$\begin{aligned} \varphi_1(r_0, e_0, s_0, r_2) &= t_{0.9} = \{t : s_b(t) = 0.1 s_0\}, \\ \varphi_2(r_0, s_0, r_2) &= 0.9 s_0 \frac{r_2^3 - (r_0 + h_1)^3}{r_2^3}, \\ \varphi_3(r_0, r_0, r_2) &= \frac{e_0 r_0^3}{r_2^3}, \end{aligned} \tag{3.53}$$

where $\varphi_1(\cdot)$ stands for the batch time $t_{0.9}$ required to convert 90% of the initial amount of the substrate [A1], $\varphi_2(\cdot)$ is the amount of the substrate per volume unit converted to the product, and $\varphi_3(\cdot)$ is the total amount of the enzyme used per volume unit of the bioreactor. The first and third objectives should be minimized while the second one should be maximized.

The appropriate intervals of the decision variables for the optimal design problem are given in Table 3.6. Assuming the highly stirred reactor, the thickness h_1 of the diffusion shell can be assumed as a constant parameter [A1,A3]. The radius r_2 of the unit cell can be expressed via the (independent) decision variables r_0, h_2 , and the parameter h_1 as follows: $r_2 = r_0 + h_1 + h_2$.

Additionally, only the bioreactor configurations with reasonable batch time were considered. If the time required to convert 90% of the initial amount of the substrate had been less than the time limit $T_{max} = 10^4$ (i.e., $t_{0.9} \leqslant 10^4$ s), the

Table 3.6: Decision variables $x = (r_0, h_2, e_0, s_0)^T$ for the bioreactor design problem

Variable	Description	Range	Units
r_0	MR radius	$[10^{-4}, 10^{-3}]$	m
h_2	Convective shell thickness	$[10^{-4}, 10^{-3}]$	m
e_0	Enzyme concentration	$[10^{-8}, 10^{-4}]$	M
s_0	Substrate concentration	$[10^{-5}, 10^{-1}]$	M

bioreactor configuration would have been considered as acceptable [44, 112]. Otherwise, the problem solution was excluded from a further analysis.

The considered optimization problem is three-objective (3.54) with four decision variables (Table 3.6). The variables in the problem description were defined in physical units. The equations of the mathematical model are well conceivable when variables are presented in natural units; however, the feasible values of variable in this case differ in several orders. Since the transition to the logarithmic scale facilitates the proper partitioning of the feasible region by the considered optimization algorithm, the variables should be re-scaled. The new variables are: $x = (x_1, \ldots, x_4)^T, x_1 = \lg r_0, x_2 = \lg e_0, x_3 = \lg s_0, x_4 = \lg h_2$, and the potential feasible region is

$$A = \{x : -4 \leqslant x_1, x_4 \leqslant -3, -8 \leqslant x_2 \leqslant -4, -5 \leqslant x_3 \leqslant -1\}. \qquad (3.54)$$

The optimization algorithm could use the internal scales where the variables vary in the interval $[0, 1]$. We used the term 'potential' in the definition of A since some infeasible subsets of A remain not defined explicitly. The infeasibility is determined during the simulation of the bioreactor action, meaning that the reactions in bioreactor are not completed during the time limit $T_{\max}$, i.e., $t_{0.9} > T_{\max}$. Since a returned undefined function value can crash the optimization process, the algorithm computing the objective functions was stopped by reaching the predefined bioreactor batch time $t_{0.9} = T_{\max}$ and returned the values of the objective functions corresponding to the maximum feasible simulation time.

3.6.2. Formulation of the bi-objective optimization problem

A graphical presentation of the Pareto front of the bi-objective optimization problems excellently aids the decision makers to compare quantitatively the available alternatives before decision making. However, in the case of a three objective problem, similar 3D graphs are rather useful for a qualitative illustration of the Pareto front than for the tradeoff between potential decisions. Fortunately, the considered problem (3.54) can be reduced to several bi-objective problems. The structure of the considered optimization problem is favorable

to reformulation which not only reduces the number of objectives but also the number of variables. The idea is the following: let us fix several favorable values of the third objective function, and compute and draw the Pareto fronts of the modified, bi-objective, optimization problems. An appropriate solution can be found by interpolating between the drawn fronts. Let us reformulate the original optimization problem by introducing a new independent variable r_2 . Variable h_2 then becomes dependent and is expressed through the variables r_2 , r_0 and the constant parameter h_1, $h_2 = r_2 - r_0 - h_1$. Instead of functions $\phi(\cdot)$, we will consider their (decimal) logarithms:

$$\begin{aligned} &\min_{x\in A} F(x), \qquad F(x) = (f_1(x), -f_2(x), f_3(x))^T, \\ f_1(x) &= \lg \varphi_1(x), \\ f_2(x) &= \lg \varphi_3(x) = \lg 0.9 + x_3 + \lg(10^{3x_4} - (10^{x_1} + h_1)^3) - 3x_4, \\ f_3(x) &= \lg \varphi_3(x) = x_2 + 3x_1 - 3x_4, \end{aligned} \tag{3.55}$$

where $x_1 = \lg r_0$, $x_2 = \lg e_0$, $x_3 = \lg s_0$ and $x_4 = \lg r_2$.

The feasible region is expressed by the bounds defined by the original independent variables

$$\begin{aligned} A = \{x: \quad & -4 \leqslant x_1 \leqslant -3, -8 \leqslant x_2 \leqslant -4, -5 \leqslant x_3 \leqslant -1, \\ & \lg(2.6) - 4 \leqslant x_4 \leqslant \lg(2.06) - 3\}. \end{aligned} \tag{3.56}$$

Let us fix an appropriate value of $f_3(\cdot)$, so that $E = f_3(x)$. The last equation of (3.56) then can be rewritten in the following form:

$$x_4 = x_1 + (x_2 - R)/3, \tag{3.57}$$

meaning that the number of independent variables can be reduced to three, and the optimization problem (3.56) can be reduced to the following bi-objective parametric minimization problem:

$$\min_{x\in A} F(x), \qquad F(x) = (f_1(x), -f_2(x))^T, x = (x_1, x_2, x_3)^T, \tag{3.58}$$

where the feasible region X of three independent variables is defined as follows:

$$\begin{aligned} A = \{&x: -4 \leqslant x_1 \leqslant -3, -8 \leqslant x_2 \leqslant -4, -5 \leqslant x_3 \leqslant -1, \\ &E/3 - 4 + \lg(2.6) \leqslant x1 + x2/3 \leqslant E/3 - 3 + \lg(2.06)\}. \end{aligned} \tag{3.59}$$

The reformulated problem is more convenient for an analysis since the number of variables and objectives is smaller than in the original problem. The time consuming computation of the first objective $f_1(\cdot)$ remains the main difficulty of the problem. However, an acceptable solution can be achieved with

a smaller number of the evaluations of the objective functions because of the reduced dimensionality.

The optimization of microbioreactors following such formulation can be found in publication [A4].

Conclusions

The analytical solutions at limiting cases have been delivered for bioreactor based on microbioreactors. For the given analytical expressions, explicit characteristics like effectiveness can be calculated analytically too, which can be useful in investigating various properties of microbioreactor systems.

The analysis of approximations delivered by the homotopy perturbation method has demonstrated various flaws of the method. First, we selected multiple models by inserting the small parameter in different parts of equation. We demonstrate that just applying the method could lead to invalid expressions, for example, an approximation could provide negative concentrations. We also demonstrated that diferent introduction of the small parameter give errors which vary by few magnitude of order (see Table 3.1). We also show that for fixed set of configuration, approximation could be sufficient. Overall, we show that, in order to use the approximations provided by HPM, the solutions should be measured, for example, by calculating the total error.

In order to find the most preferable configurations in bioreactors design, the optimization task needs to be considered. To address this, the mathematical formulation of the multi-objective optimization problem was formulated. The formulated task involves optimization of bioreactor geometries (volumes of the bioreactor) as well as the consumed enzyme quantity. Such a formulation of the optimization task can be expanded to find preferable configurations of microbioreactors.

The main conclusions from this Chapter:

1. The analytical solutions (3.13)–(3.14) at limiting cases have been delivered [A3].

2. The analytical approximations by Homotopy perturbation method at limiting cases have been delivered.

3. The limitations of Homotopy perturbation method was identified and recommendations were provided [A6].

4. The mathematical model of multi-objective optimization problem for optimal configuration was delivered, the model was published [A4]

In this Chapter the limited cases of microbioreactors were analysed analytically. In next Chapter the numerical analysis of all considered models is presented.

4. Application of Computational Models to Investigate Bioreactors Properties

As it was described in Chapter 1, mathematical modelling can be efficiently used to improve the process of new bioreactor creation, as well as the improvement of the existing ones. In this Chapter the numerical investigation of models defined in Chapter 2 is presented. The results of this Chapter are from publications [A1–A4].

The proposed model of a microbioreactor with carbon nanotubes catalysts shows the suitability with experimental data.

4.1. Continuous-flow stirred tank reactors properties

The non-linear initial boundary value problem (2.14)–(2.8) can be analytically solved only for specific values of the model parameters [6, 44, 102]. Therefore, the problem was solved numerically, using the finite difference technique [29]. In the space direction r, both segments $[0, r_0]$ and $[r_0, r_1]$ were divided into the same number N of small intervals. A uniform discrete grid was also introduced in the time direction t. An explicit finite difference scheme has been built as a result of the difference approximation [29]. Although explicit difference schemes have the strict stability limitations, these schemes have are simple for programming [28, 29].

Each segment was divided into 120 equal intervals. To make the difference scheme stable, the time step size τ was chosen from the sufficient stability conditions $\tau \leq \min\left(\min\{h_{\mathrm{m}}^2, h_{\mathrm{d}}^2\}/(2\max\{\mathrm{D_m}, \mathrm{D_d}\})\,, K_{\mathrm{M}}/(2V_{\max})\right)$, where h_{m} and h_{d} are the space step size of a microbioreactor and Nernst layer, respectively [11].

In the numerical simulation, the steady-state time t_{ss} was chosen as the earliest time when the normalised change of the substrate concentration remains very small during a relatively long term, i.e.,

$$t_{\mathrm{ss}} = \min_{t>0}\left\{ t : \frac{t}{s_0}\left| \frac{\mathrm{d}\left((3/r_0^3)\int_0^{r_0} s_{\mathrm{m}}(r,t)\, r^2 \mathrm{d}r + (3/(r_1^3 - r_0^3))\int_{r_0}^{r_1} s_{\mathrm{d}}(r,t)\, r^2 \mathrm{d}r\right)}{2\mathrm{d}t}\right| < \varepsilon \right\}, \tag{4.1}$$

$$\begin{aligned} s_{\mathrm{m,s}}(r) &\approx s_{\mathrm{m}}(r, t_{\mathrm{ss}}), \quad r \in [0, r_0], \\ s_{\mathrm{d,s}}(r) &\approx s_{\mathrm{d}}(r, t_{\mathrm{ss}}), \quad r \in [r_0, r_1]. \end{aligned} \tag{4.2}$$

Moreover, the decay rate $\varepsilon = 10^{-3}$ was used in the calculations.

The numerical solution of the problem (2.14)–(2.8) was validated by using exact analytical solutions for special cases of the model parameters when the nonlinear model approaches its linear counterpart [15, 44, 63, 109] at different values of the model parameters, $V_{\max}$, h and s_0. The percentage error was less than 1%.

In all the numerical experiments the following typical values of the model parameters were kept constant [3, 41, 44],

$$\begin{gathered} \mathrm{D_d} = 600\,\mu m^2/s, \quad \mathrm{D_m} = 200\,\mu m^2/s, \quad K_\mathrm{M} = 100\,\mu M, \\ r_0 = 250\ \mu m, \quad \phi = 0.6. \end{gathered} \tag{4.3}$$

Figure 4.1 shows the dynamics of the substrate concentration calculated for moderate concentration of the substrate ($s_0 = K_\mathrm{M}$, $S_0 = 1$), the diffusion shell thickness h of 60 μm, and the following two values of the maximal enzymatic rate $V_{\max}$: 1 and 10 μM/s. The points calculated at $s_0 = 100\,\mu$M, $h = 60\ \mu m$ and two values of $V_{\max}$ are 1 (in Fig. 4.1a) and 10 μM/s (in Fig. 4.1b). The other parameters are as defined in (4.3). The displayed numbers near arrows indicate time in seconds.

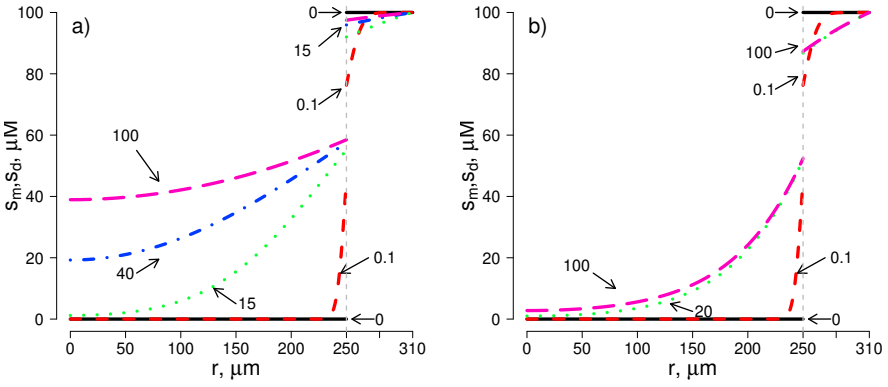

Figure 4.1: Profiles of the substrate concentration at different time (t)

Applying model parameter values defined in (4.3), the maximal enzymatic rates $V_{\max} = 1$ μM/s (Figure 4.1a) and $V_{\max} = 10$ μM/s (Figure 4.1b) correspond to the following two approximate values of the diffusion module σ: 1.8 and 5.6. Since the substrate concentration (s_0 and S_0) and the Biot number $\beta = 15.5$ were the same in both numerical experiments, Figure 4.1 illustrates mainly the effect of the diffusion module σ on the concentration within the MR as well as on the effectiveness of the MR.

For model parameter values $S_0 = 1$, $\beta = 15.5$ and $\sigma = 1.8$ (Figure 4.1a) used in the simulations, the calculated effectiveness factors are as follows: η_i

= 0.92, η_e = 0.99, η_p = 0.75, η_o = 0.68, while at a greater value of $\sigma = 5.6$ (Figure 4.1b) they become: η_i = 0.55, η_e = 0.93, η_p = 0.74, η_o = 0.38, i.e. a greater value of σ corresponds to a lower effectiveness of the MR. On the other hand, the numerical experiments showed that increasing of the diffusion module σ leads to decreasing of the holding time, e.g., $T_h = 0.85$ ($t_h = 266$ s) at $\sigma = 1.8$ and T_h = 0.146 ($t_h = 45$ s) at $\sigma = 5.6$. These effects are investigated in detail below.

In most numerical experiments carried out, the holding time t_h was significantly greater than the steady state time t_{ss}. When the steady state is reached, the substrate concentration $s_m(r,t)$ as well as the enzyme reaction rate $v(s_m(r,t))$ stays unchanged with time, i.e., $v(s_m(r,t)) = v(s_{m,s}(r))$ for $t > t_{ss}$. Because of this, the time t_h can be evaluated from the concentrations calculated as follows:

$$\begin{aligned} t_h &\approx \Big\{ t : \int_0^{t_{ss}} \int_0^{r_0} v(s_m(r,t))\, r^2 \,\mathrm{d}r\,\mathrm{d}t + \\ &\quad (t - t_{ss}) \int_0^{r_0} v(s_{m,s}(r))\, r^2 \,\mathrm{d}r = \frac{(r_1^3 - r_0^3) s_0}{3} \Big\} \\ &= t_{ss} + \Big(\frac{(r_1^3 - r_0^3) s_0}{3} \\ &\quad - \int_0^{t_{ss}} \int_0^{r_0} v(s_m(r,t))\, r^2 \,\mathrm{d}r\,\mathrm{d}t \Big) \Big/ \int_0^{r_0} v(s_{m,s}(r))\, r^2 \,\mathrm{d}r . \end{aligned} \tag{4.4}$$

4.1.1. Impact on effectiveness

To investigate the impact of the diffusion limitations on the MR effectiveness, the factor η_o was numerically calculated for different values of the diffusion module σ, the Biot number β, and the dimensionless substrate concentration S_0. Figure 4.2 shows the factor η_o versus σ and β at the dimensionless substrate concentration $S_0 = 1$.

As one can see in Figure 4.2, the overall effectiveness factor η_o increases with decreasing of the diffusion module σ and approaches to a constant value, which is approximately the same for all values of the Biot number β.

In the case of a low substrate concentration ($S_0 \ll 1$) and small values of σ, such that $\coth(\sigma) \approx (1/\sigma + \sigma/3)$, according to (3.9), the factor η_o approaches to ϕ for all possible values of β, i.e. $\eta_o \approx \phi$ for $S_0 \ll 1$ and $\sigma < 1$. Figure 4.2 shows that η_o approaches the maximum that is slightly higher than ϕ, specifically, $\eta_o \to 0.75 > \phi = 0.6$. This is due substrate concentration ($S_0 = 1$) used in the simulation. On the other hand, it was already shown that at very high concentrations ($S_0 \gg 1$) of the substrate, the effectiveness factor η_o approaches to unity. Figure 4.2 also shows that the impact of the Biot number β on the factor η_o is significant only when $\sigma > 1$, i.e., when the MR action is under diffusion control. The effect of β increases with increasing σ.

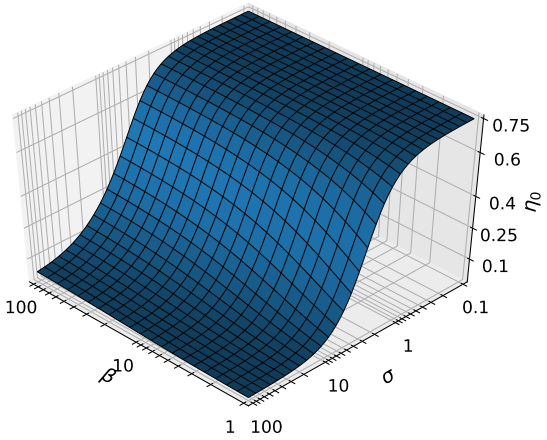

Figure 4.2: The overall effectiveness factor η_o vs. the diffusion module σ and Biot number β

To determine the influence of the substrate concentration on the effectiveness of MR, the overall effectiveness factor η_o was calculated for a wide range of values of the substrate concentration. Figure 4.3a shows the factor η_o versus the dimensionless concentration S_0 and diffusion module σ at a mean value of the Biot number, $\beta = 10$, and Figure 4.3b shows η_o versus S_0 and β at a mean value of the diffusion module $\sigma = 1$.

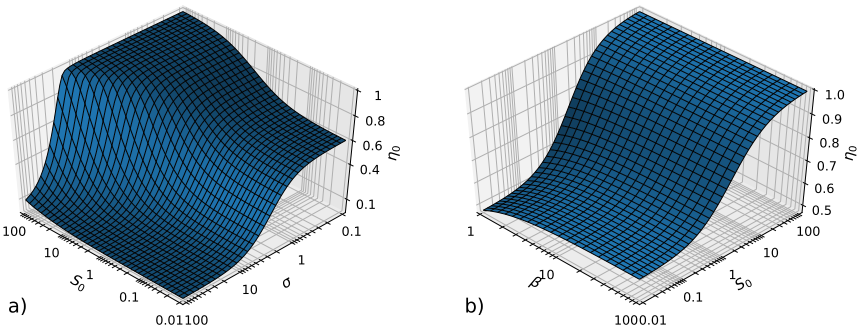

Figure 4.3: The overall effectiveness factor η_o vs. the dimensionless concentration S_0 changing the diffusion module σ (a) and changing the Biot number β (b)

Figures 4.2 and 4.3 show that the MR effectiveness can be notably increased by increasing the substrate concentration S_0 as well as by decreasing the diffusion module σ, i.e., by decreasing the intraparticle diffusion resistance. The effectiveness can be also but slightly increased by increasing the Biot number β, i.e., by decreasing the external diffusion resistance. In the case of low substrate concentration ($S_0 \ll 1$), it can be noticed that η_o is a monotonic increasing

function of β (see (3.9)).

In particular, Figures 4.2 and 4.3a demonstrate that the MR effectiveness η_o is a monotonic decreasing function of the diffusion module σ and practically stagnates at its maximum value when $\sigma < 1$, i.e., η_o is practically invariant to σ when the enzyme kinetics controls the MR action. Having a MR which action is controlled by the enzyme kinetics ($\sigma < 1$), its effectiveness can not be further increased by decreasing of the internal diffusion resistance.

Increasing the internal effectiveness factor η_i by decreasing the diffusion module σ (Thiele module or Damköhler number) has been already reported for the first-order enzyme kinetics i.e., ($S_0 \ll 1$) [41, 109]. The dependence of the external effectiveness factor η_e on the Biot number β defined through the external mass transfer coefficient is also already known [3]. Figures 4.2 and 4.3 show the overall effectiveness factor versus a wide ranges of three parameters σ, β, and S_0. Figure 4.3 exclusively shows how the MR effectiveness changes when the enzyme kinetics changes from the zero-order kinetics ($S_0 \ll 1$) to the first-order ($S_0 \gg 1$) kinetics.

4.1.2. Impact on process duration

To determine the influence of the diffusion limitations and the initial substrate concentration on the process duration, the MR action was simulated and the dimensionless holding time T_h was calculated by changing values of the diffusion module σ, the Biot number β and the dimensionless substrate concentration S_0. Figure 4.4 shows calculated values of the time T_h versus σ and β at the dimensionless concentration $S_0 = 1$. The dependence of T_h on the substrate concentration is presented in Figure 4.5.

As one can see in Figure 4.4, the time T_h increases with decreasing both, the diffusion module σ and the Biot number β. Figure 4.4 also shows that the impact of the Biot number β on the time T_h is notable only when $\sigma > 1$, i.e. when the MR action is under diffusion control.

To determine the influence of the substrate concentration om the process duration, the MR action was simulated and the dimensionless time T_h was calculated for a wide range of values of the substrate concentration. Figure 4.5a shows the time T_h versus the dimensionless concentration S_0 and diffusion module σ at a mean value of the Biot number, $\beta = 10$, and Figure 4.3b shows T_h versus S_0 and β for a mean value of the diffusion module $\sigma = 1$.

One can see in Figure 4.5 a nonlinear increase in the time T_h while increasing the substrate concentration S_0. The time T_h is particularly high at low values of the diffusion module σ, i.e., when the enzyme kinetics controls the MR action. So, increasing the MR effectiveness by decreasing the internal diffusion limitation i.e., (decreasing σ) as well as by increasing the substrate concentration when a short processing time is of crucial importance. The impact

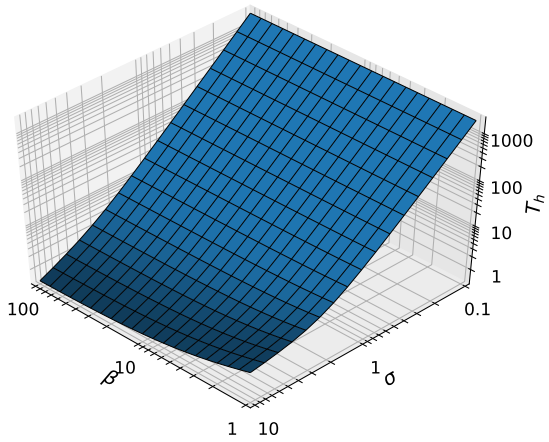

Figure 4.4: The dimensionless holding time T_h vs. the diffusion module σ and Biot number β .

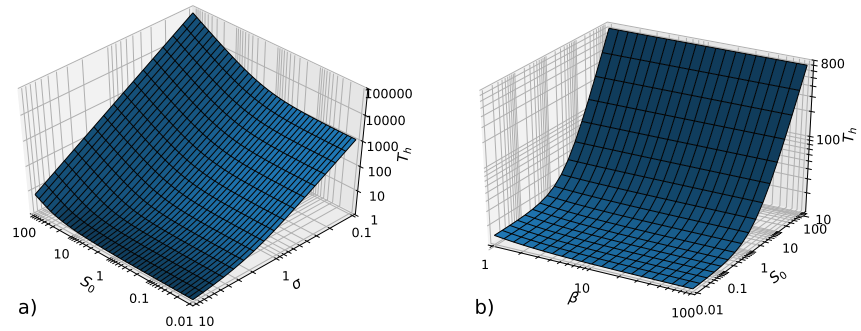

Figure 4.5: The dimensionless holding time T_h vs. the dimensionless concentration S_0 changing the diffusion module σ (a) and changing the Biot number β (b)

of the external diffusion resistance (β) on the time T_h is rather slight.

The complex nature of bioprocesses and microbioreactors leads to consideration of simultaneous optimization, of several objectives some of which are conflicting, i.e., if one of them is improved, the others get worse [70]. The multi-objective optimization together with the multi-dimensional visualization can be used for finding a trade-off solutions and making decisions when designing microbioreactors [A4].

Very recently, when analysing a stirred catalytic basket bioreactor for the production of bioethanol, it was observed that the time of the glucose consumption increases by increasing the glucose concentration in the bioreactor medium [58]. It was also observed that the time for consumption of glucose decreases with an increase in the stirrer speed. Particularly, when using the stirrer speed of 200 rpm and free cells as catalysts, the glucose consumption

time was nearly 20 h, while at 500 rpm the consumption time was about two times less [58]. Since the thickness of the Nernst diffusion layer for a flat surface decreases about $\sqrt{2.5}$ times when the stirrer speed increases 2.5 times and the radius of free cells is relatively small, the Biot number β then decreases about $\sqrt{2.5} \approx 1.6$ [14]. One can see in Figure 4.4 a similar decrease (about 2 times) in the holding time T_{h} when decreasing the Biot number in 1.6 times for small values of β. Figure 4.5 shows that the time T_{h} increases while increasing the substrate concentration, as it was observed in [58].

Figure 4.5 shows how the MR holding time changes when the enzyme kinetics changes from zero-order ($S_0 \ll 1$) to first-order ($S_0 \gg 1$) kinetics.

4.2. Batch stirred tank reactors properties

The nonlinear initial boundary value problem (2.14)–(2.23) was solved numerically, using the finite difference technique [29]. In the space direction r, the radius $[0, r_0]$ of a microbioreactor as well as the segment $[r_0, r_1]$ corresponding to the diffusion shell were divided into the same number N of subintervals. A uniform discrete grid was also introduced in the time direction t. An explicit finite difference scheme has been used as in Section 4.1.

The numerical solution of the problem (2.14)–(2.23) was validated by using the known numerical solutions obtained for similar BSTR systems, where the enzyme kinetics approaches the first-order kinetics and the external diffusion resistance is ignored ($h_1 = 0$, $\beta \to \infty$) [18, 20]. The solution was also compared with the exact analytical and approximate numerical solutions obtained for the corresponding CSTR system [A3].

In all the numerical experiments, the following typical values of the model parameters were kept constant [3, 41, 44]:

$$\begin{aligned} \mathrm{D_d} = 600\,\mu m^2/s, \quad \mathrm{D_m} = 200\,\mu m^2/s, \quad K_{\mathrm{M}} = 100\,\mu\mathrm{M}, \\ r_0 = 250\ \mu m, \quad \phi = 0.6\,. \end{aligned} \tag{4.5}$$

Figure 4.6 shows the dynamics of the substrate concentration and the transient effectiveness factors calculated for the diffusion shell thickness h_1 of $60\,\mu m$ ($r_1 = 310\,\mu m$), the convective shell thickness h_2 of $120\,\mu m$ ($r_2 = 430\ \mu m$), the maximal enzymatic rate $V_{\max}$ of $1\,\mu\mathrm{M/s}$, and the moderate initial concentration $s_0 = K_{\mathrm{M}} = 100\ \mu\mathrm{M}$. The dimensional parameters correspond to the moderate values of the dimensionless parameters as follows: the diffusion module $\sigma \approx 1.77$, the Biot number $\beta = 15.5$, the ratio $\alpha = 3$, the inverse adsorption capacity $\theta \approx 0.7$, and the initial concentration $S_0 = 1$. The MR system was simulated at $r_1 = 310\,\mu m$, $r_2 = 430\,\mu m$, $V_{\max} = 1\,\mu\mathrm{M}$, and $s_0 = 100\,\mu\mathrm{M}$. The other parameters are as defined in (4.5).

The evolution of the substrate concentration (Figure 4.6a) shows that the microbioreactor action finally approaches the steady state at the zero substrate

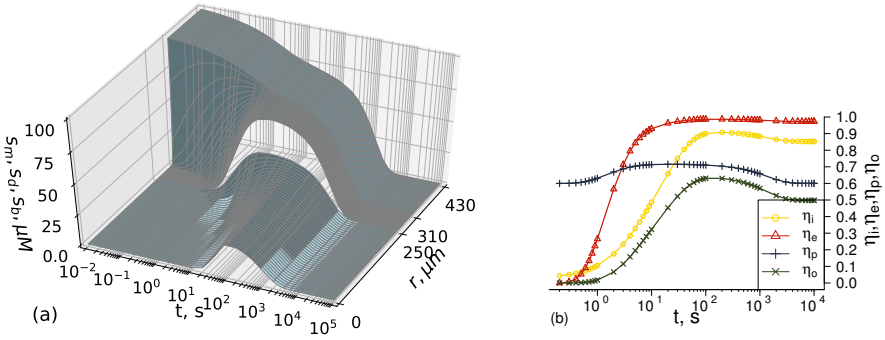

Figure 4.6: Evolution of the substrate concentration at different space points (a) and different transient effectiveness factors (b)

concentration in both MR and bulk. As one can see in Figure 4.6b, the steady state overall effectiveness factors fit well with the effectiveness factor values calculated by the formulas (1.15) and (3.9): $\eta_{\mathrm{i,ss}} = 0.839$, $\eta_{\mathrm{r,ss}} = 0.967$, $\eta_{\mathrm{p,ss}} = 0.6$ and $\eta_{\mathrm{o,ss}} = 0.487$.

Figure 4.6b shows a non-monotonic behaviour of all the transient effectiveness factors, though the substrate concentration in bulk continuously decreases (Figure 4.6a). All the effectiveness factors reach maximums after approximately the same time when the substrate concentration in the MR centre ($r = 0$) reaches its maximum ($t \approx 100\,\mathrm{s}$). After this time elapsed, the microbioreactor system approaches a pseudo-equilibrium state, where both substrate concentrations, in bulk and averaged in the MR, do change, but their relationship becomes constant [18]. In a similar well-stirred batch reactor with spherical porous catalyst particles obeying the first-order enzyme kinetics ($s_0 \ll K_{\mathrm{M}}$), the overall transient effectiveness factor was approximated as a monotonous increasing function of time [18, 19, 21]. The effect of non-monotony of the overall transient effectiveness factor is discussed in detail below.

4.2.1. Non-monotonicity of the overall transient effectiveness factors

The dynamics of the overall transient effectiveness factor η_{o}^* as a function of the dimensionless time T as follows:

$$\eta_{\mathrm{o}}^*(T) = \eta_{\mathrm{o}}^*\left(\frac{\mathrm{D_m}t}{r_0^2}\right) = \eta_{\mathrm{o}}(t)\,. \tag{4.6}$$

An example overall transient effectiveness factor dynamics can be see in Figure 4.7.

The effectiveness factor η_{o}^* was calculated at very different values of the initial dimensionless concentration S_0 of the substrate (Figure 4.7a), the dif-

fusion module σ (Figure 4.7b), the Biot number β (Figure 4.7c), the inverse adsorption capacity θ (Figure 4.7d), and the partition coefficient ϕ (Figure 4.7e). The other simulation parameters were the same as in the computational experiment shown in Figure 4.6. The solid red lines in Figure 4.7 show the particular case of the effectiveness factor η_{o}^{*} simulated exactly at the same values of the model parameters as in Figure 4.6. The values of the steady state overall effectiveness factor $\eta_{\mathrm{o,ss}}$ defined by (3.9) are depicted by solid black lines. The normalized substrate concentration S_{b}/S_0 in bulk is represented by colouring the effectiveness surface.

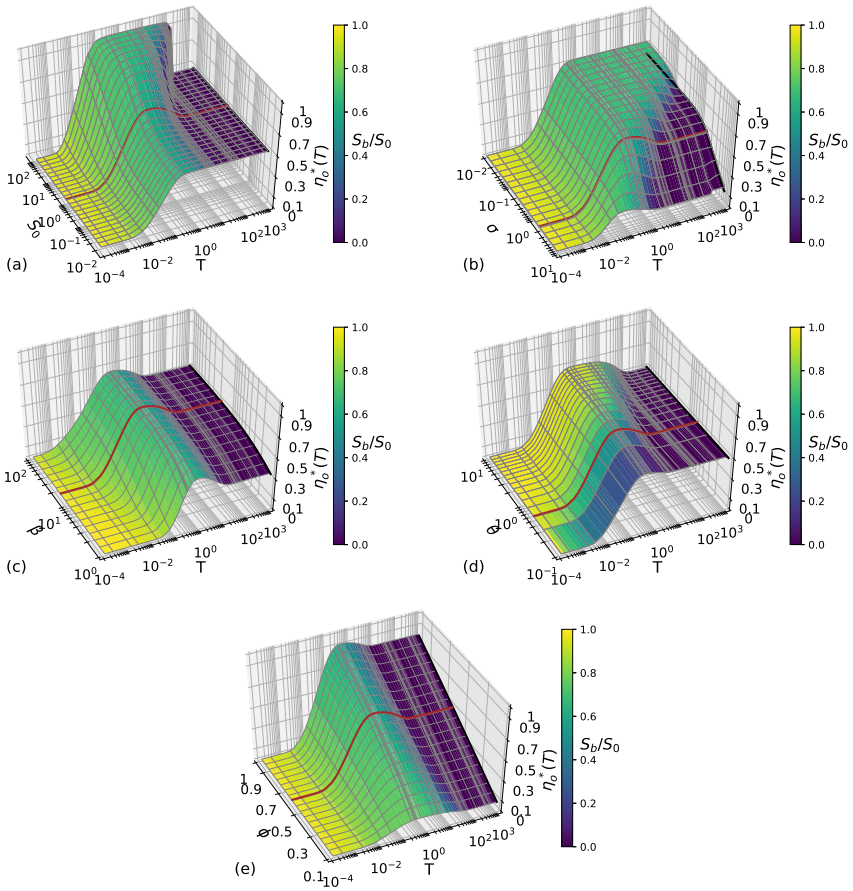

Figure 4.7: The overall transient effectiveness factor η_{o}^{*} at different values of the dimensionless substrate concentration S_0 (a), the diffusion module σ (b), the Biot number β (c), the ratio θ (d) and the partition coefficient ϕ (e)

As one can see in Figure 4.7a, the overall transient effectiveness factor reaches the steady state noticeably faster at low substrate concentrations when the Michaelis-Menten kinetics approaches first-order kinetics ($S_0 \ll 1, s_0 \ll$

K_M), than at high concentrations, when the MR acts under the zero-order enzyme kinetics ($S_0 \gg 1, s_0 \gg K_M$). Moreover, at moderate and high concentrations the overall effectiveness factor $\eta_o^*(T)$ is a non-monotonic function of dimensionless time T, and the maximum is reached approximately at the same time, when the steady state effectiveness is reached at low concentrations. At high concentrations, the transient effectiveness factor η_o^* reaches its maximum and steadies at the highest effectiveness (η_o^* near to unity) for some time, later it drastically decreases and approaches the steady state value.

As for the CSTR acting under first-order enzyme kinetics ($S_0 \ll 1$), the steady state overall effectiveness factor $\eta_{o,ss}$ is invariant to the initial concentration of the substrate (Figure 4.7a) as described in the formula (3.9). $\eta_{o,ss}$ is also invariant to the ratio θ (Figure 4.7d).

Figures 4.7a and 4.7b show that the MR effectiveness for a certain time can be notably increased by increasing the initial substrate concentration S_0 as well as by decreasing the diffusion module σ, i.e., by decreasing the intraparticle diffusion resistance. Such impacts of S_0 and σ on the MR effectiveness has been already reported for the corresponding microbioreactor acting in the CSTR mode [A3].

As one can see in Figures 4.7c, the maximum transient as well as the steady state overall effectiveness factor can be slightly increased by increasing the Biot number β, i.e., by decreasing the external diffusion resistance. Both the maximal and the steady state overall effectivenesses, decrease with decreasing the partition coefficient ϕ (Figure 4.7e), i.e., by decreasing the porosity of catalyst particles. This feature of the steady state effectiveness factor $\eta_{o,ss}$ can be also noticed from the formula (3.9).

All the solid black lines in Figure 4.7 coincide with the final values ($T = 10^3$) of the transient effectiveness factor η_o^*, except the values simulated at the smallest values of the diffusion module, i.e., $\sigma < 0.1$. Further calculations ($T > 10^3$) showed that the $\eta_{o,ss}$ is achieved also for $\sigma < 0.1$, particularly, $\eta_{o,ss} \approx \eta_o^*$ at $T > 10^6$ for $\sigma = 0.01$. Figure 4.7 shows that the overall transient effectiveness factor η_o^* approaches its steady state value $\eta_{o,ss}$ and the formula (3.9) derived for CSTR system can also be applied for a BSTR system for an analysis of the steady state effectiveness.

4.2.2. Duration of the substrate reduction

The process duration is also among the most important characteristics of biotechnological processes [60]. A minimization of time-cost is often sought by the designers of biotechnological processes [106]. The batch time required to achieve a certain conversion of the reactants is usually assumed as the main characteristic of the process duration [44].

Colouring the effectiveness surfaces in Figure 4.7 shows how fast the

substrate is reduced while the biochemical reaction is taking place in the MR. The most noticeable influence on the duration of the substrate reduction comes from the diffusion module σ and the adsorption capacity (ratio θ).

As one can see in Figure 4.7d, the time required to convert 90% of the initial amount of the substrate ($S_b/S_0 = 0.1$) at $\theta = 10$ is by a few orders of magnitude greater than at $\theta = 0.1$. A tenfold decrease in the module σ leads to more than tenfold increase of the time required to convert a certain amount of the substrate (Figure 4.7b). A similar effect of the adsorption capacity on the duration of the substrate conversion has been observed in the heterogeneous bioreactors with porous catalyst particles and no external mass transfer resistance [19, 21].

Taking into account the influence of module σ and ratio θ on the process duration (Figures 4.7b and 4.7d), the increasing MR effectiveness by decreasing internal diffusion limitation (decreasing σ) as well as by decreasing the adsorption capacity (increasing θ) is restricted when a short substrate conversion time is of crucial importance. On the other hand, the influence of the main model parameters on the substrate reduction time is similar to that observed in the corresponding microbioreactor system acting in the CSTR mode [A3].

4.2.3. Ratio of maximum to the steady-state effectiveness

As it was shown above, at certain values of the model parameters the transient overall effectiveness factor η_o (as well as η_o^*) is a non-monotonic function of time. To investigate how much the maximum of the transient overall effectiveness factor can exceed the steady state overall effectiveness factor, their ratio G_η ($G_\eta \geq 1$) was calculated for different values of the model parameters,

$$G_\eta = \frac{\max\limits_{t>0}\{\eta_o(t)\}}{\eta_{o,ss}} = \frac{\max\limits_{T>0}\{\eta_o^*(T)\}}{\eta_{o,ss}}. \tag{4.7}$$

Figure 4.8 shows the gain ratio G_η versus the dimensionless initial substrate concentration S_0 and all other main parameters of the model (2.25)-(2.27): the diffusion module σ, the Biot number β, the ratio (inverse adsorption) θ, and the partition coefficient ϕ. The other simulation parameters were the same as defined in (4.5) and used in the computational experiment shown in Figure 4.6.

The simulation results depicted in Figure 4.8 confirm that the transient effectiveness factor η_o is a monotonic function of time when the Michaelis-Menten kinetics approaches the first-order kinetics ($S_0 \ll 1$) [20, 21]. When the enzyme reaction obeys the zero-order kinetics ($S_0 \gg 1$), the factor η_o is a non-monotonic function in most cases of parameter variation. Even at moderate initial substrate concentration i.e., ($S_0 \sim 1$), the effectiveness factor η_o may be non-monotonic function of time.

In addition to the initial substrate concentration, the diffusion module σ is another governing parameter noticeably influencing the monotony of the overall

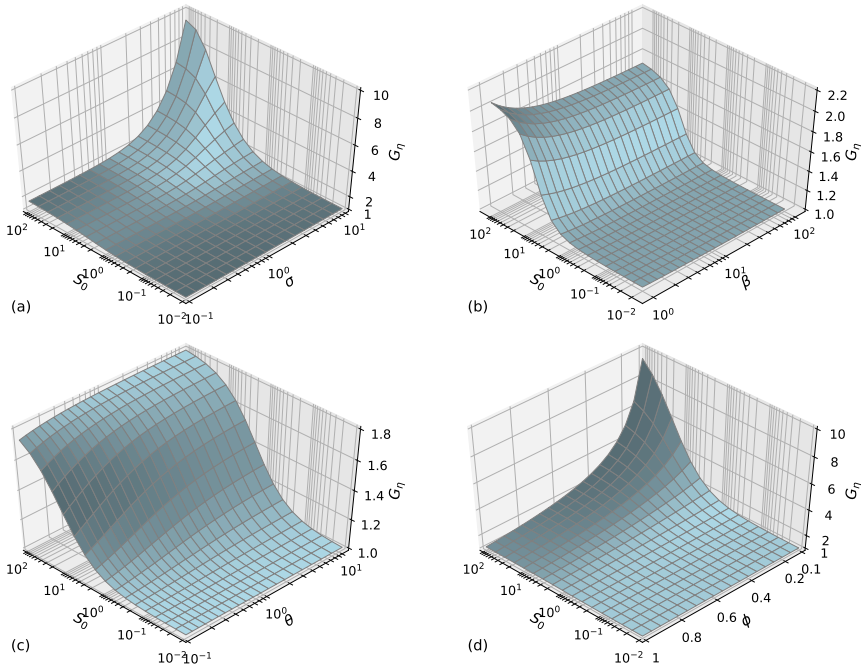

Figure 4.8: The dependence of the gain ratio G_η on the substrate concentration S_0 and other main model parameters: the diffusion module σ (a), the Biot number β (b), the ratio θ (c), and the partition coefficient ϕ (d)

transient effectiveness factor η_o. At a high substrate concentration ($S_0 = 100$), when the bioreactor action is under diffusion control ($\sigma = 10$), the maximum of the transient overall effectiveness factor exceeds the steady state overall effectiveness factor more than nine times ($G_\eta \approx 9.3$).

As one can see in Figure 4.8d, at high substrate concentrations ($S_0 > 1$) the gain ratio G_η increases while decreasing the partition coefficient ϕ. However, then the absolute value of the effectiveness factor is very low, as shown in Figure 4.7e, therefore the practical value of bioreactors of such a configuration is poor. The ratio G_η also increases while decreasing the Biot number β, i.e., by increasing the external diffusion limitation (Figure 4.8d). Figure 4.8c shows that the adsorption capacity especially affects the non-monotony of transient factor η_o at moderate concentrations of the substrate ($S_0 \sim 1$), i.e., when the enzyme kinetics changes from the first order to zero order.

4.3. Microbioreactors with carbon nanotubes properties

The mathematical model (2.33)–(2.23) has been defined as an initial boundary value problem. Due to nonlinearity of the reaction term (2.33), the problem was solved numerically using the finite difference technique [24, 28, 29]. The radius $[0, R_0]$ of the microbioreactor as well as the segment $[R_0, R_1]$ corresponding to the diffusion shell were divided into the same number $N = 120$ of subintervals. A uniform discrete grid was also introduced in the time direction t [A3],[A1]. The numerical simulator was programmed in C++ language [91].

The numerical solution of the problem was validated by using known analytical [18, 19] and numerical [A1] solutions obtained for specific cases of the model parameter values.

When the rate of one enzyme catalyzed process significantly predominates over the rate of another, one the conjugated two enzyme process (1.1) approaches to one enzyme catalyzed process. If $V_1(L_m) \ll V_2(O_m)$, then the quasi-steady-state reaction rate $V(L_m, O_m)$ of the conjugated process approaches to the rate $V_1(L_m)$. At the parameter values satisfying $V_1(L_m) \gg V_2(O_m)$, the rate $V(L_m, O_m)$ approaches to $2V_2(O_m)$. In those two very opposite cases the concentration dynamics of each substrate (lactose and oxygen) was quantitatively compared with the dynamics of the substrate concentration in the corresponding BSTR based on spherical mono catalyst particles [A1].

4.3.1. Simulation of experiments

The derived mathematical model was applied for simulation of physical experiments, performed at five initial concentrations L_0 of lactose: 2, 5, 10, 20 and 50 mM. The values of the model parameters were chosen as follows [93, 94]:

$$
\begin{aligned}
&\mathrm{K_L} = 9.6\,\mathrm{mM}, \quad V_\mathrm{L} = 0.019\,\mathrm{mM/s},\\
&\mathrm{K_O} = 0.5\,\mathrm{mM}, \quad V_\mathrm{O} = 1.170\,\mathrm{mM/s}, \quad O_0 = 0.25\,\mathrm{mM},\\
&\mathrm{D_{L,m}} = \mathrm{D_{P,m}} = 2.2\times10^{-10}\,\mathrm{m^2/s}, \quad \mathrm{D_{O,m}} = 0.67\times10^{-9}\,\mathrm{m^2/s},\\
&\mathrm{D_{L,d}} = \mathrm{D_{P,d}} = 6.6\times10^{-10}\,\mathrm{m^2/s}, \quad \mathrm{D_{O,d}} = 2.0\times10^{-9}\,\mathrm{m^2/s},\\
&R_0 = 225\,\mu m, \quad R_1 = 305\,\mu m, \quad R = 840\,\mu m, \quad \phi = 0.56.
\end{aligned}
\tag{4.8}
$$

The effective diffusion coefficients of all the species in the MR were derived from the typical values of the corresponding diffusion coefficients in the bulk by assuming, for each species, the same ratio of the diffusion coefficient in the bulk i.e., as the corresponding coefficient in the MR, $\mathrm{D_{L,d}}/\mathrm{D_{L,m}} = \mathrm{D_{O,d}}/\mathrm{D_{O,m}}$

= $D_{P,d}/D_{P,m} \approx 3$ [22, 37]. The partition coefficient ϕ was experimentally determined by calculating the void fraction of the MR [32]. The thickness $R_1 - R_0$ of the diffusion shell was adjusted to fit the experimental results. The fitted thickness $R_1 - R_0 = 80\,\mu m$ matches rather well with the diffusion layer thickness for a typical magnetic stirrer [14].

Oxygen as the substrate of laccase was experimentally detected using a selective Clark-type electrode [37]. When simulating the dynamics of the enzyme catalyzed process (1.1), the bulk concentration O_b of oxygen was assumed as the concentration corresponding to the response measured experimentally in a cell isolated from atmosphere [94].

Figure 4.9 shows the dynamics of experimental and simulated concentrations of oxygen. The inset presents the dynamics of the oxygen concentration in a linear scale only for the first 4000 s during which the physical experiments were taking place.

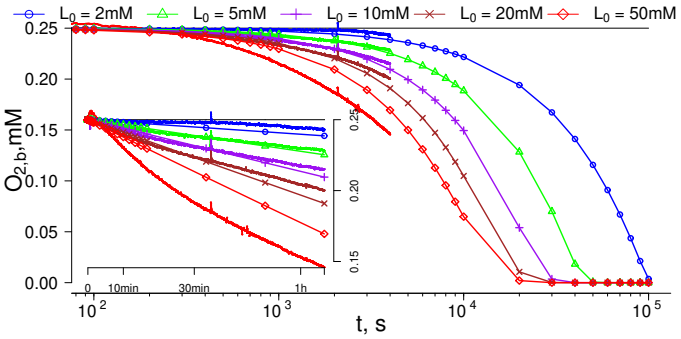

Figure 4.9: The dynamics of experimental and simulated concentrations of oxygen

Figure 4.9 shows that the mathematical model quite accurately reflects the physical experiments at moderate and low concentrations of lactose. For the lactose concentrations of 2, 5, 10 and 20 mM, the relative error between the numerical solution and the experiment data, averaged over the time from 0 up 4000 s, is less than 5%. However, at $L_0 = 50$ mM the relative modeling error approximates to 15%. Taking into consideration the instability of artificial catalyst and possible measurement errors, the achieved modeling errors can be considered as admissible [32, 72], therefore the model (2.33)–(2.23) can be used for investigating the kinetic properties and optimizing the configuration.

4.3.2. Dynamics of concentrations

Figure 4.10 shows the dynamics of the concentrations of lactose, oxygen, and product, calculated at the moderate initial concentration of lactose $L_0 =$ 10 mM $\approx K_L$. The other parameters are as defined in (4.8). The product

concentration is represented by colouring surfaces of the lactose (a) and oxygen (b) concentrations.

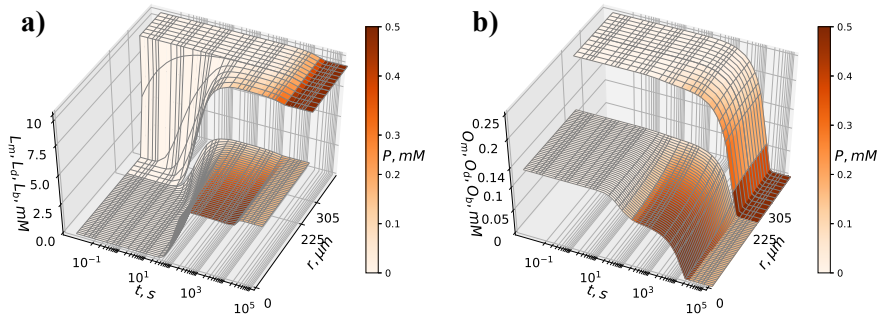

Figure 4.10: Evolution of the concentrations of lactose (a) and oxygen (b) at different space points

As one can see in Figure 4.10, practically whole oxygen has been consumed at $t \approx 3 \times 10^4$ s, while the lactose amount at that moment has been only slightly reduced. Figures 4.9 and 4.10 show that all the oxygen can be also reduced by exploiting significantly less amount of lactose than $L_0 = 10$ mM. However, decreasing the initial concentration L_0 of lactose noticeably reduces the rate of the oxygen reduction. One can see in Figure 4.9 that the time required for conversion of half of the oxygen (the half-time) is achieved in ≈ 1 h at 50 mM, ≈ 1.5 h at 20 mM, ≈ 2.5 h at 10 mM, ≈ 4.5 h at 5 mM, and in ≈ 12.5 h at 2 mM.

Figure 4.10 also shows that the maximal product concentration is achieved when approximately whole oxygen is consumed. The final concentration P_b of the product in the bulk becomes approximately equal to the double initial concentration O_0 of oxygen, $P_\mathrm{b}(t) \approx 2O_0 = 0.5$ mM when $t \to \infty$. The lactose concentration reduces only slightly, $L_\mathrm{b} \approx L_0 - 2O_0$, i.e., $L_0 - L_\mathrm{b}(t) \approx 2O_0 \approx P_\mathrm{b}(t)$ when $t \to \infty$. These approximate values also derived from the mathematical model (2.33)–(2.23).

The configuration (4.8) of the modeled bioreactor corresponds to the following values of the main dimensionless parameters: $\Phi_\mathrm{L} = 0.67$, $\Phi_\mathrm{O} = 13.3$, $\beta_\mathrm{L} = \beta_\mathrm{O} = 11.43$, i.e., the oxygen reduction acts under diffusion control $\Phi_\mathrm{O} > 10$.

4.3.3. Impact of lactose concentration on the effectiveness

The transient effectiveness factor η_t is presented in Figure 4.11 by changing the initial lactose concentration L_0 : (a) $\Phi_\mathrm{L} = 0.1$, (b) $\Phi_\mathrm{L} = 0.67$, (c) $\Phi_\mathrm{L} = 1$, (d) $\Phi_\mathrm{L} = 10$. The other parameters are the same as in Figure 4.10. The normalized oxygen concentration O_b/O_0 in the bulk is represented by colouring

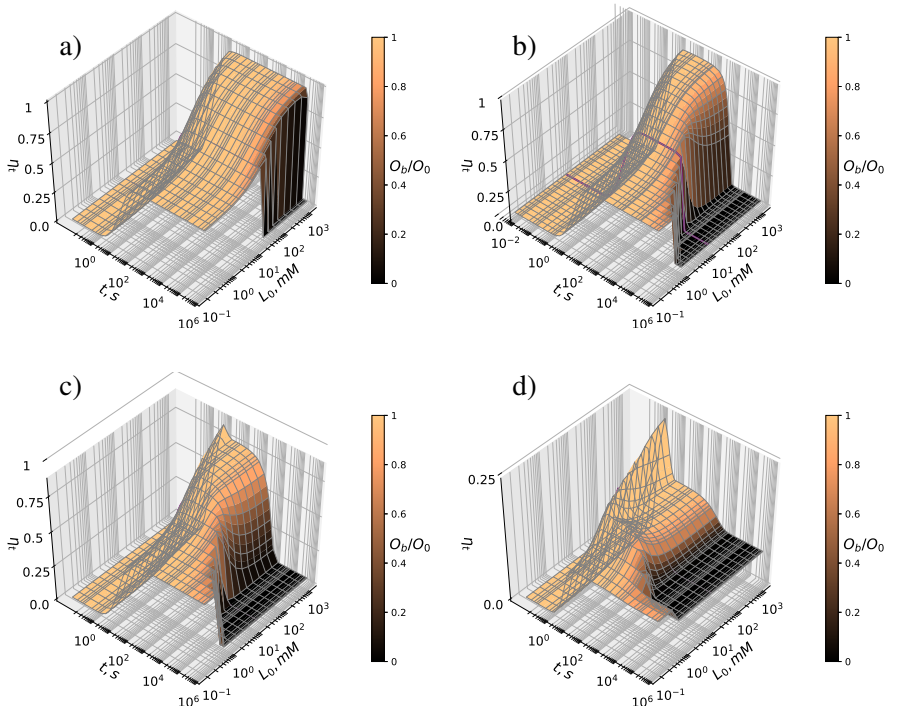

Figure 4.11: The transient effectiveness factor η_t when changing the initial lactose concentration L_0

the effectiveness surface. The solid violet line stands for a numerical experiment shown in Figure 4.10.

Figure 4.11b shows non-monotonic behaviour of the transient effectiveness factor η_t at high and moderate initial concentrations of lactose ($L_0 > 0.5$ mM = $2O_0$), while at low concentrations the effectiveness factor η_t is a monotonous increasing function of time. At any concentration of lactose the transient effectiveness factor $\eta_t(t)$ finally ($t \to \infty$) approaches its steady state value.

As one can see in Figure 4.11b, the transient effectiveness reaches the steady state noticeably faster at low lactose concentrations ($L_0 \lesssim 2O_0$) than at higher concentrations. Moreover, at high concentrations the effectiveness factor reaches its maximum approximately at the same time when the steady state effectiveness is reached at low concentrations. At high concentrations, the effectiveness factor reaches its maximum and steadies at the highest value (near to unity) for some time, later it drastically decreases and approaches a steady state value.

As it was mentioned above, when the first process (1.1a)–(1.1b) predominates ($V_1(L_\mathrm{m}) \gg V_2(O_\mathrm{m})$) in the conjugated two enzymes catalyzed process (1.1), the conjugated process operates under oxygen limited conditions, and the rate $V(L_\mathrm{m}, O_\mathrm{m})$ becomes almost invariant to the lactose concentration,

$V(L_\mathrm{m}, O_\mathrm{m}) \approx 2V_2(O_\mathrm{m})$. In the opposite case, when the other process (1.1d)–(1.1c) predominates i.e., ($V_2(O_\mathrm{m}) \gg V_1(L_\mathrm{m})$), the rate $V(L_\mathrm{m}, O_\mathrm{m})$ which is almost invariant to the oxygen concentration, $V(L_\mathrm{m}, O_\mathrm{m}) \approx V_1(L_\mathrm{m})$ (see Figure 4.11a- 4.11d).

The conjugated process (1.1) starts i.e., ($t = 0$) under lactose limited conditions because the initial rate $V_2(O_0)$ at the model parameter values (4.8) is much greater than the rate $V_1(L_0)$, independently of the initial lactose concentration L_0, i.e., $V_2(O_0) \approx 1.17\,\mathrm{mM/s} \gg V_\mathrm{L} > V_1(L_0)$ for $\forall L_0 > 0$.

Figure 4.11b shows that at high and moderate initial concentrations of lactose ($L_0 \gtrsim 2O_0$), after a relatively short time ($10^2 - 10^3$ s) the oxygen concentration as well as the effectiveness factor start to decrease drastically. The oxygen concentration becomes so low that $V_2(O_\mathrm{m})$ becomes much less than $V_1(L_\mathrm{m})$, and then the process acts under oxygen limited conditions, i.e., $V(L_\mathrm{m}, O_\mathrm{m}) \approx 2V_2(O_\mathrm{m})$. At so low concentrations of oxygen as $O_\mathrm{m} \ll \mathrm{K_O}$, the non-linear reaction term $V_2(O_\mathrm{m})$ reduces to a the first-order reaction term i.e., $V_2(O_\mathrm{m}) \approx O_\mathrm{m} V_\mathrm{O}/\mathrm{K_O}$.

As one can see in Figure 4.11b, the initial lactose concentration can be so low ($L_0 \lesssim 2O_0$) that the oxygen can be only partially reduced and the process (1.1) stays under lactose control as it was initially. At so very low concentrations of lactose ($L_\mathrm{m} \ll \mathrm{K_L}$), the rate $V_1(L_\mathrm{m})$ approaches to the first order rate, $V_1(L_\mathrm{m}) \approx L_\mathrm{m} V_\mathrm{L}/\mathrm{K_L}$. So, at the steady state conditions, the rate $V(L_\mathrm{m}, O_\mathrm{m})$ of the conjugated two enzymes catalyzed process (1.1) approaches to the first order rate: to $2O_\mathrm{m} V_\mathrm{O}/\mathrm{K_O}$, if $L_0 \gtrsim 2O_0$, or to $L_\mathrm{m} V_\mathrm{L}/\mathrm{K_L}$, if $L_0 \lesssim 2O_0$. In such linear cases, the steady state effectiveness factor can be calculated analytically [A3][A1]. Applying that formula for two linear cases of the reaction rate $V(L_\mathrm{m}, O_\mathrm{m})$ leads to two expressions of the steady state effectiveness factor, one for lactose (η_L) and another for oxygen (η_o),

$$\eta_C = \frac{3\beta_C \phi(\Phi_C \coth \Phi_C - 1)}{\Phi_C^2(\beta_C + \phi(\Phi_C \coth \Phi_C - 1))}, \quad C = L, O. \tag{4.9}$$

Values of the steady state factors calculated at the parameter values defined in (4.8) are as follows: $\eta_\mathrm{L} \approx 0.54$ and $\eta_\mathrm{o} \approx 0.073$. As one can see in Figure 4.11a- 4.11d, the transient effectiveness factor $\eta_t(t)$ finally ($t \to \infty$), depending on L_0, approaches to either η_L or to η_o, both calculated from (4.9).

4.3.4. Impact of the diffusion limitations on the effectiveness

The transient effectiveness factor η_t when changing the Thiele modulus Φ_L at two concentrations of lactose L_0: 10 (a) and 0.1 (b) mM. Then the parameters obtain values $\Phi_\mathrm{O} = 13.3$ for L_0: 10 (c) and 0.1 (d) mM ($\Phi_\mathrm{O} = 1$) (see Figure 4.12). The other parameters and notation are the same as in Figure 4.11.

Figure 4.12 shows the evolution of the transient effectiveness factor η_t simulated at a wide range of values of the Thiele modulus Φ_L and two initial concentrations of lactose L_0: 10 and 0.1 mM. The dependencies of the evolution of η_t on another Thiele modulus Φ_O and the Biot number $\beta = \beta_L = \beta_O$ are depicted in Figure 4.13 (also in Figures 4.12c–4.12d).

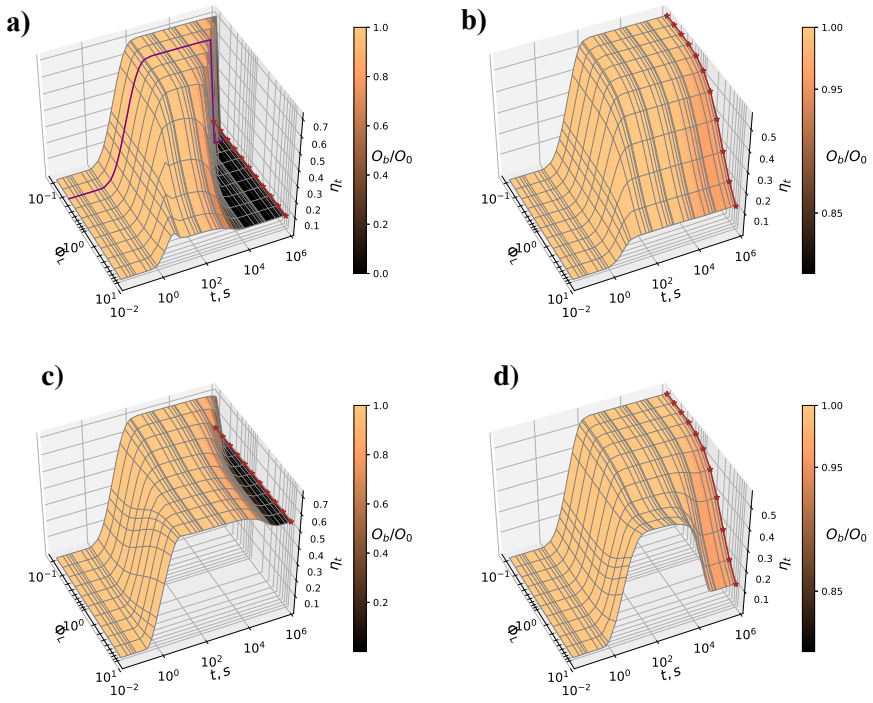

Figure 4.12: The transient effectiveness factor η_t when changing the Thiele modulus Φ_L at two concentrations of lactose L_0: 10 (a) and 0.1 (b) mM

The simulation results depicted in Figure 4.12a correspond to the simulated physical experiment shown in Figure 4.10 with addition of Φ_L variation. Although the concentration $L_0 = 10$ mM is comparable with the Michaelis constant K_L, the concentration is high enough ($L_0 > 2O_0$) that all oxygen is consumed (see Figure 4.11)b, and the conjugated process acts distinctly under oxygen limited conditions when the process approaches the steady state. Since both Biot numbers (β_O and β_L), the partition coefficient ϕ and the Thiele modulus Φ_O were constant in simulations shown in Figure 4.12a, the steady state effectiveness factor is invariant to the Thiele modulus Φ_L and equal to $\eta_o \approx 0.073$ for all values of Φ_L.

To show that the Thiele modulus Φ_L can really affect the steady state effectiveness factor, the bioreactor system was simulated at hundredfold less lactose concentration $L_0 = 0.1$ mM, when the conjugated process acts under lactose limited conditions from the beginning up to the steady state. Figure

4.12b shows that the steady state effectiveness factor monotonously increases with decreasing the Thiele modulus Φ_L and can be expressed as a function $\eta_L = \eta_L(\Phi_L)$ calculated from (4.9) and is depicted by a red dotted line.

At $L_0 = 0.1$ mM, the transient factor η_t monotonously increases with time for all values of Φ_L ranging from 0.1 up to 10 (Figure 4.12b), while η_t is a non-monotonic function of time at $L_0 = 10$ mM as shown in Figure 4.12a. Figure 4.12b also shows that only a small part of oxygen is reduced at so low ($L_0 = 0.1$ mM) lactose concentration. The non-monotony of η_t can be achieved also at moderate values of L_0 by adjusting different physical and catalytic parameters of the MR [A1] (also refer to Figure 4.12d).

One can see in Figure 4.12a a spike of the transient effectiveness factor η_t at $t \approx 10$ s when the system acts under diffusion limitation ($\Phi_L > 1$). This shows that process reduces to limited one under $R_1 - R_0 = 80\,\mu m$. A very similar spike was also observed when modeling the mono-enzyme immobilized MR [A1].

Figures 4.12 and 4.13a–4.13e show that the MR effectiveness can be notably increased, at least for a certain time, by decreasing the Thiele modules, i.e., by decreasing the intraparticle diffusion resistance. Such impact of the diffusion resistance on the MR effectiveness has been already reported for the corresponding mono-enzyme MR [A3][A1].

Assuming the same Biot number for both substrates, $\beta = \beta_L = \beta_O$, the dependence of the MR effectiveness on the external diffusion resistance is depicted in Figure 4.13c. As one can see in Figure 4.13c, the maximum transient as well as steady state effectiveness factors can be slightly increased by increasing the Biot number β, i.e., by decreasing the external diffusion resistance. Since the MR action was simulated for a relatively high lactose concentration ($L_0 = 10$ mM), the steady state effectiveness factor η_o is rather low and changes only slightly as in Figure 4.12a.

4.3.5. Duration of oxygen reduction

Colouring surfaces of the transient effectiveness factor in Figures 4.11–4.13 show how fast oxygen is reduced in the biochemical reactions taking place in the MR. The most noticeable influence of the oxygen reduction on the duration comes from the lactose concentration L_0 and both Thiele modulus, Φ_L and Φ_O.

As one can see in Figure 4.11 the time required to convert 90% of the initial amount of oxygen ($O_b/O_0 = 0.1$) at $L_0 = 10^3$ mM is in a few orders of magnitude less than at $L_0 = 1$ mM. On the other hand, at relatively low lactose concentration ($L_0 < 2O_0$) the 90% reduction of oxygen cannot be achieved at all.

At high concentrations of lactose all oxygen can be reduced notably faster than the steady state effectiveness is reached. Thus, all the oxygen can be

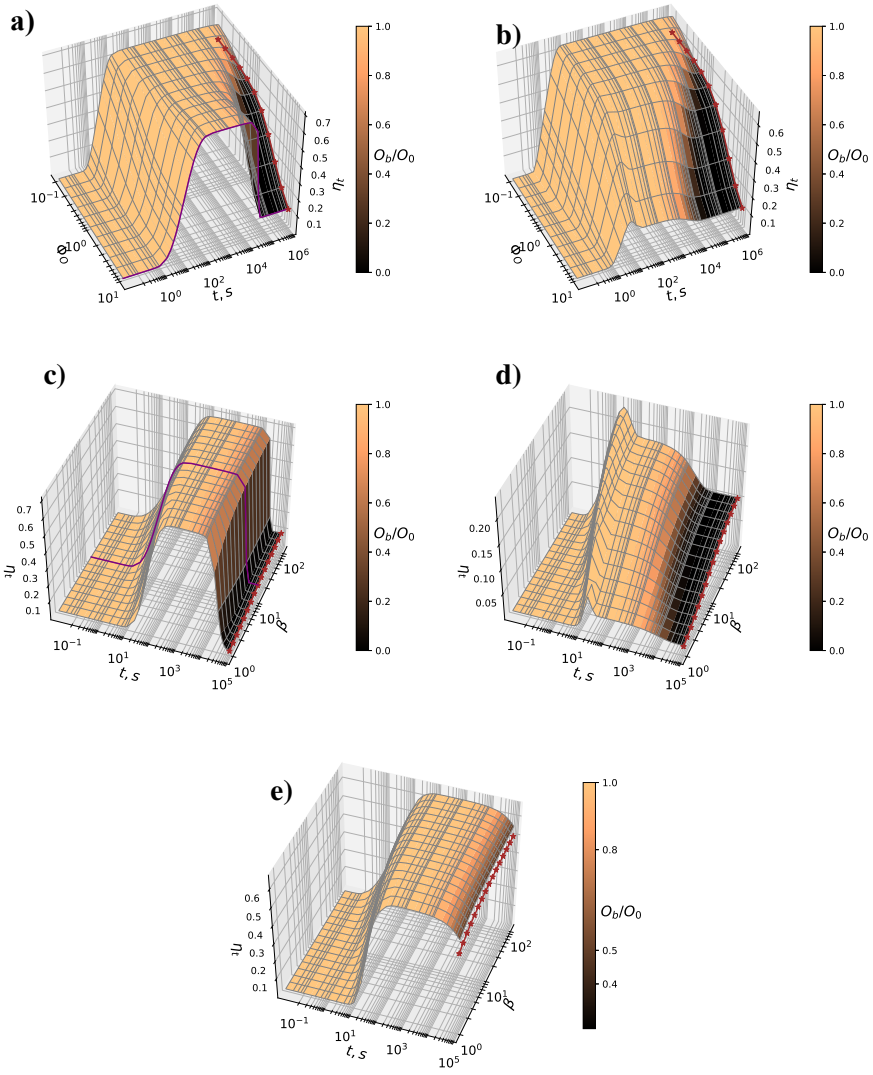

Figure 4.13: The transient effectiveness factor η_t when changing the Thiele modulus Φ_O (a–b) and the Biot number $\beta = \beta_L = \beta_O$ (c–e)

reduced at significantly higher effectiveness than that at the steady state. Therefore, the often used classical steady state approach can lead to serious errors affecting bioreactor design efforts [19].

Figures 4.12a and 4.13a show that at moderate and high concentrations of lactose a tenfold decrease in the Thiele modulus can lead to more than a tenfold increase of the time required to convert a certain amount of oxygen. The similar behavior is observed when $\Phi_L = 10$ see Figure 4.13b.

Due to stirring of the solution, the influence of the Biot number (Figure

4.13c) on the duration of the oxygen reduction is notably less important than the influence of the Thiele modulus and lactose concentration. The total effectiveness increases with decrease of Φ_O (see Figure 4.13d), where $\Phi_O = 10$, and 4.13e, where $\Phi_O = 1$.

Additional simulations have showed that the influence of the Biot number, the adsorption capacity $(1/q)$, and of the formal partition coefficient ϕ on the transient effectiveness factor as well as to the process duration is very similar to that observed in computational modeling the mono-enzyme immobilized MR [A1] (Figure 4.13d- 4.13e).

Taking into account the influence of the Thiele modulus on the process duration, increasing MR effectiveness by decreasing internal diffusion limitation (decreasing Φ_L and Φ_O) is restricted when a short substrate conversion time is of crucial importance.

Conclusions

The two-compartment mathematical model (2.33)–(2.23) can be used to investigate regularities of a batch stirred tank reactor based on an array of identical spherical porous microbioreactors loaded with bienzyme when both enzyme catalyzed processes obey the Michaelis-Menten kinetics. The mathematical model rather accurately reflects the physical experiments with microbioreactors loaded with non specific glucose dehydrogenase and oxygen reducing laccase (Figure 4.9).

The transient overall effectiveness factor η_t of a microbioreactor is a non-monotonic function of time if the initial lactose concentration is notably greater than the initial oxygen concentration ($L_0 \gtrsim 2O_0$) (Figures 4.11, 4.12a and 4.13). At high lactose concentration, most of the oxygen is reduced at significantly higher effectiveness than that at the steady state. At law initial concentrations of lactose ($L_0 \lesssim 2O_0$), the effectiveness factor η_t is a monotone increasing function of time (Figures 4.11 and 4.12b). The non-monotony of η_t can be achieved also at moderate values of L_0 by adjusting the physical and catalytic parameters. Depending on the concentration L_0, the transient effectiveness factor η_t approaches its steady state value equal to either η_L (if $L_0 \lesssim 2O_0$) or to η_o (if $L_0 \gtrsim 2O_0$), both calculated from (4.9).

The bioreactor effectiveness can be notably increased, at least for a certain time, by decreasing both Thiele moduli, Φ_L and Φ_O, i.e., by decreasing the intraparticle diffusion resistance. However, increasing bioreactor effectiveness by the decreasing internal diffusion limitation (decreasing Φ_L and Φ_O) is restricted when a short substrate conversion time is of crucial importance (Figures 4.12 and 4.13a).

The main conclusions from this Chapter:

1. The mathematical model presented in Section 2.1 was investigated numericaly [A3].

2. The mathematical model presented in Section 2.2 was investigated numericaly [A1].

3. It was demonstrated that transient effectiveness of a closed system (batch type bioreactors) reduces to characteristics of open steady-state system (continuous type models) under large time.

4. The novel mathematical model presented in Section 2.2 was investigated numericaly [A2].

5. The comparison of numerical experiments with experimental data demonstrated that the proposed novel three layer mathematical model are suitable to formalize experiments proposed by [93, 94].

6. The kinetics of bioreactor, based on microbioreactors, can be succesfully modeled in one dimmentional space, using unit cell (a microbioreactor) and the surrounding (diffusion) shell.

Conclusions

1. The developed mathematical model of a microreactor with carbon nanotubes, which include combining chemical reactions via elections wiring conversion, can be successfully used to investigate the kinetic properties of the bioreactor behavior.

2. The transient effectiveness of a closed bioreactor system reduces to the transient effectiveness of an open bioreactor system under large time. The delivered analytical characteristics are valid for a much wider class of models.

3. The considered method of homotopy perturbation could be suitable to provide good approximations at fixed system hyper-parameters. Sufficient approximations with error $< 10^{-10}$ could be achieved. However, different microbioreactor configurations require different formulations of HPM (different initial introduction of the small parameter into equation).

4. The chemical kinetics of bioreactor, based on large number uninteracting microbioreactors, can be successfully modeled as unit cell (a microbioreactor) and the surrounding shell in one dimensional space.

Bibliography

[1] Ali E. AL-Muftah and Ibrahim M. Abu-Reesh. Effects of simultaneous internal and external mass transfer and product inhibition on immobilized enzyme-catalyzed reactor. *Biochem. Eng. J.*, 27(2):167–178, 2005.

[2] Mohammad Al-Shannag, Zakaria Al-Qodah, Joan Herrero, Joseph A.C. Humphrey, and Francesc Giralt. Using a wall-driven flow to reduce the external mass-transfer resistance of a bio-reaction system. *Biochem. Eng. J.*, 38(3):554–565, 2008.

[3] Illanes Andrés. *Enzyme Biocatalysis: Principles and Applications*. Springer, Dordrecht, 2008.

[4] Rutherford Aris. *The Mathematical Theory of Diffusion and Reaction in Permeable Catalysts: The theory of the steady state*, volume 1. Clarendon Press, 1975.

[5] Rutherford Aris. *The Mathematical Theory of Diffusion and Reaction in Permeable Catalysts: Vol. 1: The Theory of the Steady State*. Oxford Studies in Physics. Oxford University Press, Oxford, 1975.

[6] Rutherford Aris. *Mathematical Modeling: A Chemical Engineer's Perspective*. Academic Press, London, 1999.

[7] E. Babolian, A. Azizi, and J. Saeidian. Some notes on using the homotopy perturbation method for solving time-dependent differential equations. *Math. Comput. Model.*, 50:213–224, 2009.

[8] Robert Bailey, Frank Jones, Ben Fisher, and Bill Elmore. Enhancing design of immobilized enzymatic microbioreactors using computational simulation. *Appl. Biochem. Biotechnol.*, 122(1–3):639–652, 2005.

[9] R. Baronas, F. Ivanauskas, and J. Kulys. Modelling a biosensor based on the heterogeneous microreactor. *J. Math. Chem.*, 25:245–252, 1999.

[10] R Baronas, F Ivanauskas, and A Survila. Simulation of electrochemical behavior of partially blocked electrodes under linear potential sweep conditions. *J. Math. Chem.*, 27(4):267–278, 2000.

[11] Romas Baronas, Feliksas Ivanauskas, and Juozas Kulys. Mathematical modeling of biosensors based on an array of enzyme microreactors. *Sensors*, 6(4):453–465, 2006.

[12] Romas Baronas, Feliksas Ivanauskas, and Juozas Kulys. *Mathematical Modeling of Biosensors*. Springer, Dordrecht, 2010.

[13] Romas Baronas, Feliksas Ivanauskas, and Juozas Kulys. *Mathematical Modeling of Biosensors*, volume 9 of *Springer Series on Chemical Sensors and Biosensors*. Springer Netherlands, Dordrecht, 2010.

[14] Philip N. Bartlett. *Bioelectrochemistry: Fundamentals, Experimental*

Techniques and Applications. John Wiley & Sons, Chichester, UK, 2008.

[15] Laurence A. Belfiore. *Transport Phenomena for Chemical Reactor Design*. John Wiley & Sons, Hoboken, New Jersey, 2003.

[16] Carl M. Bender and Steven A. Orszag. *Advanced Mathematical Methods for Scientists and Engineers I: Asymptotic Methods and Perturbation Theory*. Springer Science & Business Media, 2013.

[17] Hugues Berry. Monte carlo simulations of enzyme reactions in two dimensions: fractal kinetics and spatial segregation. *Biophys. J.*, 83(4):1891–1901, 2002.

[18] Claudia María Bidabehere, Juan Rafael García, and Ulises Sedran. Use of stirred batch reactors for the assessment of adsorption constants in porous solid catalysts with simultaneous diffusion and reaction. Theoretical analysis. *Chem. Eng. Sci.*, 61(6):2048–2055, 2006.

[19] Claudia María Bidabehere, Juan Rafael García, and Ulises Sedran. Transient effectiveness factor in porous catalyst particles. application to kinetic studies with batch reactors. *Chem. Eng. Res. Des.*, 118:41–50, 2017.

[20] Claudia María Bidabehere, Juan Rafael García, and Ulises Sedran. Transient effectiveness factor. simultaneous determination of kinetic, diffusion and adsorption equilibrium parameters in porous catalyst particles under diffusion control conditions. *Chem. Eng. J.*, 345:196–208, 2018.

[21] Claudia María Bidabehere and Ulises Sedran. Transient effectiveness factors in the dynamic analysis of heterogeneous reactors with porous catalyst particles. *Chem. Eng. Sci.*, 137:293–300, 2015.

[22] R. Byron Bird, Warren E. Stewart, and Edwin N. Lightfoot. *Transport Phenomena*. John Wiley & Sons, New York, 2 edition, 2006.

[23] J. Biswas, D.D. Do, P.F. Greenfield, and J.M.Smith. Evaluation of bidisperse diffusivities and tortuosity factors in porous catalysts using batch and continuous adsorbers: a theoretical study. *Appl. Catal.*, 22(1):97–113, 1986.

[24] Katarzyna Bizon and Bolesław Tabiś. Dynamics of an isothermal catalyst pellet with simultaneous chemical reaction and adsorption. *Chem. Eng. Res. Des.*, 115:221–229, 2016.

[25] Nadia Bortone, Marcello Fidaleo, and Mauro Moresi. Internal and external mass transfer limitations on the activity of immobilised acid urease derivatives differing in enzyme loading. *Biochem. Eng. J.*, 82:22–33, 2014.

[26] Tomáš Brányik, António A Vicente, Pavel Dostálek, and José A Teixeira. Continuous beer fermentation using immobilized yeast cell bioreactor systems. *Biotechnol. progr.*, 21(3):653–663, 2005.

[27] Christopher Earls Brennen and Christopher E Brennen. *Fundamentals of multiphase flow*. Cambridge university press, 2005.

[28] Dieter Britz, Romas Baronas, Evelina Gaidamauskaitė, and Feliksas Ivanauskas. Further comparisons of finite difference schemes for computational modelling of biosensors. *Nonlinear Anal. Model. Control*, 14(4):419–

433, 2009.

[29] Dieter Britz and Jörg Strutwolf. *Digital Simulation in Electrochemistry*. Monographs in Electrochemistry. Springer, Cham, 4 edition, 2016.

[30] Mohamed Amara Camara, Miaomiao Tian, Liping Guo, and Li Yang. Application of capillary enzyme micro-reactor in enzyme activity and inhibitors studies of glucose-6-phosphate dehydrogenase. *Journal of Chromatography B*, 990:174–180, 2015.

[31] D. Cascaval, A.I. Galaction, and R. Rotaru. Effect of glucose internal diffusion on alcoholic fermentation in a stationary basket bioreactor with immobilized yeast cells. *Rom. Biotech. Lett.*, 16(3):6200–6208, 2011.

[32] Hsien-Chang Chang, Ching-Chou Wu, Shinn-Jyh Ding, I-Shiun Lin, and I-Wen Sun. Measurement of diffusion and partition coefficients of ferrocyanide in protein-immobilized membranes. *Anal. Chim. Acta.*, 532(2):209–214, 2005.

[33] Tian Qi Chen, Yulia Rubanova, Jesse Bettencourt, and David K Duvenaud. Neural ordinary differential equations. In *Advances in neural information processing systems*, pages 6571–6583, 2018.

[34] Raimondas Čiegis and Remigijus Čiegis. Numerical algorithms for solving the optimal control problem of simple bioreactors. *Nonlinear Anal. Model. Control*, 24(4):626–638, 2019.

[35] Raimondas Čiegis, Olga Suboč, and Remigijus Čiegis. Numerical simulation of nonlocal delayed feedback controller for simple bioreactors. *Informatica*, 29(2):233–249, 2018.

[36] Douglas S Clark and Harvey W Blanch. *Biochemical engineering*. CRC press, 1997.

[37] Douglas S. Clark and Harvey W. Blanch. *Biochemical Engineering*. Marcel Dekker, New York, 2 edition, 1997.

[38] Liliane Coche-Guerente, Piere Labbé, and Virginie Mengeaud. Amplification of amperometric biosensor responses by electrochemical substrate recycling. 3. Theoretical and experimental study of the phenol-polyphenol oxidase system immobilized in laponite hydrogels and layer-by-layer self-assembled structures. *Anal. Chem.*, 73(14):3206–3218, 2001.

[39] John Crank. *The Mathematics of Diffusion*. Oxford University Press, London, 1975.

[40] Berardino D'acunto. *Computational Methods for PDE in Mechanics:(With CD-ROM)*, volume 67. World Scientific Publishing Company, 2004.

[41] Mark E. Davis and Robert J. Davis. *Fundamentals of chemical reaction engineering*. McGraw-Hill, New York, 2003.

[42] Duong D. Do and Paul F. Greenfield. The concept of an effectiveness factor for reaction problems involving catalyst deactivation. *Chem. Eng. J.*, 27(2):99–105, 1983.

[43] Pauline M. Doran. *Bioprocess Engineering Principles*. Academic Press, 1995.

[44] Pauline M. Doran. *Bioprocess Engineering Principles*. Academic Press, Waltham, MA, 2 edition, 2013.

[45] D. A. Edwards, B. Goldstein, and D. S. Cohen. Transport effects on surface-volume biological reactions. *J. Math. Biol.*, 39(6):533–561, 1999.

[46] Messoud Efendiev. *Mathematical Modeling of Mitochondrial Swelling*. Springer, 2018.

[47] A. Eswari and L. Rajendran. Analytical solution of steady state current at a microdisk biosensor. *J. Electroanal. Chem*, 641(1):35–44, 2010.

[48] Adolph Fick. On liquid diffusion. *J. Membrane Sci.*, 100(1):33–38, 1995.

[49] David J. Fink, Tsungyen Na, and Jerome S. Schultz. Effectiveness factor calculations for immobilized enzyme catalysts. *Biotechnol. Bioeng*, **15**(5):879–888, 1973.

[50] Rafael F. Fonseca, Caio C. B. Melo, Beatriz, B. C. P. Sanches, Victor Bertucci-Neto, Cristiane S. Farinas, and Wu H. Kwong. Modelling of solid-state fermentation over wide operational range for application in process optimization. *Can. J. Chem. Eng*, 96:1723–1734, 2018.

[51] Buntu Godongwana. Effectiveness factors and conversion in a biocatalytic membrane reactor. *PLoS ONE*, 11(4):e0153000, 2016.

[52] Ireneusz Grubecki. External mass transfer model for hydrogen peroxide decomposition by terminox ultra catalase in a packed-bed reactor. *Chem. Process Eng.*, 38(2):307–319, 2017.

[53] Tatsuro Gueshi, Koichi Tokuda, and Hiroaki Matsuda. Voltammetry at partially covered electrodes: Part i. chronopotentiometry and chronoamperometry at model electrodes. *J. Electroanal. Chem and Interfacial Electrochemistry*, 89(2):247–260, 1978.

[54] H. Gutfreund. *Kinetics for the Life Sciences*. Cambridge University Press, Cambridge, 1995.

[55] Peter Harriott. *Chemical Reactor Design*. Marcel Dekker, New York, 2003.

[56] Ji-Huan He. Homotopy perturbation technique. *Comp. Meth. Appl. Mech. Eng.*, 178(3–4):257–262, 1999.

[57] Ji-Huan He. Homotopy perturbation method: a new nonlinear analytical technique. *Appl. Math. Comput.*, 135(1):73–79, 2003.

[58] Amir Hussain, Martin Kangwa, and Marcelo Fernandez-Lahore. Comparative analysis of stirred catalytic basket bio-reactor for the production of bio-ethanol using free and immobilized Saccharomyces cerevisiae cells. *AMB Expr.*, 7(1):158, 2017.

[59] Jamshed Iqbal, Shoaib Iqbal, and Christa E Müller. Advances in immobilized enzyme microbioreactors in capillary electrophoresis. *Analyst*, 138(11):3104–3116, 2013.

[60] Jamshed Iqbal, Shoaib Iqbala, and Christa E. Müller. Advances in immobilized enzyme microbioreactors in capillary electrophoresis. *Analyst*, 138(11):3104–3116, 2013.

[61] M Jahoda, M Moštěk, A Kukuková, and V Machoň. Cfd modelling of liquid homogenization in stirred tanks with one and two impellers using large eddy simulation. *Chem. Eng. Res. Des.*, 85(5):616–625, 2007.

[62] Edward Jones, Kay McClean, Sally Housden, Gilda Gasparini, and Ian Archer. Biocatalytic oxidase: Batch to continuous. *Chem. Eng. Res. Des.*, 90:726–731, 2012.

[63] Rafael Kandiyoti. *Fundamentals of Reaction Engineering*. Ventus Publishing, Frederiksberg, Denmark, 2009.

[64] Badr Kaoui, Marco Lauricella, and Giuseppe Pontrelli. Mechanistic modelling of drug release from multi-layer capsules. *Comput. Biol. Med.*, 93:149–157, 2018.

[65] V. Kasche, A. Kapune, and H. Schwegler. Operational effectiveness factors of immobilized enzyme systems. *Enzyme Microb. Technol.*, 1(1):41–46, 1979.

[66] Anees Y. Khan, Santosh B. Noronha, and Rajdip Bandyopadhyaya. Glucose oxidase enzyme immobilized porous silica for improved performance of a glucose biosensor. *Biochem. Eng. J.*, 91:78–85, 2014.

[67] O.M. Kirthiga and L. Rajendran. Approximate analytical solution for non-linear reaction diffusion equations in a mono-enzymatic biosensor involving Michaelis-Menten kinetics. *J. Electroanal. Chem.*, 751:119–127, 2015.

[68] Aikaterini Konti, Diomi Mamma, Dimitios G. Hatzinikolaou, and Dimitris Kekos. 3-Chloro-1,2-propanediol biodegradation by Ca-alginate immobilized pseudomonas putida DSM 437 cells applying different processes: mass transfer effects. *Bioprocess. Biosyst. Eng.*, 39(10):1597–1609, 2016.

[69] J Kulys. The development of new analytical systems based on biocatalysts. *Analytical Letters*, 14:377–397, 1981.

[70] Martin Kunze, Clemens Lattermann, Sylvia Diederichs, Wolfgang Kroutil, and Jochen Büchs. Minireactor-based high-throughput temperature profiling for the optimization of microbial and enzymatic processes. *J. Biol. Eng.*, 8:22, 2014.

[71] Bronius Kvedaras and Mifodijus Sapagovas. Skaičiavimo metodai. *Vilnius:" Mintis*, 1974.

[72] Jerzy Leszczynski, editor. *Handbook of Computational Chemistry*. Springer, Dordrecht, 2012.

[73] Haiying Liu, Xinming Qian, Zhiming Du, Ping Huang, and Zhenyi Liu. Thermal explosion model and calculation of sphere fireworks and crackers. *J. Therm. Anal. Calorim.*, 110(3):1029–1036, 2012.

[74] Martin F. Luna and Ernesto C. Martínez. Optimal design of dynamic experiments in the development of cybernetic models for bioreactors. *Chem. Eng. Res. Des.*, 136:334–346, 2018.

[75] William L Luyben. *Chemical reactor design and control*. John Wiley & Sons, 2007.

[76] Michael E. G. Lyons. Transport and kinetics at carbon nanotube – redox enzyme composite modified electrode biosensors. *Int. J. Electrochem. Sci.*, 4(1):77–103, 2009.

[77] Gheorghe Maria. Enzymatic reactor selection and derivation of the optimal operation policy, by using a model-based modular simulation platform. *Comput. Chem. Eng.*, 36:325–341, 2012.

[78] Ray Medina. *Fermentation Technology*. Scientific e-Resources, 2019.

[79] A. Meena and L. Rajendran. Analytical solution of system of coupled non-linear reaction diffusion equations. Part II: Direct reaction of substrate at underlying microdisc surface. *J. Electroanal. Chem*, 650(1):143–151, 2010.

[80] J Monod et al. Thetechnique of continuous culture. *Ann. Inst. Pasteur*, 79:390–410, 1950.

[81] Jacques Monod. Recherches sur la croissance des cultures bacteriennes. 1942.

[82] Endre Nagy. Survey on biocatalytic membrane reactor and membrane aerated biofilm reactor. *Curr. Org. Chem.*, 21:1713–1724, 2017.

[83] Endre Nagy, Jozsef Dudás, Rosalinda Mazzei, Enrico Drioli, and Lidietta Giorno. Description of the diffusive-convective mass transport in a hollow-fiber biphasic biocatalytic membrane reactor. *J. Membr. Sci.*, 482:144–157, 2015.

[84] Jens Nielsen, John Villadsen, and Eli Keshavarz-Moore. Bioreaction Engineering Principles. *Trends Biotechnol.*, **13**(4):156, 1995.

[85] Aaron Novick and Leo Szilard. Experiments with the chemostat on spontaneous mutations of bacteria. *Proc. Natl. Acad. Sci. U. S. A.*, 36(12):708, 1950.

[86] Bernt Øksendal. Stochastic differential equations. In *Stochastic differential equations*, pages 65–84. Springer, 2003.

[87] Gottfried J Palm, Lukas Reisky, Dominique Böttcher, Henrik Müller, Emil AP Michels, Miriam C Walczak, Leona Berndt, Manfred S Weiss, Uwe T Bornscheuer, and Gert Weber. Structure of the plastic-degrading ideonella sakaiensis mhetase bound to a substrate. *Nature communications*, 10(1):1–10, 2019.

[88] Emmanouil Papadakis, Sven Pedersen, Anjan K. Tula, Marina Fedorova, John M. Woodley, and Rafiqul Gani. Model-based design and analysis of glucose isomerization process operation. *Comput. Chem. Eng.*, 98:128–142, 2017.

[89] Sarunas Petronis, Michael Stangegaard, Claus Bo Vöge Christensen, and Martin Dufva. Transparent polymeric cell culture chip with integrated temperature control and uniform media perfusion. *Biotechniques*, 40(3):368–376, 2006.

[90] Jakeline Kathiele Poppe, Roberto Fernandez-Lafuente, Rafael C. Rodrigues, and Marco Antônio Záchia Ayub. Enzymatic reactors for biodiesel

synthesis: Present status and future prospects. *Biotechnol. Adv.*, 33(5):511–525, 2015.

[91] William H. Press, Saul A. Teukolsky, William T. Vetterling, and Brian P. Flannery. *Numerical Recipes: The Art of Scientific Computing*. Cambridge University Press, Cambridge, 3 edition, 2007.

[92] L. Rajendran and S. Anitha. Reply to "Comments on analytical solution of amperometric enzymatic reactions based on Homotopy perturbation method", by Ji-Huan He, Lu-Feng Mo [Electrochim. Acta (2013)]. *Electrochim. Acta*, 102:474–476, 2013.

[93] Dalius Ratautas, Liucija Marcinkevičienė, Rolandas Meškys, and Juozas Kulys. Mediatorless electron transfer in glucose dehydrogenase/laccase system adsorbed on carbon nanotubes. *Electrochim. Acta*, 174:940–944, 2015.

[94] Dalius Ratautas, Eimantas Ramonas, Liucija Marcinkevičienė, Rolandas Meškys, and Juozas Kulys. Wiring gold nanoparticles and redox enzymes: A self-sufficient nanocatalyst for the direct oxidation of carbohydrates with molecular oxygen. *Chem. Cat. Chem.*, 10:971–974, 2018.

[95] James B. Rawlings and John G. Ekerdt. *Chemical Reactor Analysis and Design Fundamentals*. Nob Hill Publishing, LLC, Madison, WI, 2 edition, 2015.

[96] Ursula Rinas, Hesham El-Enshasy, Markus Emmler, Andrea Hille, Dietmar C. Hempel, and Harald Horn. Model-based prediction of substrate conversion and protein synthesis and excretion in recombinant Aspergillus niger biopellets. *Chem. Eng. Sci.*, 60(10):2729–2739, 2005.

[97] Lars Ruthotto and Eldad Haber. Deep neural networks motivated by partial differential equations. *arXiv preprint arXiv:1804.04272*, 2018.

[98] Abraham Sagiv. Exact solution of mass diffusion into a finite volume. *J. Membr. Sci.*, 186(2):231–237, 2001.

[99] Abraham Sagiv. Exact solution of mass diffusion into a finite volume. *J. Membr. Sci.*, 186:231–237, 2001.

[100] J. Saranya, L. Rajendran, L. Wang, and C. Fernandez. A new mathematical modelling using Homotopy perturbation method to solve nonlinear equations in enzymatic glucose fuel cells. *Chem. Phys. Let.*, 662:317–326, 2016.

[101] Daniel Schäpper, Muhd Nazrul Hisham Zainal Alam, Nicolas Szita, Anna Eliasson Lantz, and Krist V. Gernaey. Application of microbioreactors in fermentation process development: A review. *Anal. Bioanal. Chem.*, 395(3):679–695, 2009.

[102] T. Schulmeister. Mathematical modelling of the dynamic behaviour of amperometric enzyme electrodes. *Sel. Electrode Rev.*, 12:203–260, 1990.

[103] Th Schulmeister. Mathematical modelling of the dynamic behaviour of amperometric enzyme electrodes. *Sel. Electrode Rev.*, **12**(2):203–260, 1990.

[104] Szymon Skoneczny and Monika Cioch-Skoneczny. Mathematical modelling and approximate solutions for microbiological processes in biofilm through homotopy-based methods. *Chem. Eng. Res. Des.*, 139:309–320, 2018.

[105] T Skybová, M Přibyl, and P Hasal. Mathematical model of decolourization in a rotating disc reactor. *Biochem. Eng. J.*, 93:151–165, 2015.

[106] T. Skybová, M. Přibyl, and P. Hasal. Mathematical model of decolourization in a rotating disc reactor. *Biochem. Eng. J.*, 93:151–165, 2015.

[107] Ernest W Thiele. Relation between catalytic activity and size of particle. *Ind. Eng. Chem.*, 31(7):916–920, 1939.

[108] Nestor V. Torres. Application of the transition time of metabolic systems as a criterion for optimization of metabolic processes. *Biotechnol. Bioeng.*, 44(3):291–296, 1994.

[109] Francisco J. Valdés-Parada, J. Alvarez-Ramirez, and J. A. Ochoa-Tapia. Analysis of mass transport and reaction problems using Green's functions. *Rev. Mex. Ing. Quim.*, 6(3):283–294, 2007.

[110] Momchil Velkovsky, Rachel Snider, David E. Cliffel, and John P. Wikswo. Modeling the measurements of cellular fluxes in microbioreactor devices using thin enzyme electrodes. *J. Math. Chem.*, 49(1):251–275, 2011.

[111] Guillermo Vidriales-Escobar, Raul Rentería-Tamayo, Felipe Alatriste-Mondragón, and Omar González-Ortega. Mathematical modeling of a composting process in a small-scale tubular bioreactor. *Chem. Eng. Res. Des.*, 120:360–371, 2017.

[112] John Villadsen, Jens Nielsen, and Gunnar Lidén. *Bioreaction Engineering Principles*. Monographs in Electrochemistry. Springer, New York, 3 edition, 2011.

[113] H. J. Vos, P. J. Heederik, J. J. M. Potters, and K. Ch. A. M. Luyben. Effectiveness factor for spherical biofilm catalysts. *Bioprocess Eng.*, 5(2):63–72, 1990.

[114] Vern W Weekman. Laboratory reactors and their limitations. *AIChE J.*, 20(5):833–840, 1974.

[115] Stephen Whitaker. *The Method of Volume Averaging*, volume 13. Springer Science & Business Media, 2013.

[116] Jonathan WC Wong, R. D. Tyagi, and Ashok Pandey. *Current Developments in Biotechnology and Bioengineering: Solid Waste Management*. Elsevier, 2016.

[117] Shosuke Yoshida, Kazumi Hiraga, Toshihiko Takehana, Ikuo Taniguchi, Hironao Yamaji, Yasuhito Maeda, Kiyotsuna Toyohara, Kenji Miyamoto, Yoshiharu Kimura, and Kohei Oda. A bacterium that degrades and assimilates poly (ethylene terephthalate). *Science*, 351(6278):1196–1199, 2016.

[118] Li-Tao Zhu, Wang-Yu Ma, and Zheng-Hong Luo. Influence of distributed

pore size and porosity on MTO catalyst particle performance: Modeling and simulation. *Chem. Eng. Res. Des.*, 137:141–153, 2018.

[119] Antanas Žilinskas and Gražina Gimbutienė. A hybrid of bayesian approach based global search with clustering aided local refinement. *Commun. Nonlinear. Sci. Numer. Simul.*, 78:104857, 2019.

[120] Péter Érdi and Gábor Lente. Stochastic chemical kinetics. 2014.

Publications by the Author

Articles in journals indexed in Claritive Analytics Web of Science:

[A1] R. Baronas, J. Kulys, and **L. Petkevičius**. Computational modeling of batch stirred tank reactor based on spherical catalyst particles. *Journal of Mathematical Chemistry*, 57(1):327–342, 2019, Springer.

[A2] R. Baronas, J. Kulys, and **L. Petkevičius**. Modeling carbohydrates oxidation by oxygen catalyzed by bienzyme glucose dehydrogenase/laccase system immobilized into microreactor with carbon nanotubes. *Journal of Mathematical Chemistry*, 2019, Springer. (in review processes)

[A3] R. Baronas, J. Kulys, and **L. Petkevičius**. Modelling the enzyme catalysed substrate conversion in a microbioreactor acting in continuous flow mode. *Nonlinear Analysis: Modelling and Control*, 23(3):437–456, 2018, Vilnius University.

[A4] A. Žilinskas, R. Baronas, L. Litvinas, and **L. Petkevičius**. Multi-objective optimization and decision visualization of batch stirred tank reactor based on spherical catalyst particles. *Nonlinear Analysis: Modelling and Control*, 24(6):1019-1033, 2019, Vilnius University.

Articles in periodical peer-reviewed journals:

[A5] **L. Petkevičius** and R. Baronas. Modeling and simulation of enzyme-catalysed substrate conversion in a microbioreactor. *International Journal on Advances in Systems and Measurements*, 11(1 & 2):173–182, 2018, IARIA.

Articles in International conference proceedings

[A6] **L. Petkevičius**. Applying homotopy perturbation method to non-linear differential equations. *In 33rd annual European Simulation and Modelling Conference* (ESM 2019). Eurosis, pages 1–3, 2019.

[A7] **L. Petkevičius** and R. Baronas. Modeling and simulation of porous multi layer microbioreactors. *In 33rd International Conference on Modelling and Simulation* (ECMS 2019), pages 190-196. SCS-Europe, 2019.

[A8] **L. Petkevičius** and R. Baronas. Numerical analysis of the dynamics of reactant conversion in batch stirred tank reactor. *In 2018 IEEE 6th Workshop on Advances in Information, Electronic and Electrical Engineering* (AIEEE), pages 1–6. IEEE, 2018.

[A9] **L. Petkevičius** and R. Baronas. Numerical simulation and analysis of enzyme-catalysed substrate conversion in a microbioreactor. *In SIMUL 2017: The Ninth International Conference on Advances in System Simulation*, pages 8–12, 2017, IARIA.

Curriculum Vitae

Personal information

Linas Petkevičius
Email: linas.mif.vu@gmail.com
Birth: 1990-10-09. Plungė, Lithuania

Education

PhD 2015-2019 Informatics
MSc 2013-2015 Statistics
BSc 2009-2013 Statistics

Teaching and research experience

VU MIF 2017-now jr. researcher
VU MIF 2015-2017 jr. assistant

Work Experience

VU MIF 2010-2015 Laboratory assistant
Neurotechnology 2012-present Analyst

Scholarships

2019 Lithuanian research council

NOTES

Vilnius University Press
9 Saulėtekio Ave., Building III, LT-10222 Vilnius
Email: info@leidykla.vu.lt, www.leidykla.vu.lt
Print run copies 30